Politecnico di Torino

Politecnico di Torino

Corso di Laurea Magistrale in Ingegneria Energetica e Nucleare

A.a. 2023/2024

Sessione di Laurea Marzo 2024

Thermal runaway experimental analysis on 18650 Lithium-ions batteries during nail penetration test

Relatore:
Davide Papurello

Candidato:
Stefano Donati

Abstract

The need to find an alternative to transport powered by fossil fuels to reduce our impact on the planet is accompanied by the constant search for energy storage technologies. The excessive use of fossil fuels has led to a serious state of air pollution and is complicit in global warming; for these reasons, it has become of fundamental importance to change, gradually, the power system of transportation. Lithium-ions batteries are the most widespread technology for this purpose, but a fundamental parameter to take into consideration is the risk in case of an accident: during a collision with another vehicle, the batteries located inside the car are stressed considerably and this can be the cause of a puncture or irreversible deformation of the cell; events of this type are considered a risk for the occupants of the vehicle and all those involved in the accident as it can result in a high-temperature fire that can be potentially lethal. The stresses to which the vehicle is subjected during driving on the road such as vibrations, shocks and temperature changes must also be considered, stresses that, in the long run, can damage the battery pack.
This work will examine the effects of different forms of abuse on Lithium-ions batteries, with a focus on mechanical and thermal abuse; specifically, the experimental section will collect data about the behaviour of 18650 cylindrical cells after nail penetration: tests were performed in different temperature conditions to better understand how the environment influences the thermal runaway. Thanks to temperature and gas sensors, it was possible to characterize the 18650 thermal runaway to find analogies and differences between each cell in different ambient conditions. The collected data can be useful to better understand the behaviour of Lithium-Ion cells subjected to different forms of abuse and can help to find solutions to reduce the dangerous effects for the safety of people who use this storage technology.

Contents

List of Figures

1 Lithium Ions Batteries: State of the art

1.1 Introduction

The consumption of energy is at the basis of the development of a society; according to the Russian astronomer Nikolaj Kardašëv, the degree of technological advancement of a civilization is classified in a scale (Kardašëv's scale) based on the amount of energy it consumes. It is divided into:

- Type I: planetary civilization, that is able to obtain energy from all the resources present in the host planet (10^{16} W)
- Type II: stellar civilisation, able to exploit the energy produced by a star such as the sun (10^{26} W)
- Type III: galactic civilisation, capable of obtaining useful energy from an entire galaxy (10^{36} W)

At the moment, human civilization is at position 0.7276 on the Kardashev scale, but by the year 2060 it could reach position 0.7474 [57]. Although the change is only a few decimal digits, it must be remembered that the power involved is very high and therefore even a small increase can result in an additional power of millions of Watts.
Energy consumption is measured in Mtoe (Millions tonnes of oil equivalent) and includes energy produced by: oil, natural gas, coal, nuclear energy, and renewable energy. From Figure 1, it can be noticed that from 1985 the world population has increased by almost 50%, and with it, energy consumption has also increased, going from about 7000 Mtoe to 13500 Mtoe.

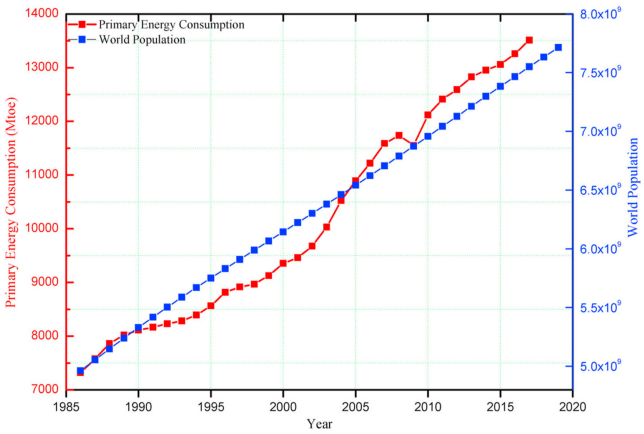

Figure 1: Primary energy consumption and population growth[40]

According to the report from the International Energy Agency (IEA), in 2019 35% of the energy consumed was used in the transport sector, of which 22% was used for private passenger transport: this corresponds to the majority share, followed by the manufacturing sector (23%) and residential sector (20%), as shown in figure 2.

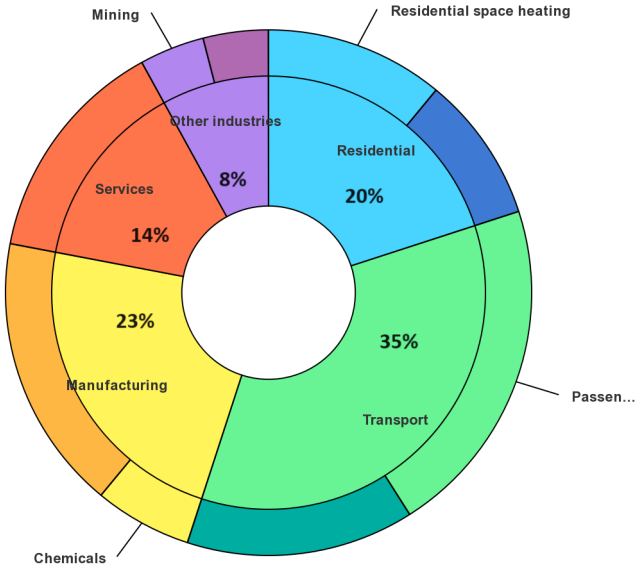

Figure 2: Largest end uses of energy by sector in 2019 [21]

According to an analysis by the IEA on oil consumption between 1979 and 2019, it appears that the largest amount of fossil fuel was consumed in the transport sector, amounting to 83.1 EJ, as shown in Figure 3. These data allow us to understand how impactful the automotive sector is in terms of fossil resource consumption, especially oil. This hydrocarbon has become the first choice in terms of energy vector for the automotive sector thanks to its high energy density, which is about 43.6 MJ/kg (8.2 kWh/liter) [27]. This characteristic allows car manufacturers to store large amounts of energy (and therefore vehicle autonomy) in small tanks, optimizing space and consumption. However, the conversion efficiency must be taken into account and for an internal combustion engine, there are multiple variables to consider: atmospheric conditions, compression ratio, number of revolutions, and stoichiometric ratio between air and fuel, to name a few examples. Under the best conditions, a thermal engine has an efficiency of 40% measured at the crankshaft [28], without taking into account the other losses that can take place like the ones in the transmission organs. Improving the effi-

ciency of the transport sector is therefore of fundamental importance to gradually reduce the direct consumption of fossil fuels: both to ensure a healthier environmental condition for the inhabitants of this planet by reducing the production of CO2, and from an economic point of view as the price of fuel represents a significant unknown for the future.

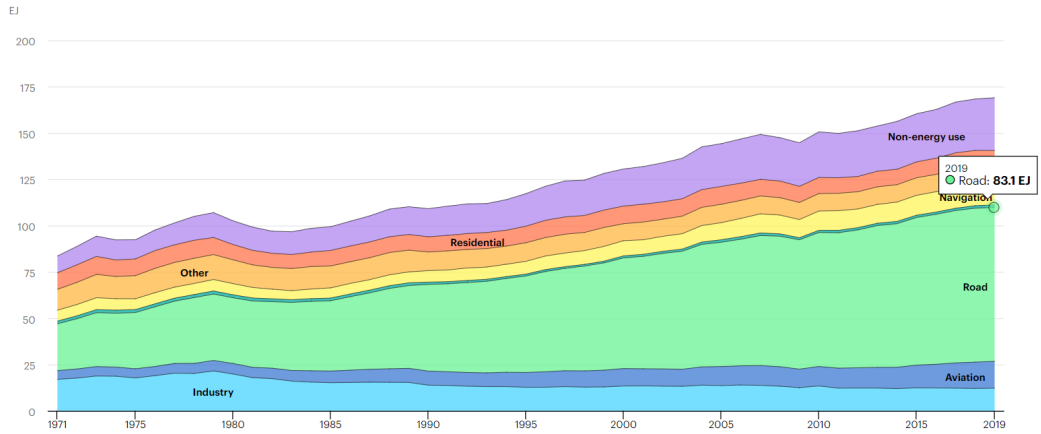

Figure 3: Oil total final consumption by sector [21]

In the end 35% of primary energy is consumed in the transport sector; it is therefore important to analyze how the car market changed in the past years. According to the report from the International Council on Clean Transportation (2022/2023), in 2021 the registration of new cars in the European Union decreased by 3% compared to 2020 and by 26% compared to 2019. At the same time, new registrations of plug-in hybrid and full electric vehicles went from 3% in 2019 to 19% of new registrations in 2021. China also increased the share of electric cars (full and plug-in hybrids) registered, going from 5% in 2019 to 24% in mid-2022. Similarly, the electric car market in the United States reached the highest growth rate in the first half of 2022, reaching a 7% share [9], as shown in figure 4.

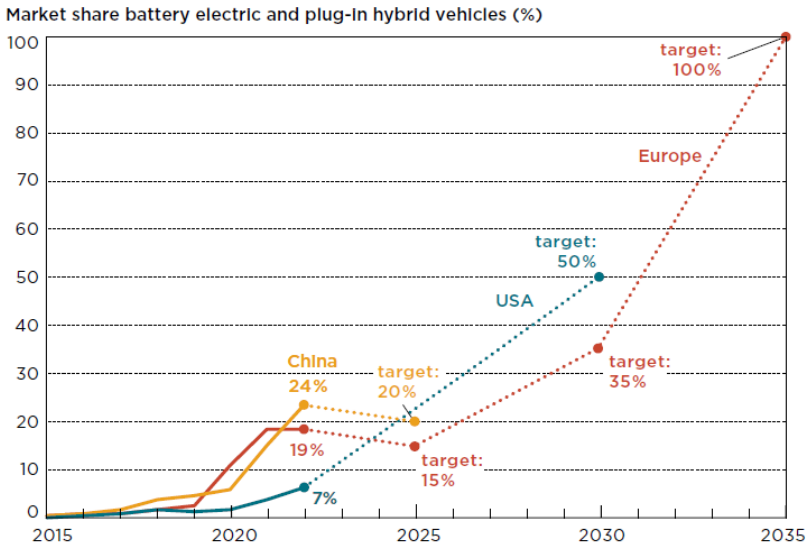

Figure 4: Share of battery electric and plug-in hybrid vehicles [9]

The European Union has already reached the target set for 2025 for a share of 15% of new vehicles registered powered by hybrid or full electric powertrains. The target has then been set at 100% by 2035 to bring to zero the emissions of vehicles put into circulation after that date, according to the "Fit for 55" package approved by the European Union Council in 2023 [20].
Another parameter to consider is the cost of technologies and raw materials for the production of electricity. As shown in Figure 5, the trend of crude oil prices varies considerably over time, and is strongly influenced by geopolitical phenomena; the high concentration of fossil resources by some states makes countries that are scarcer in these ones (such as oil and natural gas) more vulnerable. A country's energy independence is the key to unconditional development. Price variations of primary resources also affect those that derive from their consumption, such as electricity. Over time, however, technologies for alternative generation of electrical energy have made big progress and this fact has been accompanied by a strong reduction in the cost of technology.

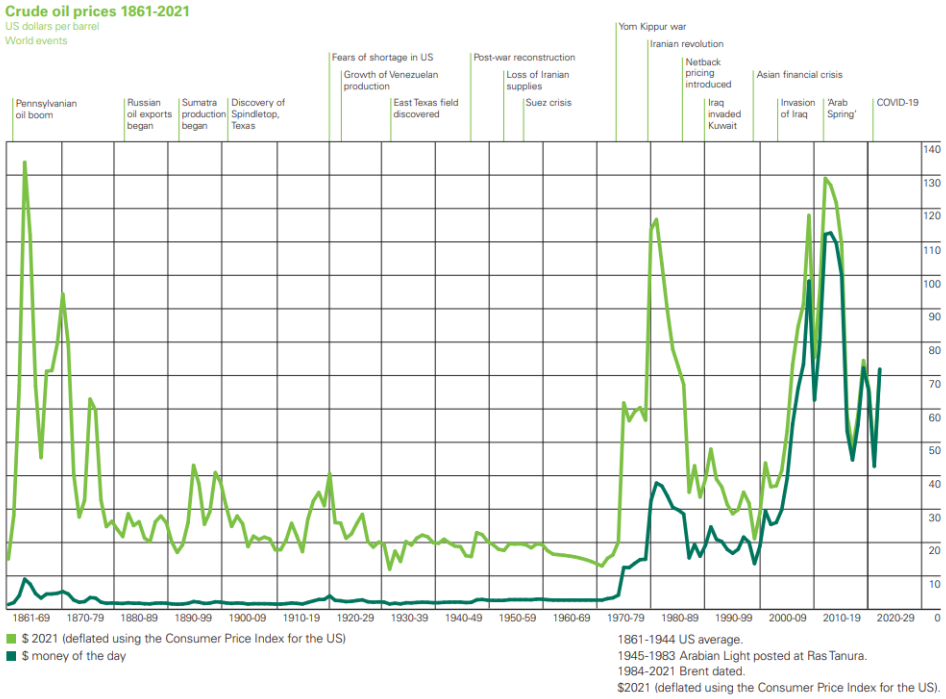

Figure 5: Crude oil prices from 1861 to 2021 [6]

In figure 6 it is shown how some fundamental parameters varied for the major technologies used for the production of electricity from renewable sources, such as:

- **Total installed costs**: amount of money spent for a technology divided by the power output
- **Capacity factor**: dimensionless ratio between the actual electrical energy used and the maximum electrical energy that would have been used by considering a constant load pattern with values equal to the reference power[8]
- **Average LCOE**: electricity tariff at which an investor would precisely break even after paying the required rates on return on capital, given the costs incurred during the lifetime of a technology [29]

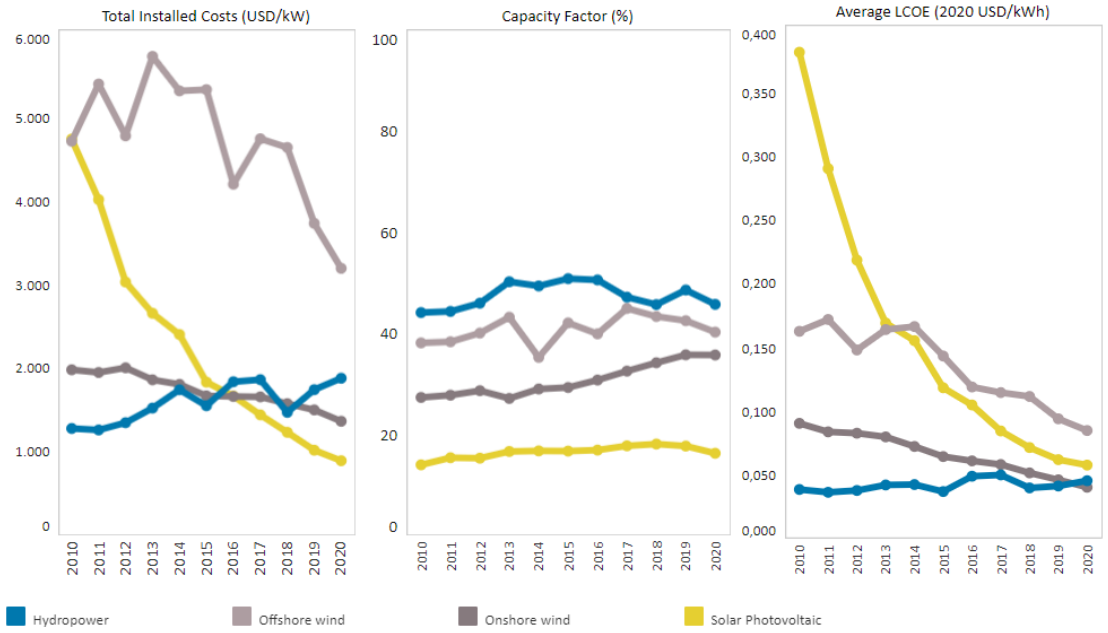

Figure 6: Total installed cost, Capacity factor and average LCOE for different technologies [22]

We can see how the LCOE for the production of energy from photovoltaics has drastically decreased in the last decade, going from about 0.4$/kWh in 2010 to 0.06$/kWh in 2020. The same phenomenon also applies to the installation costs of photovoltaic panels, which have been reduced by 80% compared to the initial cost. The costs for on-shore and off-shore wind turbines are also following the same trend, making these technologies increasingly competitive over time. A disadvantageous characteristic of renewable technologies like those mentioned above is the inconsistent generation, that means dependent on environmental conditions: due to this characteristic, the value of the capacity factor is lower compared to the centralized production of traditional plants; in the case of natural gas-fired power plants, the CF is around 56% while for nuclear power plants, the highest value recorded is equal to 92% [50].
Technological advancement has therefore allowed the wider diffusion of renewable technologies, which present, as previously stated, several advantages such as the reduction of pollutants emitted into the atmosphere, the reduction of dependence on countries with large deposits of fossil fuels and at the same time a reduction in energy prices. All these advantages are however limited by the randomness of the primary sources of renewable energy (sun, wind, tides); for these reasons, an efficient and accessible storage system is among the priorities and for this purpose,

lithium-ion batteries prove to be a key component [2]. The reason for the success of this storage technology will be explored in the following paragraphs.

1.2 Types of storage

Energy storage systems are of fundamental importance for the management of renewable resources which often have intermittent and unpredictable behavior. However, the use of renewable sources to replace fossil ones requires a change of mentality by the population and greater research and technological adaptation by energy producers.
Often the moments of maximum production of electrical and thermal energy do not coincide with those of maximum demand: for example, the production of domestic hot water in summer through the use of solar collectors; as for electricity, an example can be the maximum production through photovoltaic panels at noon and in the afternoon hours, but the total absence of coverage in the evening when there is a need to turn on the light or other appliances. Storage systems are also of fundamental importance for reducing the price of energy. Without storage, the energy produced by power plants must always be equal to the energy consumed [8]; the power plant must therefore be sized to cover the needs of all those who are connected, even in times of high demand. This therefore presupposes that the plant works at partial load during phases of lower demand (reducing efficiency) to cover the hours of maximum demand; the use of storage systems instead allows to reduce the maximum power of the plant since part of the demand will be covered by the energy accumulated previously during periods of lower request.
There are different types of energy storage for electrical energy: in fact, it can be stored in mechanical or chemical form. As for storage in the form of mechanical energy, we have:

- **Hydro-pumped storage**: during the night, when the demand for electricity is low, water is pumped and stored from a lower elevation area to a higher one (storage of potential energy). During the day, the water is allowed to expand again in the turbine to produce energy and cover peak demand times
- **Compressed air energy storage**: During periods of low demand, using excess electrical energy, air is compressed inside large underground tanks. During periods of maximum demand, the air is allowed to expand in a turbine to produce electricity
- **Gravity energy storage**: This involves storing energy in the form of gravitational potential energy by lifting weights using electric motors powered by a surplus of electrical current; the weights are then dropped and during the

fall they drag the electric motor which therefore works as a generator [49]

- **Flywheel energy storage**: A large rotating mass is set in motion by an electric motor to which it is axially connected. Once set in motion, it stores energy ($E = \frac{1}{2}I\omega^2$) which is then able to transfer back to the motor while operating as a generator [32]

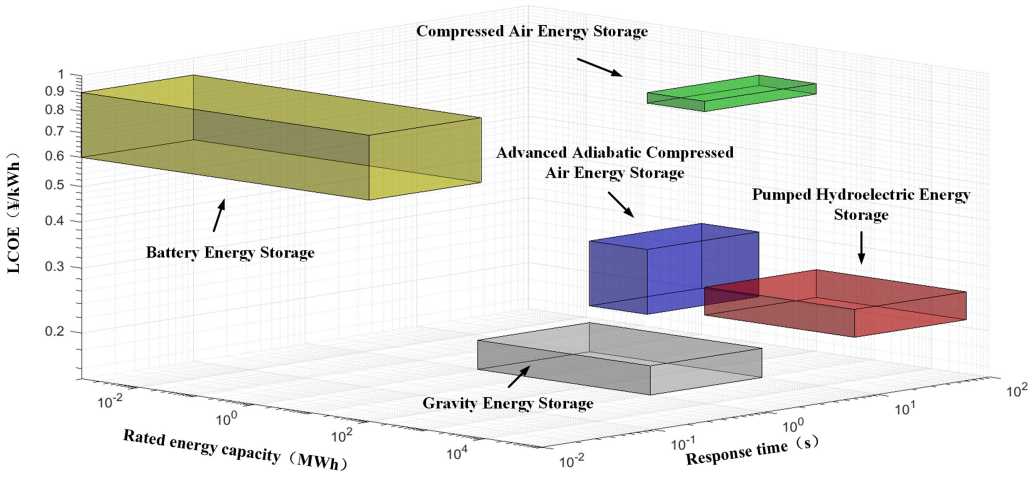

Figure 7: Comparison of different energy storage technologies[49]

As shown in Figure 7, the Levelized Cost Of Electricity is significantly higher for batteries compared to mechanical storage; for this reason, the latter is preferred for large energy systems such as power plants. Furthermore, all mechanical storage systems, with the exception of the Flywheel, are used only in stationary applications and for this reason cannot be used as a power system for cars. In table 1, is shown a comparison between every storage system in terms of their most important characteristics to better understand their range of implementation.

	Hydro-pumped	CAES	Flywheel	Li-ion
Energy Capacity [MWh]	100-20000	580-2860	0,0052-5	0-10
Power Rating [MW]	1-5000	100-1000	0,1-20	0-100
Specific Energy [Wh/kg]	100-400	30-60	5-100	80-200
Energy Efficiency [%]	65-85	40-70	85-95	75-97
Lifetime [years]	30-60	20-40	15-20	5-15
Energy Cost [$/KWh]	5-100	2-120	3000-6000	900-1300

Table 1: Comparison between most common electrical energy storage systems[5][40]

Lithium-ion batteries are therefore at a disadvantage compared to stationary storage systems such as Hydro-pumped and CAES, however, the latter are only to be used for stationary applications. For mobile storage, such as transportation or for electronic devices like computers and smartphones, batteries are the most widespread solution, especially thanks to their high energy density. However, there are exceptions where batteries are used also for big stationary storage systems, such as the Vistra's Moss Landing energy storage facility: it is the world's largest lithium-ion battery-based storage system, with a peak power of 750 MW and a storage capacity of 3000 MWh [51]. This storage system, however, is still incomparable with the largest hydro pumping storage system, located in Virginia (USA): the Bath County Pumped Storage System. Operational since 1985, it can generate a net power of 3000 MW and a capacity of 24000 MWh, with an efficiency equal to 79% [8][11].
About electrochemical storage, the cells are divided based on how the reactants are consumed for the production of electricity, in particular:

- **Primary Cells**: the reactants are consumed during discharge, generating electric current. The reaction is not reversible and they cannot be recharged, such as alkaline batteries.
- **Secondary cells**: the reactants are consumed during discharge but can be reconstituted during the charging phase, like Lithium-ion and NiMH batteries.
- **Flow Batteries**: two tanks contain electrolytic substances in liquid form in which elements with different oxidation states are dissolved, the most used technology is Vanadium Redox Flow Battery (VRFB). The Vanadium ions dissolved in the electrolytic substance contained in the two tanks are made to circulate in the two half-cells (where the oxidation and reduction reactions take place). Each half-cell includes an electrode, on which the redox species react generating a flow of electrons that can flow through the collector; the two half-cells are separated by an ion exchange membrane. Figure 8 on the left shows a functional scheme [52].
- **Fuel Cells**: reagents, usually gaseous, are sent to react on the anode and on the cathode in presence of a catalytic layer (e.g. Platinum). The two electrodes are separated by a membrane for the passage of ions consisting of an electrolytic material (e.g. Nafion). They can work at low and high temperatures (60-800°C) depending on the characteristics required by the application [43].

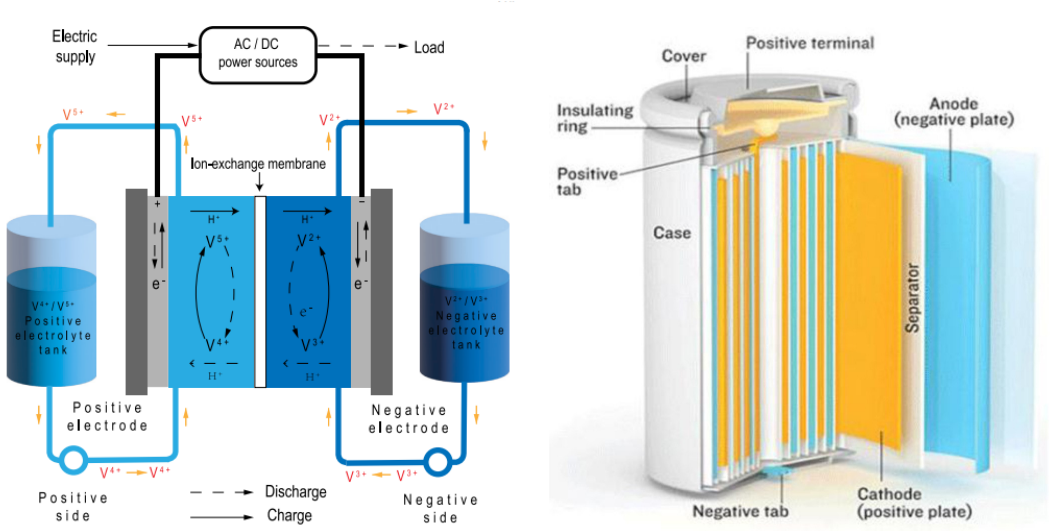

Figure 8: Vanadium Redox Flow Battery (left) [52] and Lithium Ions Battery (right) [61]

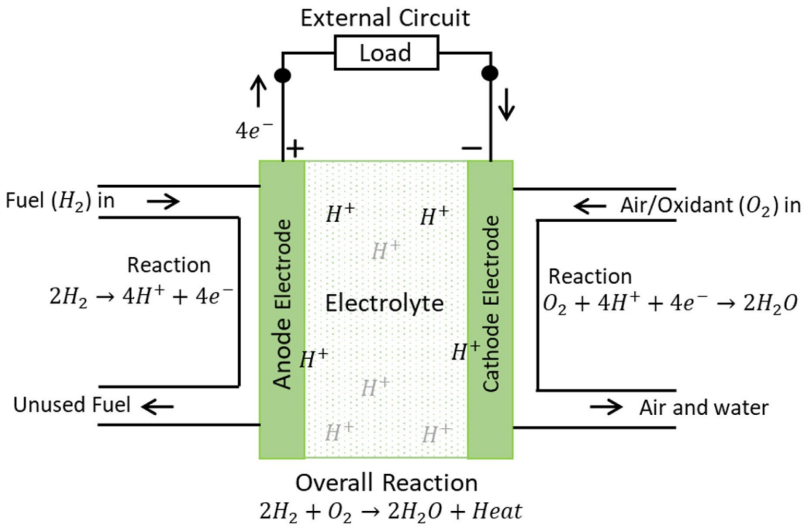

Figure 9: Hydrogen Fuell Cell scheme [24]

The main difference between flow batteries and lithium-ions batteries lies in the capacity: the amount of energy stored within a flow battery depends on the amount of electrolytic substances accumulated in the reservoirs; during the discharge phase, the concentration of ions decreases until the reaction stops. The recharging phase can be carried out either by replacing the electrolyte reservoirs (fast charging) or by conventional recharging. In the case of lithium-ions batteries, on the other hand, the capacity depends on the amount of reactive material

used in the manufacture of the anode and cathode; moreover, recharging can only be performed using the traditional method, as it is not possible to replace the reagents inside the battery. Nevertheless, compared to lithium-ions batteries, VRFBs have lower energy density, lower round-trip efficiency, higher toxicity of vanadium oxides and risk of precipitation within the electrolyte [52]. They do, however, have advantages over lithium-ions batteries such as a longer service life, no self-discharge and a depth of discharge equal to 100% [53]. For what concerns Fuel Cells, the diagram of which is shown in figure 9, they are closer to flow batteries than to traditional batteries. In fact, the amount of energy stored depends on the size of the tanks in which the reactants are stored, and the power output is a function of the fuel flow rate that is sent to the electrodes; furthermore, recharging can only be done by replacing the fuel tanks, conceptually similar to refuelling. Among the main obstacles to their deployment is the method of storing reagents, in particular hydrogen. Hydrogen can be stored at high pressure (700 bar), in liquid form at a temperature of 21 K or through adsorption and absorption processes in solid matrices such as zeolite or metal hydrides; however, these processes require large amounts of energy and are still difficult to implement [43].

1.3 Working principle of batteries

The storage of electrical energy within an electrochemical cell is based on redox reactions that take place between the anode and cathode. At the anode, the oxidation reaction takes place (transfer of electrons) while at the cathode, the reduction reaction takes place (reception of electrons). In the case of a general electrochemical reaction, two metals are brought into contact by immersing them in an electrolyte solution: due to the different electropositivity of the two metals, electrons and cations are released from the more electropositive metal, i.e. more prone to release electrons; the electrons find a point of passage in an external circuit while the released ions pass through the electrolyte.
The first electrolytic cell was invented by Luigi Galvani and for this reason is also called the galvanic cell. Later, others created new types of electrochemical cells, an example is the Daniell cell whose two half-reduction reactions are:

$$Anode : Zn \rightarrow Zn^{2+} + 2e^{-} \tag{1}$$

$$Cathode : Cu^{2+} + 2e^{-} \rightarrow Cu \tag{2}$$

For Lithium-ion technology, the principle remains the same but the reagents involved change as the anode and cathode materials change. The Lithium-Cobalt Oxide cell will be taken into consideration for the half-reactions, as it was the first cell put on the market in 1991 [61].

$$Anode : LiC_6 \rightarrow Li^{+} + e^{-} + 6C \tag{3}$$

$$Cathode : CoO_2 + Li^{+} + e^{-} \rightarrow LiCoO2 \tag{4}$$

The four basic components of a Lithium-ions battery are the cathode, anode, electrolyte and separator. During the charging phase, the Lithium ions move from cathode, passing through the electrolyte, to anode and move back during discharge. Current commercial battery technologies are named after the Lithium donor in the cathode. Pure lithium metal is extremely reactive, which is why it cannot be used directly as an ion donor, but is often used in the form of a metal oxide: this makes it more chemically stable, but results in a loss of electrical conductivity and thus an increase in electrode impedance. In order to increase the conductive properties of the cathode, lithium oxide is reduced to a very fine powder and dissolved in a conductive carbon-based material through a solvent

and then a binder. For the anode, the most commonly used material is graphite, which is characterized by a low cost and a structure which facilitates the exchange of lithium ions, leading to a good capacity density [55]; the process is similar to that of the cathode, but in this case the collector, which in the previous case was aluminium, is copper. Aluminium and copper are the two most suitable materials to perform the function of current collector: they have high electrical and thermal conductivity, and, once transformed into thin foils, are able to facilitate the passage of electrons and in addition ensure heat exchange to dissipate energy due to oxidation-reduction reactions.
The electrolyte is positioned between the anode and cathode and allows the ions to pass through and it consists of a mixture of lithium salts and organic solvents. The organic solvent is of vital importance as it promotes the passage of lithium ions: an example of a solvent is dimethylethylcarbonate $(C_3H_6O_3)$. The electrolyte is not chemically stable due to a passivation phenomenon, that is a chemical phenomenon due to which a protective layer forms on the anode called Solid Electrolyte Interface (SEI). This layer separates the anode from the electrolyte but still allows the ions to pass through; this protective film stabilises the system at the expense of a reduction in the battery's capacity, but increases its lifespan. The same phenomenon also occurs at the contact point between cathode and anode [19].
To avoid direct contact between anode and cathode, resulting in a short circuit and destruction of the cell, a separator is placed between the two electrodes; the most common materials for the separator are Polyethylene and Polypropylene. A fundamental property of the separator is to allow the passage of ions into the electrolyte while ensuring the physical separation of the two electrodes. Although the separator does not have an active role within the battery, characteristics such as porosity, pore size, mechanical strength and thermal stability influence the life and safety of batteries. Charging/discharging processes can lead to the formation of lithium dendrites, which can perforate the separator, leading to direct contact between anode and cathode; in addition, mechanical, thermal and electrical abuse can affect the strength of the separator, leading to failure. The main characteristics requested to the separator are, in general: stability, thickness, porosity and tortuosity. The thickness of the separator must be sufficient to withstand the stresses to which the cell will be subjected during its life cycle. The typical thickness for consumer electronics is 25 μm; below 20 μm, ionic conductivity increases but at the expense of resistance. Porosity, on the other hand, is defined as the amount of empty space within the material: high porosity facilitates ion transport by increasing the conductivity of the electrolyte, while low porosity presents the risk of

pore clogging, but in favour of greater mechanical resistance; the recommended porosity for commercial batteries is 40 %. Tortuosity, on the other hand, represents the difficulty of the path that the ions must follow: higher tortuosity may limit dendritic formations, but reduce ion conduction and mass transport. Another fundamental parameter of the separator is the mechanical resistance: this component must be able to withstand stress to ensure the safety of the battery. Tensile strength measures the effort required to break the separator, in general for commercial applications, a minimum strength of 100 Mpa is guaranteed; puncture resistance, on the other hand, is defined as the maximum load for a needle capable of puncturing the separator: for commercial applications, a minimum load of 300 g is guaranteed [34]. Finally, after the production phase, batteries are subjected to a process with the aim of pre-ageing them: a charging current is slowly injected to allow the formation of the SEI to protect the anode; at the same time, battery are tested to find any abnormal cells to be removed to avoid risks for safety [55].
To understand how batteries work, it is necessary to know some basic parameters:

- Roundtrip efficiency (η): is the ratio between the energy spent to recharge and that obtained during the discharge phase

- State of charge (SOC): percentage of the amount of energy stored compared to the maximum amount of energy that can be stored [8]

$$SOC(t) = SOC(t_0) + \int_{t_0}^{t} \frac{I_{bat}}{C_{bat}}\, dt \tag{5}$$

- State of Health: actual capacity divided by initial capacity [48]

$$SOH = \frac{Capacity}{Capacity_{Initial}} \tag{6}$$

- Depth of discharge (DOD): the complementary of the state of charge [8]

$$DOD(t) = 1 - SOC(t) \tag{7}$$

- Ideal Capacity: is the maximum charge quantity according to the reagents contained in the battery, it is expressed in Ah.

- Real Capacity: is the capacity the cell is capable of delivering during dis-

charge up to the cut-off voltage[1]

$$Q_r = \int_0^t I_{cell}\, dt \tag{8}$$

The actual capacity of the battery is also a function of environmental conditions such as temperature, and decreases both as the cell ages and as the discharge current increases [48]

- C-rate: discharge current expressed as a function of nominal capacity. It corresponds to the value of the (constant) current that would discharge the cell in a certain number of hours divided by the total capacity of the battery
- Theoretical energy: product of theoretical capacity and open circuit voltage V_{oc}
- Real energy: value measured during the entire discharge process, also depends on environmental parameters such as temperature

$$W_r = \int_0^t V_{cell} I_{cell}\, dt \tag{9}$$

In order to study the cell voltage, it is necessary to elaborate on certain parameters; in (3) the reaction occurring at the anode is given, and in (4) that of the cathode of a generic Lithium-ions cell. During the charge and discharge phases, the potential of the two electrodes changes over time, and the potential difference (Voltage) of the cell also changes. When the cell is not connected to any electrical load, i.e. is not supplying or drawing current, it has a voltage called Open Circuit Voltage (OCV). This is the maximum potential difference at which the cell is at equilibrium. This voltage is defined as:

$$U_{oc} = E_{cathode} - E_{anode} \tag{10}$$

The potentials of the two electrodes can be calculated via the Nernst equation:

$$E = \frac{-\Delta G_{reaction}(T, P_0)}{ZF} + \frac{RT}{ZF} ln(\frac{\prod_{n=1}^{N} C_r^n}{\prod_{n=1}^{N} C_p^n}) \tag{11}$$

where:
$\Delta G_{reaction}$ = Gibbs free energy of the semi-reaction
Z = number of electrons exchanged in the semi-reaction

[1]Cut-off voltage: minimum cell voltage value below which the cell must not continue the discharge process in order to avoid cell damage

$F = 96485\ Cmol^{-1}$ Faraday's constant
$R = 8,314\ JK^{-1}mol^{-1}$ Universal Gas constant
$C_r = mol/m^3$ concentration of reagents
$C_p = mol/m^3$ concentration of products

The Nernst equation is useful for calculating the potential gradient within the cell under equilibrium conditions, without transport phenomena [43].
Transport phenomena inside the cell are:

1. Charge Transfer: due to activation of electrochemical potential (oxidation and reduction processes)
2. Charge Migration: due to migration of ions and electrons
3. Mass transport: diffusion of molecules inside the electrodes

Transport phenomena are responsible for overvoltages, i.e. voltage gradients that change the value of the potential difference of the cell with respect to the open circuit voltage, these are: Activation overvoltage (η_{act}), Ohmic overvoltage (η_{ohm}) and Diffusion overvoltage (η_{diff}). The cell voltage under operating conditions can be expressed as follows:

$$V_c = OCV - [\eta_{act} + \eta_{ohm} + \eta_{diff}] \tag{12}$$

Equation 12 therefore shows that the operating voltage is reduced by voltage drops due to transport phenomena during the discharge phase. Activation overvoltage is related to the kinetics of charge transfer, and, in general, this process is favoured as the temperature increases, so at higher temperatures activation reactions are stimulated, reducing the voltage drop [43]. The voltage drop due to the activation of electrochemical phenomena is present at both the cathode and anode, as these are the places where oxidation and reduction half-reactions occur.
Ohmic overvoltage, on the other hand, is related to charge migration (electrons and ions); it is linked to both the passage of electrons through the circuit outside the cell, and the passage of ions in the electrolyte solution, and can be expressed as:

$$\eta_{ohm} = RI = \rho\frac{l}{s}is \tag{13}$$

where:
$\rho[\Omega m]$ =resistivity
$l[m]$ =length of conductor

$s[m^2]$ =active surface
$i[A/m^2]$ =specific current

The ohmic voltage drop therefore depends on the properties of the material that allows ions and electrons to pass through; in general, ionic conductivity ($\sigma_{ion}[1/\Omega m] = 1/\rho$) increases with increasing temperature, while electrical conductivity decreases with increasing temperature, but overall, the increase in ionic conductivity is more influential, so a higher temperature favours charge transport phenomena [43].
Finally, diffusion (or concentration) overvoltage is related to mass transport phenomena, i.e. diffusion phenomena within the electrodes, and is a phenomenon that especially affects open cells such as fuel cells but also electrochemical cells in general. For high current values, molecular diffusion is not fast enough to sustain the reaction, causing the cell voltage to drop. It occurs when the discharge reaction is fast enough to generate a reduction in the surface concentration of the charge carriers on the electrode; this generates a limiting factor to the continuation of the reaction, related to the ability of the reactant to diffuse on the electrode surface [43]. In figure 10 is reported the discharge phase (at constant current) of one of the 18650 batteries used in the experimental section.

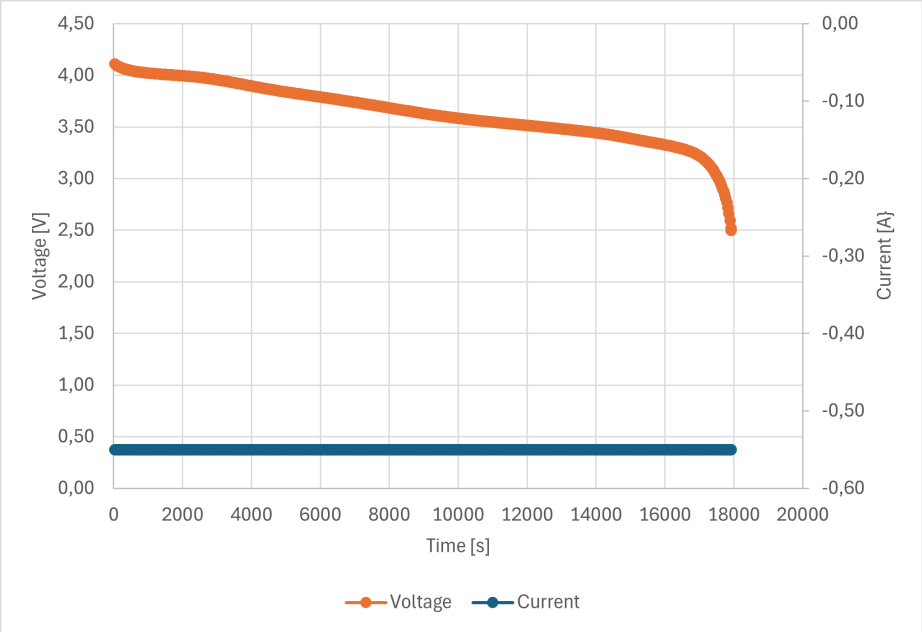

Figure 10: Discharge curve of 18650 Lithium-ion battery with 2850 mAh capacity used in the experimental section

In general, a single electrochemical cell is not able to meet the storage needs,

unless it is for small consumer electronics. For larger systems, individual cells must be assembled to increase power and capacity. When one or more cells are placed in series, the total voltage is the sum of the voltages of the individual cells: this is necessary to increase the supply voltage when the required voltage level is higher than that of the individual cell. On the other hand, by placing the cells in parallel with each other, the voltage at the ends remains the same, but the total current flowing out of the two nodes increases, which helps to increase the capacity. A Battery Management System (BMS) is required to manage the discharge and charge phases and monitor the health of a battery pack. The BMS checks the battery pack by means of sensors, monitoring its operating parameters, such as voltage, state of charge and temperature, and intervenes in the event of anomalies; it becomes crucial when several individual cells are connected to form a battery pack. As cycles of use pass, batteries respond differently to stress and charge/discharge processes and deteriorate differently from one to another. After several cycles, the gap in capacity can become considerable, even if the cells initially had very similar characteristics; without the BMS monitoring the processes, the pack may have cells at the limit of overcharging together with partially discharged cells during the charge phase, while during discharge there may be cells close to the cut-off voltage while others can still supply energy, as shown in the figure 11. This phenomenon prevents the full utilisation of cell capacity, increasing the charging cycles of the battery pack and shortening its service life [48].

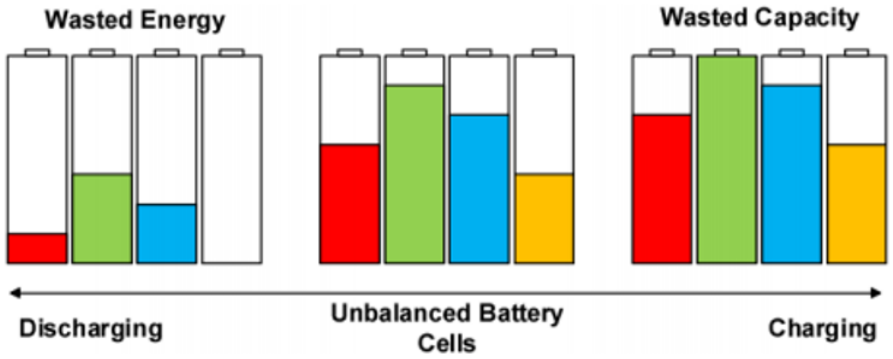

Figure 11: Effects of unbalanced cells during charge/discharge[48]

In order to optimise the operation of the battery pack and thus increase its efficiency and lifetime, the BMS must be used to monitor its parameters, one of which is the State of Charge (SOC). SOC represents the amount of energy present inside the cell compared to the maximum amount that can be stored, as shown

in the equation 5. Among the most widely used methods for measuring the state of charge are direct methods, based on the physical properties of the cells; these methods are based on measurement of Open Circuit Voltage (OCV), Internal Resistance (IR), Impedance Spectroscopy (IS) and Electromotive Force (EMF) [3]. OCV method measures the open-circuit voltage after a period of battery rest, to allow the reactants within the cell to return to equilibrium; it is a simple and accurate method but requires the cell to be rested before measurement is performed. Another method is to measure the Electromotive Force (EMF), which is the voltage in the battery under open circuit conditions when the reactants are in equilibrium. Determining the SOC of the cell is possible by measuring its internal resistance by taking voltage and current measurements during charge/discharge: this resistance is also called DC resistance. Generally speaking, internal resistance values are very low and therefore difficult to measure, which is why it is hardly implemented. Finally, the Impedance Spectroscopy method requires the application of currents at different frequencies to the battery terminals in order to determine the impedance; this impedance is then put on a graph together with the SOC [3].

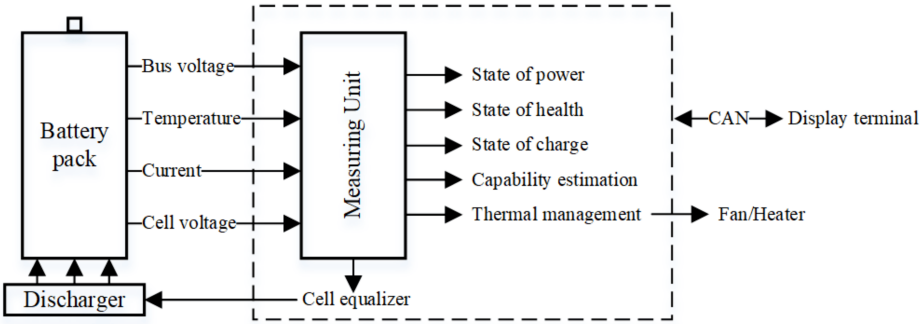

Figure 12: Scheme of BMS working principle[3]

As shown in figure 12, the BMS also monitors the cell temperature to perform thermal management: this process is of fundamental importance for the safe management of the battery pack and to avoid irreversible and dangerous phenomena such as thermal runaway. The BMS monitors the temperature of the cells through a probe and if one or more batteries reach too high temperatures, it activates the cooling system, which can be forced convection air (fans) or natural convection air or liquid. Temperature control is carried out not only for overheating, but also in the case of low temperatures; as mentioned above, the cell temperature influences the parameters that characterise its discharge and charge. For example, a very low temperature decreases the open circuit voltage and at the same time reduces the ionic conductivity (σ_{ion}) [43]. For this reason, the BMS also heats the batteries

by means of electrical resistance to keep them in optimal condition and, in the case of electric vehicles, carries out pre-heating before the charging phase to increase the efficiency of the process and, above all, preserve battery life. Charging or discharging batteries in very cold environments can considerably reduce their life, even if the current is in an acceptable range (1C[2]) and can be more damaging than higher discharge values (16C) at room temperature, as shown in figure 13 [16].

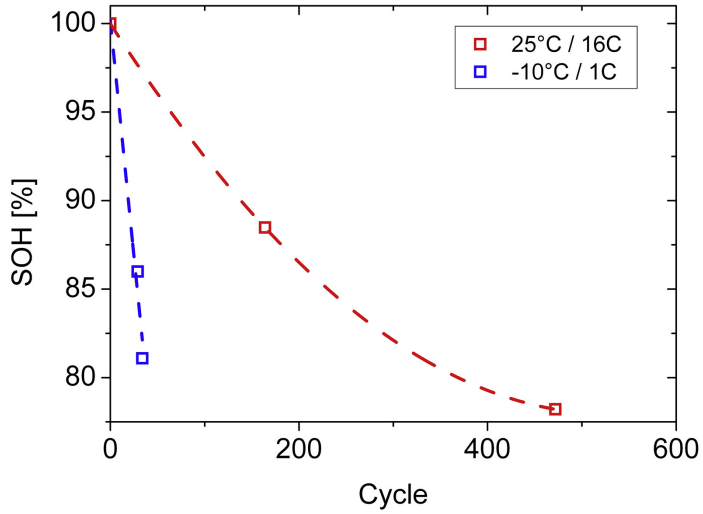

Figure 13: Effect of temperature on ageing of a 18650 Lithium-ion cell [16]

A study [16] shows that a cell working at -10 °C reaches 80% of its initial capacity almost immediately, while the same cell working at room temperature reaches the same SOH in more cycles but working at its maximum discharge current. For this reason, the intervention of the BMS becomes of crucial importance both in overtemperature conditions to avoid thermal runaway, and in very low temperature conditions to preserve the life of the battery pack.

[2] 1C: the C-rate at which the battery is discharged or charged. For example, a C-rate of 1C means that a 10 Ah battery is discharged with a current of 10A

1.4 Comparison of electrochemical storage technologies

In this section, the most widespread electrochemical storage technologies will be compared, with a focus on technologies implemented in e-mobility. Characteristics such as power density, specific energy, cost and safety are of fundamental importance for a storage system, particularly in the field of mobility. For a long time, the direct competitor of LIBs were Lead-Acid batteries, and it was thanks to these that the spread of electric vehicles began in the early 1900s: they were powered by Lead-Acid batteries with a range of around 80 km; when full discharge had been reached, the vehicle would stop for cell replacement, and then resume its journey. By the beginning of the 20th century, twice as many electric vehicles were sold in the United States as those powered by petrol [48], but were replaced by cars with internal combustion engines by the First World War, due to their high cost and low range, but sacrificing advantages such as quietness, less vibration during driving and the absence of exhaust fumes. The need for alternative energy production systems has brought the need for an effective storage system back to the surface. A new era for lithium-ion batteries has begun, thanks mainly to an increase in storage capacity and a decrease in the cost of the technology [26].
Lithium is an excellent material for use in batteries due to its light weight and high electropositivity, but, as stated earlier, due to its high reactivity it cannot be used directly for the manufacture of the cathode. This is why it is used in its oxidised state, and some examples of oxides through which it is used in batteries are:

- LCO ($LiCoO_2$)
- LMO ($LiMn_2O_4$)
- LFP ($LiFePO_4$)
- NCA ($LiNiCoAlO_2$)
- NMC ($LiNiMnCoO_2$)

In figure 14 spider charts are collected for the most popular LIBs technologies: these charts allow us to understand the strengths and weaknesses of each technology, to find the most suitable one for the intended purpose. In general, LIBs can be divided into power applications and energy applications: the former are used for purposes where high specific power needs to be delivered while sacrificing autonomy; for the latter, the application is more focused on storage, leaving out the maximum power that can be delivered. For full electric vehicles, for example,

high specific energy is required to maximise the vehicle's range while limiting its weight.

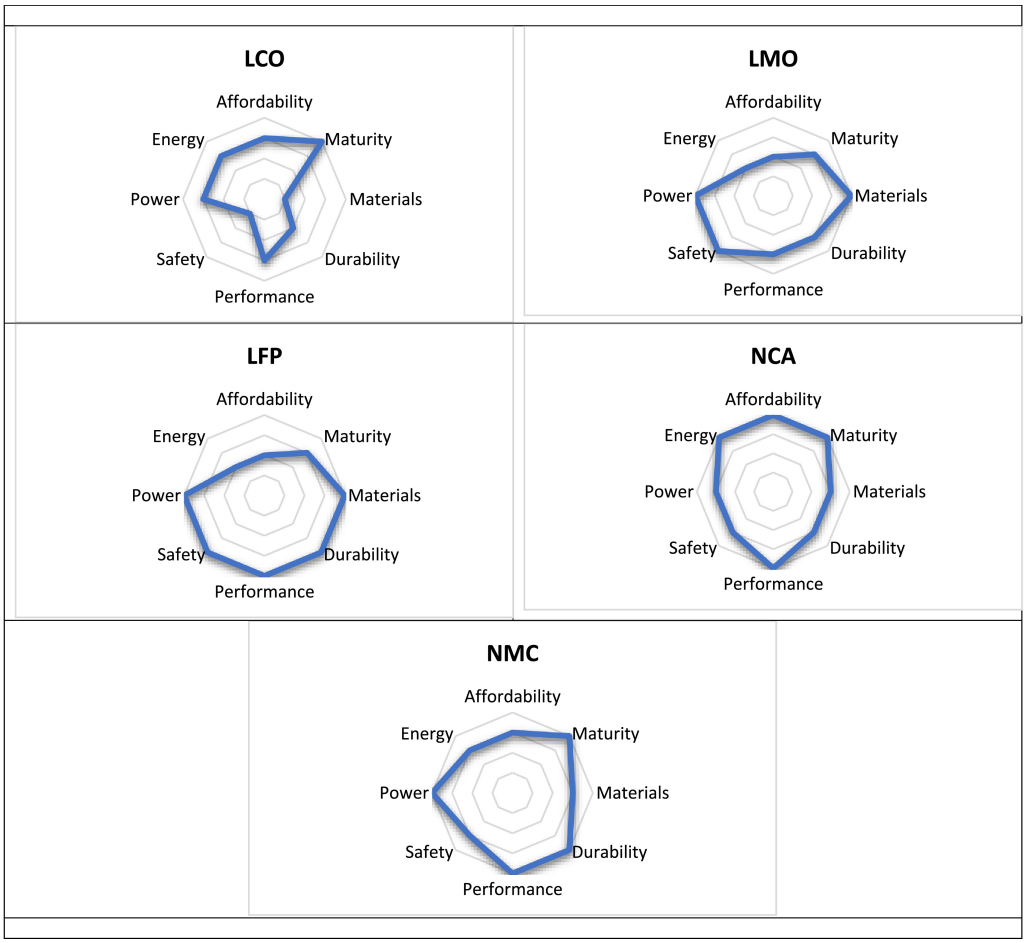

Figure 14: Different spider charts of LIB technologies[60]

LCO Technology was the first to be commercialised in 1991[61], and has long been used in portable electronics such as smartphones and tablets. The specific energy for this technology is between 150-220 Wh/kg [60]. One problem with this technology is the use of Cobalt: in 2020, 68% of Cobalt was mined in the Democratic Republic of Congo, which has long been characterised by high political instability; to combat this problem, car manufacturers are shifting research to lithium storage technologies that are less dependent on Cobalt, such as Volkswagen or Tesla. The latter has stated that more than half of its current car production is based on Cobalt-free technologies such as LFP batteries [44].
In contrast, LMO technology is Cobalt-free and provides a high level of safety, but is characterised by a lower specific energy value (100-140 Wh/kg). This technology

has a limited market share and is therefore characterised by higher prices. LFP, on the other hand, are among the most popular technologies: they are characterised by high safety, specific power and durability. NCA and NMC cells contain Cobalt, but in smaller quantities than LCO batteries, and provide a higher safety level. They are characterised by high specific power and energy, which is the reason why they are among the batteries used, along with LFP batteries, in the automotive industry: manufacturers such as Tesla, BMW, BYD, Volkswagen, Nissan and others have been using NCA and NMC cells over the last decade, contributing to their increased popularity and thus reducing their price by almost 90% over the last ten years [26].

Lithium-ions batteries are produced in 3 different configurations: cylindrical, prismatic and pouch. Cylindrical batteries are the most popular for the automotive market due to their compactness and mechanical strength, which are necessary for this type of application. Most of these cells are produced in the 18650 format (18 mm in diameter and 65 mm in length) and 21700 format (21 mm in diameter and 70 mm in length); the 21700 are therefore larger than the 18650, which translates into a higher capacity but also a worse heat exchange capability. Cylindrical batteries are connected together to form battery packs: when this happens, a space is formed between each cell for cooling during discharging and recharging, in which air can be forced in to remove heat or provide it for pre-heating the cells a few minutes before recharging, increasing the efficiency of the process.

Prismatic cells have an iron or aluminium case that contributes to their strength, and thermal management is facilitated by their square shape. Their capacity may vary according to size, but they are characterised by a higher cost than cylindrical cells.

Finally, the pouch configuration differs from prismatic cells in the material of the external case: instead of aluminium, a lighter but less resistant material such as a polymer is used. These cells are widely used as storage systems for mobile devices such as smartphones and laptops due to their low weight and ability to adapt to the shape of the device that holds them. However, a dangerous phenomenon often occurs at the end of their life: due to the deterioration of the electrolyte and thermal and electrical abuse, the cell swells. To minimise the risk of this phenomenon, these batteries are recommended for low-intensity use and several smartphone manufacturers adopt slow charging practices (when fast charging is not required) to slow cell deterioration and increase safety during the life of the device [60]. In figure 15 are reported some examples.

Figure 15: 18650 cylindrical cell (left) prismatic cell (right) [13]

In figure 16, the main electrochemical storage technologies employed today in various application fields are compared. As can be seen, LIBs rank best both in terms of specific energy and energy density compared to competing technologies. However, Lead-acid batteries are still in use today, for example as starter batteries for cars with internal combustion engines; while Ni-MH batteries are rechargeable batteries that are used in low-energy electronic devices such as remote controls and small household appliances. Lithium batteries can replace lead-acid batteries in the automotive sector, but despite their advantages, in some situations, Lead-Acid are still employed; the reason for this is the large price difference between the two technologies. A 12 V battery with a capacity of 50 Ah and a maximum discharge current of 470 A is required to start and operate the services of a small internal combustion engine car; a lead-acid battery with these characteristics can be purchased in a spare parts shop for around 70 euros. If the car is used continuously and therefore the state of charge is maintained above 80 per cent, the estimated life of the battery is around 4 to 5 years [23]. Replacing this system with a Lithium-ions battery presents a higher initial investment accompanied by advantages that are not being exploited, such as the greater depth of discharge that can be achieved and the longer lifespan. This situation makes easier and cheaper to replace the Lead-acid battery every 4-5 years rather than installing a Lithium-Ion battery for the starter motor; in the end, for simple problems is sometimes better to adopt simple solutions.

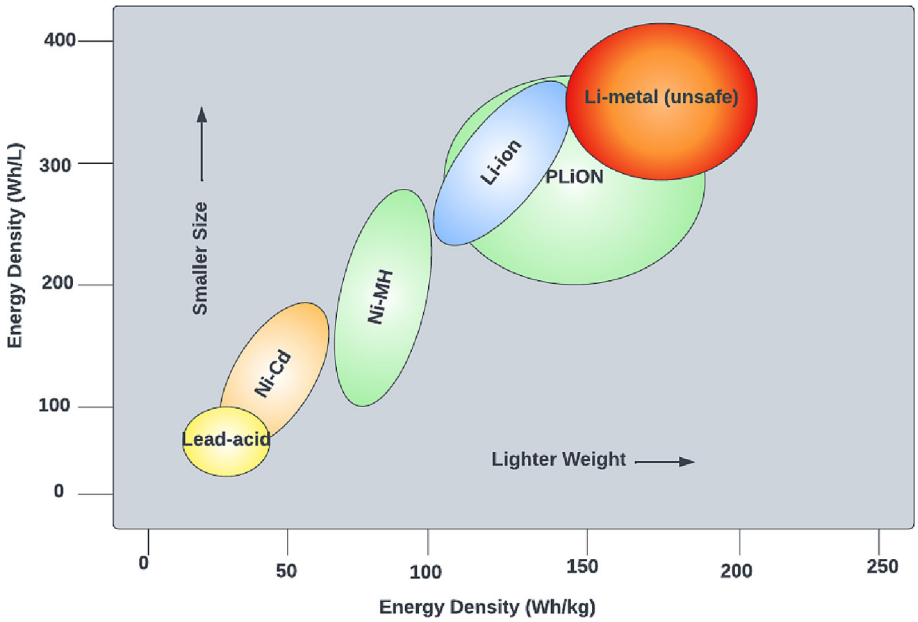

Figure 16: Comparison of different electrochemical storage systems[26]

For stationary storage, Lithium-ions batteries offer greater flexibility and specifications to better meet consumers' needs compared to Lead-Acid technology. One of the advantages lies in the variety of LIB technologies: each of them differs in terms of power and specific energy, cost and degree of safety, offering consumers a specific solution for their requirements. In the case of storage for domestic photovoltaic generation, individual cylindrical cells can be combined to form battery packs of a specific size in terms of storage capacity and specific power; achieving this level of adaptability with Lead-acid storage systems is more difficult and specific solutions can increase the costs of the system [23]. And, in this case, the above mentioned advantages of Lithium-Ions batteries can be exploited and thus justify the higher initial investment compared to that of Lead-Acid batteries.
Another method for comparing lead-acid and Lithium-ions technology is the environmental impact of their use, specifically, as a stationary grid energy storage system. The effect that a process or activity has on the environment due to the consumption of energy and materials is analysed through an objective procedure called Life Cycle Assessment (LCA); the evaluation includes the energy and materials consumed and the waste released into the environment [42]. The purpose of the LCA is to find a way to improve performances of products and activities in their whole life cycle. Life cycle assessment is divided into several phases and, in the case of batteries, includes the extraction of raw materials for the manufacture of the cells, e.g. Lead, Manganese, Aluminium, Nickel, and the manufacturing and

assembly processes of the battery packs; it then leads to the consumer use phase and concludes with the end of life phase, which includes the disposal and eventual recovery of materials. Each of these processes has an impact on the surrounding environment due to, for example, the consumption of electricity or fuel to power the machinery for extracting and processing materials and transporting the processed elements; at the same time it generates waste material flows that can be harmful to humans, such as processing waste and greenhouse gases produced by fuel consumption. The impacts of these processes are analysed in a comparative LCA, with the aim of identifying the technology with the lowest environmental impact for the same functional unit produced: the functional unit is a standardisation parameter used to compare the final results of the study and provides criterion against which inputs and outputs are normalised [42]. Processes are associated with impact categories for the same functional unit; impact categories are negative effects on people and the environment, e.g. water acidification potential and global warming, expressed as tonnes of CO_2 equivalent. At the end of the analysis, the process with the lower impact in each impact category is considered the best one. In the case of stationary battery storage, one study selected, as the functional unit, the kWh of energy delivered during the battery lifetime (kWh_D) [56]. The storage system is assumed to operate for a period of 20 years in stand-by mode, this means it only intervenes in case of a lack of supply from the electricity grid. Energy density and lifetime values of different battery energy storage are given in table 2

Battery type	**Energy density [kg/kWh]**	**Lifetime [years]**
LFP	9.1	15
NMC	7.1	20
NCA	4.8	20
Lead-Acid	37.2	8.5

Table 2: Battery characteristics for the study [56]

Concerning the impact categories, the study [56] provides: climate change (kg of CO_{2eq}), acidification potential, fossil resource use (MJ), minerals and metals use (kg of Sb_{eq}[3]). The data obtained from the study proves that the impact of lead-acid batteries for the impact categories is, relative to 1 kWh of stored energy:

- 2 kg of CO_{2eq}
- 33 MJ of fossil resource consume

[3]Abiotic depletion potential expressed as equivalent kg of Bismuth (Sb). Abiotic resources are nonliving natural substances

- $8 * 10^{-4}$ kg of Sb_{eq} for consume of minerals and metals
- 0.01 $molH+_{eq}$ for acidification potential

In figure 17, results are collected for the respective impact categories compared to lead-acid batteries for which the impact is set to 100 %. The storage technologies that demonstrate significantly lower impact are NMC and NMA, for which impact values of less than 50% are obtained for climate change and fossil resource consume. For the consumption of mineral resources, on the other hand, excellent values are obtained for all lithium technologies, with impact reductions close to 90%, especially for the LFP technology; the only category in which there is a higher impact of Lithium technology with respect to Lead-Acid is acidification potential for LFP cells. Lead-acid batteries in general cause a greater impact due to lower energy density: in order to obtain the same amount of stored energy, more material has to be extracted and this leads to a greater consumption of resources both in terms of elements to be extracted and in terms of energy required for their extraction. For LIBs, on the other hand, the most impactful phase is the utilisation phase, related to climate change: the effect depends on the energy mix of the country where the electricity is produced, the higher the share of renewable energy, the lower the impact; for the manufacturing process, the extraction and processing of the minerals needed for the cathode cover a significant share. However, one phase of the life cycle where lead-acid has an advantage on LIBs is the end-of-life phase: thanks to the maturity of this technology, there are recycling strategies that allow greater recovery of raw materials and this translates into saved emissions in the production phase of new cells [56].

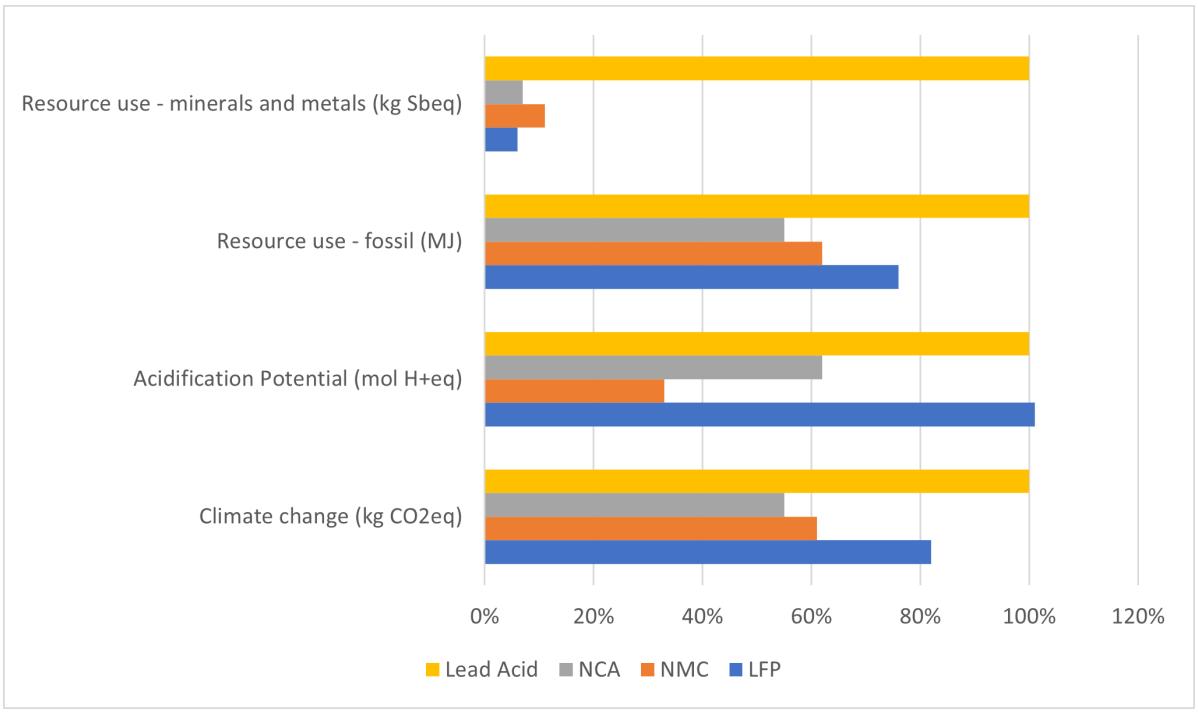

Figure 17: Results of LCA for each battery type compared to Lead-Acid [56]

1.5 Recycling and second-life

The production of LIBs involves the extraction of raw materials, such as Lithium and Cobalt, and their processing to produce the electrodes. These processes require the consumption of other raw materials such as oil and natural gas; at the same time, spent lithium-ions batteries are used by people for their own purposes and then disposed to occupy landfills. The recycling process of spent batteries must become a prerogative both to reduce the impact on the environment due to new material extraction processes and to preserve precious metals reserves by recovering those that have already been extracted. The recovery of precious metals not only has an environmental benefit, but also an economic advantage: to give an example, aluminium used as a current collector within the cathode is obtained mainly from a sedimentary rock called Bauxite. The processing of Bauxite to produce aluminium is called the Bayer process and requires the use of heat and steam both produced, locally, from fossil sources such as oil and natural gas [25]. The recovery and recycling process of aluminium can be carried out indefinitely, eliminating the extraction stage and, in this way, saving the energy used in such processes each time it is recycled. Aluminium is just one of the precious materials that compose Lithium-ion batteries, and considering that the equivalent of 1.2 million tonnes of LIBs were placed on the market in 2019, their recovery becomes more important every year [30].
The recovery of LIBs is a process still in the development phase and it is difficult to implement due to the different metals that are used to produce the cathode: on one hand the variety of technologies used for LIBs guarantees great flexibility of use and allows the creation of specific solutions, on the other hand it causes complications for the standardisation of recycling processes. Today, the most commonly used processes are:

- Hydrometallurgy
- Pyrometallurgy
- Biometallurgy
- Direct regeneration

Pyrometallurgy involves the use of high temperature furnaces for the recovery of precious metals. During this process, electrodes are exposed to temperatures higher than the melting temperatures of their component metals (>1000 °C), which transform into their liquid form. This is a very efficient process and is useful for

large-scale implementation, but it involves the loss of other components such as the electrolyte, which evaporates at those temperatures and cannot be recovered. Another advantage of this technique lies in the ability to recover precious metals from different cell technologies in the same furnace: this means a reduction of costs as a separation process based on cell chemistry is not required.
Hydrometallurgy does not require the use of high-temperature furnaces, but exploits a chemical process called leaching: this process involves the use of acid based substances to dissolve metals, which are then separated from the solution and recovered. This method has several advantages over pyrometallurgy, one in particular being the lower energy consumption as the process is maintained at a lower temperature (100 °C); lower temperatures makes it easier to implement waste heat recovery systems, which also leads to a reduction in greenhouse gases emitted into the atmosphere. The acids commonly used for the leaching process are HCl, H_2SO_4, HNO_3 and H_3PO_4; the use of these substances results in the production of environmentally harmful waste substances and gases such as SO_2, SO_3 and NO_x. The leaching process achieves a very high metal recovery efficiency, for example: for LCO technology, using hydrochloric acid (HCl) and hydrogen peroxide (H_2O_2) is obtained a recovery efficiency for Cobalt and Lithium of 99% [30]. Despite the high effectiveness of these inorganic acids, research is also moving towards less environmentally harmful organic acids, such as citric acid obtained from food waste; citric acid as a leaching agent can be obtained from citrus fruits waste such as oranges and lemons peels by means of a fermentation process. A study shows that the recovery efficiency of Lithium and Cobalt obtained by implementing citric acid as a leaching agent reached values of more than 90 % at 100 °C, and the cathode produced with the recovered Lithium and Cobalt used for a $LiCoO_2$ cell guarantees a discharge capacity close to the theoretical one of a newly manufactured cell (98 mAh/g) [10]. The use of organic acids obtained from food waste therefore leads to a reduction of the harmful gases produced by the use of inorganic acids for the leaching process, and, since it is originated by waste food, implies a reduction of process costs up to 69% [10].
An alternative to the two methods mentioned above, which are currently the most popular for large-scale recovery, is biometallurgy, which uses microorganisms such as bacteria and fungi to dissolve metal oxides; these adopt metabolic processes to release the metal ions and dissolve them in an aqueous solution to be subsequently separated through, for example, precipitation. One example is Aspergillus Niger, a fungus that by producing an acid is able to recover up to 100% of lithium from a spent battery; this is a completely natural process and therefore not harmful to

the environment. It is, however, a method still in the development phase, but one that has excellent prerequisites for future use [30].
Finally, direct regeneration involves repairing a spent cell by regenerating the degraded lithium within the cathode. During charge/discharge cycles, the availability of ions Li^+ decreases due to dendritic formations that reduce the amount of ions available to cross the electrolyte. One regeneration method consists of using a lithium salt that bonds with the degraded cathode, providing new ions available on the electrode surface. This is a low-cost process that allows the cell to be regenerated without starting over from individual elements, however, there are not yet prerequisites for its large-scale development. However, there is another way for batteries when they reach their end-of-life: instead of being disposed and recycled, they can be used as a stationary storage system. With the growing popularity of electric vehicles, the amount of batteries available for this phase is constantly increasing. Battery packs for automotive applications require a residual capacity of more than 80% of the initial capacity and self-discharge of less than 5% per day [14]. When battery packs are no longer able to meet these requirements due to ageing, batteries can be reused to store energy produced from renewable sources (solar and wind power) when production is higher than demand, or to assist distribution grid during peak phases, providing an economic advantage for both energy producers and consumers; in fact, it is estimated that the capacity generated by batteries removed from electric vehicles could exceed 200 GWh by 2030 [3]. At the moment, a lithium-ions battery storage system for domestic use with a capacity of 14 kWh and a power output of 5 kW is sold at a price of 7500 $; taking into consideration the use of second-life lithium-ions battery packs from an electric car, e.g. Tesla Model S with a residual capacity of about 80 %, we obtain a storage capacity of 80 kWh. The battery pack can be reconditioned to replace the most damaged cells, although it can be assumed that the overall condition is good as the cells are subjected to the same conditions of use and monitored by the car's control system during their lifetime. The average price for a reconditioned battery pack can be estimated at around 28$/kWh [46], in this way, the entire battery pack can be sold at around 2240$. It is, however, a reconditioned system so the cells need more control, but since it is a stationary application, all mechanical stresses due to rough terrain are eliminated; moreover, domestic applications are generally less challenging with respect to the one of transportation sector, for this reason the stresses to which the battery pack is subjected are easier to manage.

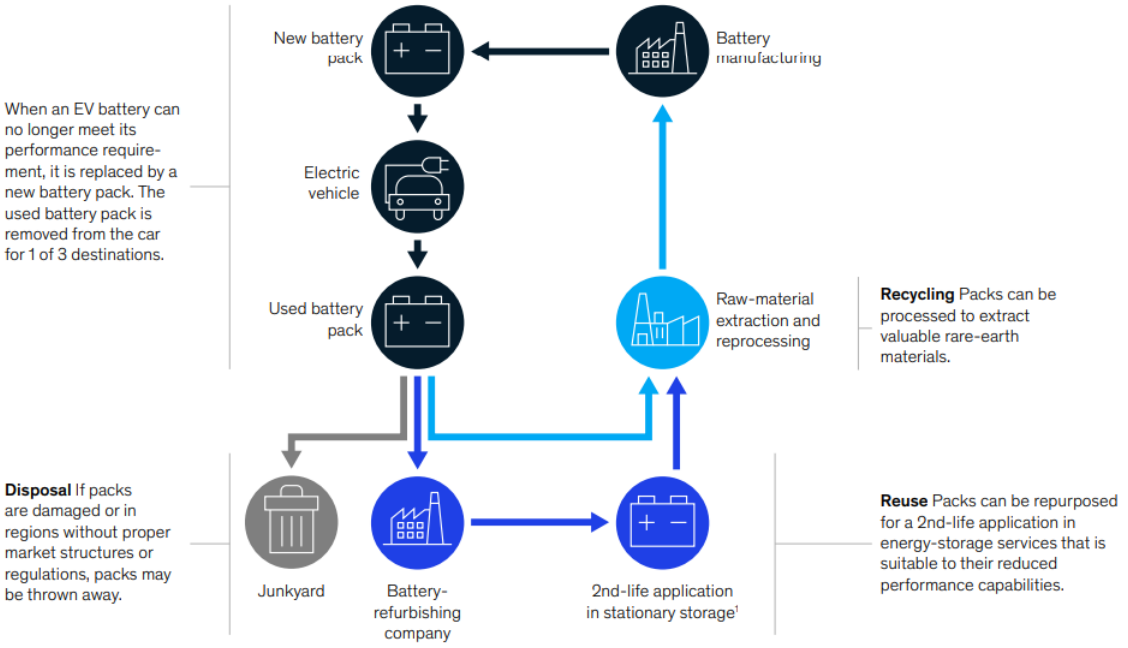

Figure 18: Illustration of different paths for spent LIB[14]

In conclusion, the paths that a battery pack faces once it reaches the end of its life are many and each of them implies advantages and disadvantages; it is not possible to find a single, ideal solution for each type, as storage technologies differ from one another and recovery strategies are still being developed and constantly improved. However, it is important to emphasise how the recycling process can be made less frequent starting from the use phase: proper battery management prolongs the life of batteries, reducing the amount of waste produced; on the contrary, improper use shortens their life, increasing the impact on the environment and resources. Some strategies can be applied to increase battery life, including:

- Use the cells in a narrower voltage range: instead of operating the cell in the 2.65-4.2 V (0-100%) range, charge and discharge it in a lower range, i.e. 3.1-4.2 V (10-100%). This procedure can increase cell life up to 38% [58]
- Charging with a lower current whenever possible; this increases both the service life and the total capacity of the battery during the discharge phase
- Keep the battery pack in optimal temperature conditions for charging/discharging, avoiding temperature fluctuations and especially very low temperatures (below 0 °C). The optimum temperature range for the operation of a cell is between 20 and 40 °C [12]

2 Safety of LIBS

2.1 Safety issues

Lithium-ions batteries are the most widespread electrochemical storage technology for electric mobility. With the increasing popularity of electrically driven vehicles, the issues of accident management and risks to the population are beginning to appear. For a car with an internal combustion engine, the risks are mainly related to the combustible material contained within the car's fuel tank: in the event of an accident, the flammable content can come into contact with hot surfaces such as exhaust manifolds and ignite, putting in danger the health of the occupants. A study carried out by AutoensuranceEZ collecting data from the National Transportation Safety Board (NTSB) and Bureau of Transportation Statistics (BTS) states that, out of 100,000 cars sold, those that catch fire after an accident are 1530 powered by internal combustion engine and 25 powered by full electric powertrains, but the highest number (3474) is attributed to hybrid cars[4]. In another study done by the Swedish Civil Contingencies Agency between 2018 and 2022 in Sweden, 20 cases of electric car fires were reported, in some cases due to impact during a traffic accident and in other cases during recharging; in the same period of the study, the number of electric cars on Swedish roads increased from 16664 to 197709 [47]. This data highlights how the fire risk associated with the LIBs that power electric cars is low, but still not zero. Fire risk is therefore a factor to be taken into account when an electric car is designed, and it is necessary to know the factors that can trigger LIB fires, in order to prevent the problem and, if this is not possible, limit the damage to the occupants of the vehicle. The risk factor associated with LIBs is linked to the development of thermal runaway during the use and abuse phases; the conditions of use to which batteries are subjected, in the case of e-mobility, are diverse and include: temperature changes, vibrations and shocks. Under these conditions, the probability of failure is higher than with stationary use; in addition to this, there are also risks during the use phases that involve the progressive ageing of the cell, with consequent rupture of the separator and risk of internal short circuit. In addition, despite BMS management, some cells may deviate from the others in the same battery pack, and, as time passes, the gap becomes more and more pronounced, leading to risks of overcharging and consequent risk of explosions. A further risk factor lies in the fact that the batteries are positioned closely together to increase their storage capacity for the same volume (a necessary feature to ensure a good vehicle autonomy) and, in case of thermal runaway, the large amount of heat and high temperature can trigger a

chain reaction to adjacent cells, generating a fire that is very easy to spread and difficult to extinguish [55].
The factors that trigger thermal runaway are many and include situations of abuse (mechanical, thermal and electrical), but also situations related to normal use such as cell deterioration. The deterioration of LIBs is in most cases due to: thickening of the SEI (Solid Electrolyte Interface), development of dendritic formations and evaporation of the electrolyte. Increasing the thickness of the SEI reduces the diffusion of the Lithium ions and increases the impedance of the cell, reducing the power output; the increase in this layer is not the same for all cells and this leads to an increase in the imbalance between one cell and another. The SEI is, however, of fundamental importance as it makes the cell more chemically stable and thus safer, while still ensuring excellent performance in terms of ion exchange; the high temperatures to which a cell may be subjected lead to the destruction of this protective layer and this can trigger thermal runaway. During its life cycle, Lithium crystals (dendrites) may form inside the cell: this phenomenon is linked to the decrease in the anode's ability to reabsorb the Lithium ions. As time passes, the Lithium that is not reabsorbed by the anode but it is deposited on its surface in crystalline form and the accumulation of this crystals can, over time, perforate the separator, leading to direct contact between the anode and cathode and, as a consequence, to an internal short circuit. Another risk factor is the inhomogeneity between the cells in the battery pack: each cell, from the manufacturing stage, presents small differences with respect to another one with which it is connected, for example it may present a higher internal resistance; over time these differences become more pronounced, leading to a differentiated ageing process between one cell and another, complicating the management of the state of charge by the BMS and leading, in some cases, to overcharging phenomena with a risk of fire [55].
LIBs can be subjected to various forms of abuse, especially in accidental situations; mechanical abuse occurs when the cells are subjected to shocks and vibrations, thermal abuse occurs in the case of high temperatures such as in fires, and finally electrical abuse occurs in the case of overcharging or short-circuiting: internal short circuit in the case of damage to the separator and external when the batteries are connected to a low resistance load.
The consequences of the stresses to which LIBs are subjected during use constitute a risk for vehicle occupants, especially when a large quantity of cells is stored in a close space inside the car; moreover, mobile storage is known to be subjected to a higher amount of stress. Speaking of mechanical abuse, examples are vibrations while driving due to the asperities of the road and stresses due to impacts

in a car accident. For thermal abuse, on the other hand, cases are linked to the atmospheric conditions of the places where the car is parked and, at the same time, the heat generated during the charging phases, especially at high power. Finally, electrical abuse can be generated during phases of normal use due to, for example, incorrect management of the charging state resulting in overcharging, but also in the event of a malfunction of an external component resulting in an external short circuit. The phenomena resulting from these forms of stress pose a great risk to the occupants who are inside a confined space such as the cabin of the car, and especially when the accident occurs in spaces with few escape routes such as car parks and tunnels. It is therefore of fundamental importance to understand which phenomena trigger such events in order to prevent them and, if this is not possible, to prevent their propagation.

2.2 LIBs abuse

The categories into which the different abuses applied to LIBs are distinguished are electrical, thermal and mechanical. About electrical abuse, it can be triggered by incorrect battery management by the BMS, but it can also be a consequence of, for example, mechanical stress, where the cell is deformed and thus the two electrodes are internally short-circuited. Electrical abuse involves high currents, often caused by internal or external short circuits. The cell that is short-circuited inevitably becomes very hot during discharge and this causes the separator to break, resulting in direct contact between the anode and cathode; this situation contributes to the rise in temperature of the cell until thermal-runaway is reached. The short-circuit can also be triggered from the outside, due to an accident or water entering the battery pack. This phenomenon becomes more dangerous as the higher the state of charge of the battery: a high state of charge allows the cell to maintain a high voltage during discharge, even at high currents, and keeps the reaction active, which would instead end more quickly with a lower state of charge; the prolonged reaction promotes a rise in temperature until thermal runaway is reached. Another phenomenon of electrical abuse occurs when the cell is charged even when the state of charge is 100%, this phenomenon is called overcharge [55]. For modern batteries, fast charging is preferred as it reduces the time spent at the charging station; however, the risk is that the cell will overheat due to the higher currents required, and has a higher probability to overcharging. Due to the dispersion of the cells within the battery packs, some of them may be subjected to overcharging due to incorrect measurements by the BMS, triggering thermal runaway phenomena. According to a study, batteries subjected to electrical overload react differently depending on their surroundings and their ability to exchange heat with the outside world [37]: in this study, pouch cells with a capacity of 1000 mAh and a rated voltage of 3.7 V were analysed; the cells were cycled before the overcharging tests to verify proper functioning. After being discharged to the cut-off voltage of 2.5 V, the cells were overcharged until thermal runaway was reached in 3 different environments: ambient air, quasi-adiabatic and adiabatic environment. The cells were subjected to overcharge with currents of 0.5C, 1C and 2C; the results show that thermal runaway occurs faster in the case of an adiabatic environment than in ambient air due to the lower heat exchange capability which allows the cell to cool down, demonstrating that a low heat exchange can accelerate reactions and promote heat generation. Another factor that influence the thermal runaway is the overcharge current: under ambient air conditions, batteries charged at 1C and 2C respectively reach the thermal runaway with a state

of charge of 210%, while those charged at 0.5C reach it with a state of charge of 329%, as shown in figure 19.

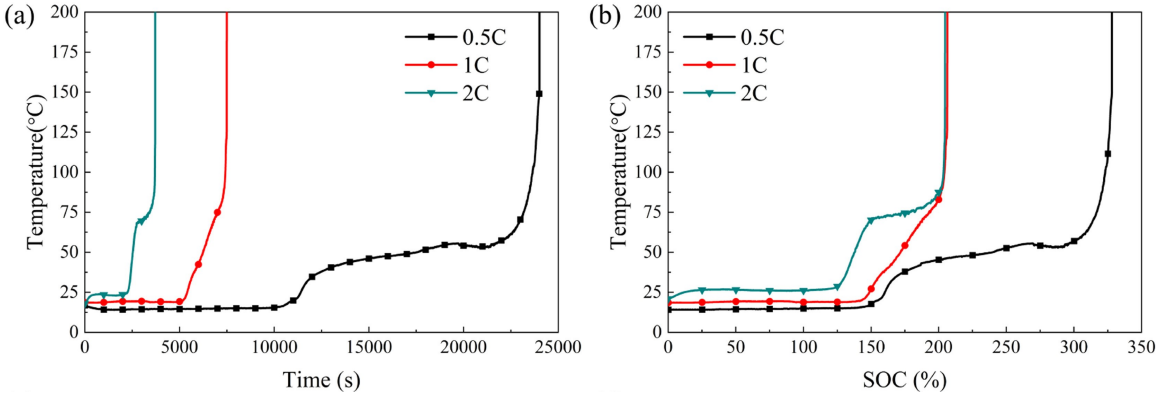

Figure 19: Temperature of cells under different charging rate [37]

When the charging rate is low (0.5C) the amount of heat generated by the joule effect does not cause a large increase in battery temperature, especially when the cell is in ambient air, which allows it to dissipate heat to the outside environment. This is not the case for cells with higher charging rates, where the amount of heat generated is greater due to the higher current delivered, and in the absence of a more efficient medium to dissipate this heat, the cell heats up much faster; at the same time, the generation of dendritic crystals is favoured at higher currents due to the lower absorption capacity of the Lithium ions, which are deposited on the electrodes and then cause perforation of the separator and the resulting internal short-circuit. In the same study, by an analysis with the microscope, it was possible to note how the structure of the cathode changes at different states of charge: as the 100% SOC is overcome, gaps begin to form between the particles, particularly around SOC of 140%. For the anode, at low values of overcharge, i.e. around 120%, no important changes to the structure are noted, while above 140% state of charge, Lithium accumulations begin to be noted on the surface of the anode, which continue to increase for even higher values of SOC [37]. Cells are therefore very susceptible to overcharging conditions, due to the increase in cell temperature and to the decomposition of the cell's constituent materials; conditions that lead to the triggering of the thermal runaway are favoured as the charging current increases, such as the accumulation of Lithium. In addition, the chain reaction leading to thermal runaway takes less time when charging rates are higher, making it more difficult to take preventive action in the event of abnormal signals, which takes longer to occur at lower charging rates. The conditions of the environment

surrounding the batteries are also critical for the development of thermal runaway: low heat transfer coefficient values (found in areas where air cannot flow freely) prevent the cell from cooling down, which leads to its overheating. The worst conditions develop, as expected, under adiabatic conditions while they improve under ambient air conditions; however, cells are often located in areas where airflow is limited due to their close positioning to increase the amount that can be stored. Accumulating the cells in packs is necessary to reduce the occupied volume as much as possible, but while this has an advantage, especially for mobile storage, it is also a risk factor for thermal runaway phenomena; in addition, the proximity of cells can cause a chain reaction triggered by the malfunction of a single overcharged cell, which can lead to very dangerous consequences. The phenomena of overcharging at high currents are real risks associated with modern battery use, especially in the transport sector: in order to make electric and hybrid vehicles a competitive solution compared to internal combustion engine vehicles, recharging times have been reduced over the years to the point where they are now almost comparable with refuelling times at the fuel station. This has been made possible by the higher charging currents that batteries can handle, but this feature also means greater safety risks, not considerably high when the battery pack is new, but after several cycles of use; as individual cells diversify over time, overcharging phenomena become a more likely eventuality, despite the control of the BMS. Another phenomenon of electrical abuse is the internal and external short circuit. As for the internal short circuit, it can be the consequence of other abuse phenomena, such as the penetration of a sharp object of conductive material (e.g. a nail), or the breakage of the separator due to mechanical stress; the external short circuit, on the other hand, is caused when both electrodes are connected to each other by a circuit with a very low resistance: this phenomenon causes the generation of a very high current with consequent overheating of the cell due to the Joule effect. Both in the case of an internal short circuit caused by the penetration of a conductive body and in the case of an external short circuit, the response of the cell depends on the short circuit current, which depends on the intrinsic resistance of the medium through which the electrons can pass: in the case of an external short circuit, the current circulates through the medium with which the battery is connected, exactly as under nominal operating conditions; on the other hand, in the case of an internal short circuit, the current does not follow the traditional path, but exploits the conductive medium that put anode and cathode in direct contact, generating a different current distribution from the previous case. This creates different temperature distributions due to the different zones of electron

passage: for the external short circuit, the zones most affected by heating are those located at the connection between the cell and the circuit, since this is the zone of greatest resistance due to contact resistance; for the internal short circuit, the zones most affected by heating are those at the interface between the cell and the pointed object [1]. The main difference between the two types of stress lies in the fact that perforation of the cell causes its irreversible damage, resulting in the release of gases: these substances can easily ignite in the presence of heat sources, causing what is known as jet-fire. However, it must be pointed out that internal short-circuit phenomena are often the consequence of mechanical abuse, as in the example cited above caused by the perforation of a conductive material; the external short circuit, on the other hand, does not require some form of mechanical abuse, but is due to direct contact of the battery poles, and is therefore a phenomenon that can result from many events, including those caused by normal battery use. From a study [1], tests performed on 15 Ah LMO pouch cells for external short-circuit show that, during discharge, the cell voltage depends on the short-circuit resistance of the medium to which the battery is connected: for very low resistance values (0.5-0.8 mΩ) the voltage drops to zero quickly and the cell is fully discharged in about ten seconds. The second group, on the other hand, has a resistance of intermediate value (24 mΩ), the discharge causes a voltage drop up to 3.6 V, after which this value stabilises and the discharge occurs more evenly until the state of charge is completely exploited. Finally, for resistance values above the previous two, voltage and current follow a trend similar to a normal discharge process. In the case of medium-high resistances, the current reaches steady-state values almost immediately without any particular variations, but in the case of very low resistance values, the current rises instantaneously to around 1000 A, this phase is followed by a gradual decrease and then a slight increase within the first ten seconds: this phenomenon is probably linked to the heating of the cell by the Joule effect caused by the high current [1]; this phenomenon leads to an increase in temperature and, as mentioned in section 1.3, results in an increase in the ionic conductivity of the electrolyte. The ionic conductivity is considered the limiting factor in the discharge process: when the currents involved are very high, the reaction is limited by the capacity of the electrolyte to conduct the Lithium ions, so an increase in temperature increases this capacity, causing a slight increase in current. The study shows that the temperature the cells reach depends on the short-circuit resistance to which they are connected: the lower the resistance, the higher the maximum temperature reached and also the speed at which it is reached; this behaviour is also linked to the magnitude

of the discharge current, so the lower the resistance, the higher the current and consequently the temperature the cell reaches. In figure 20, graphs of voltage, current and temperature profiles are reported [1].

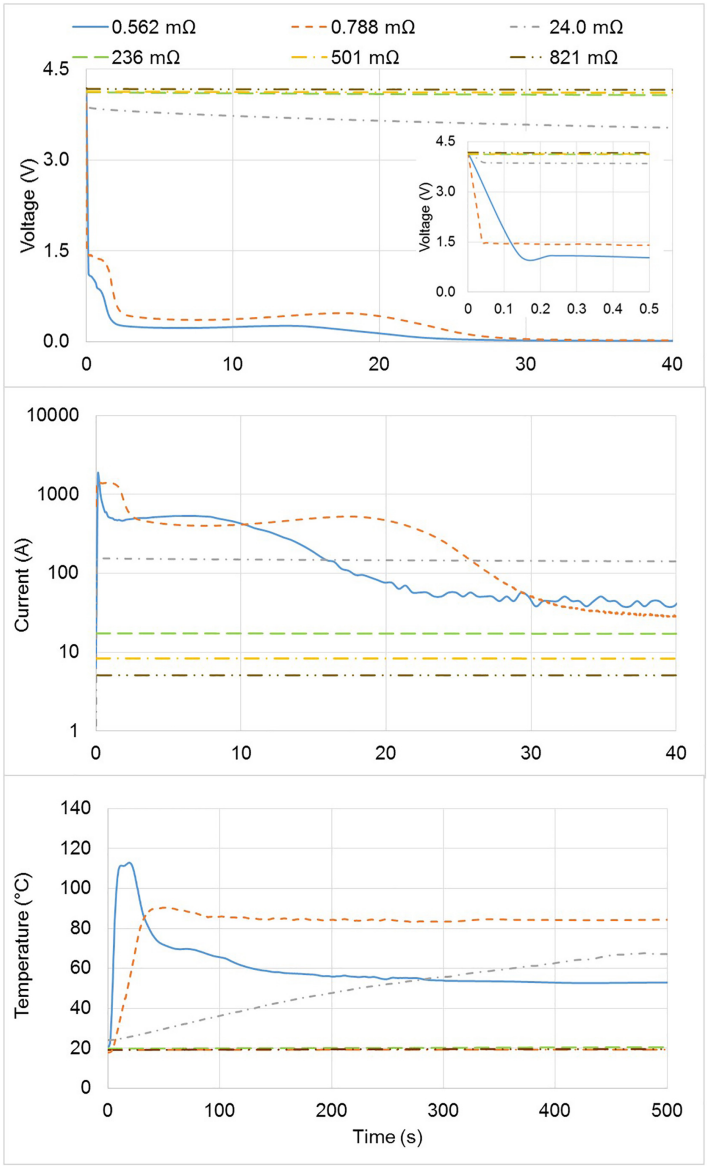

Figure 20: Behaviour of Li-ion cells under different short-circuit resistance [1]

The second form of abuse that batteries can be subjected to is thermal abuse; this occurs when cells are operated at temperatures that are not suitable for their optimal functioning. These situations are less frequent in automotive use, but can still occur in extreme weather or accident conditions; during an accident the car may be subjected to high heat fluxes due to fires from the car with which the im-

pact occurred or the fire itself may be caused by some batteries that were damaged in the impact. Similarly, weather conditions with excessively cold temperatures, such as those experienced in the coldest parts of the planet, subject batteries to thermal stress and, as mentioned above, temperatures below 0 °C can damage batteries by limiting ion exchange capability. To solve these problems, the BMS is responsible for keeping the cells in the optimum temperature range by heating and cooling the packs by means of forced air or electrical resistances. The temperature of the cell depends both on the current it is delivering, as every non-ideal generator has an internal resistance that dissipates part of the electric current into heat, but also on the conditions of the external environment: when current demand is high, the cell temperature can rise rapidly, especially if the car is already in high outside temperature conditions. If the cooling system is unable to dissipate the heat produced by the reactions taking place inside the battery, the temperature will start to increase. Under low-temperature conditions, the ionic conductivity of the electrolyte decreases and this characteristic becomes even more critical at high currents such as those used during fast charging. Under these conditions, lithium ions are deposited on the surface of the anode instead of being reabsorbed; this phenomenon is less likely to occur at warmer temperatures or above 0 °C: Lithium accumulations can eventually perforate the separator, causing an internal short-circuit. Cell temperature is a fundamental parameter to be taken into consideration when using LIBs, both to achieve maximum performance and prolong their life, and to ensure their safety and prevent serious phenomena such as thermal runaway. For this reason, it is important that the control system is able to intervene to avoid temperatures that are too far from safety conditions; however, the control system cannot react in accidental situations, such as fires, for example. For this reason, a system capable of suppressing them is required.
Thermal abuse is a phenomenon that can trigger thermal runaway, which involves the release of a large amount of energy and gases that can ignite in the presence of a heat source; the gases released include: CO, H_2, CH_4, C_2H_4 and C_2H_6 [59].The incident heat flux on the batteries capable of triggering thermal runaway can come from other nearby cells that may have ignited, or from external heat sources in the proximity of the battery packs such as internal combustion engines in the case of hybrid cars. A study shows the effect of incident heat flux on two kind Li-ion cells: a 38 Ah NCM cell in prismatic format and a 78 Ah NCM cell in pouch format; the heat flux to which they were subjected varied from 10 to 50 kW/m^2 [59]. In comparison to cylindrical cells, pouch and prismatic cells are at a disadvantage in terms of external heat flux management: for the same volume, they have a greater

exposed surface area than conventional cylindrical cells, which is an advantage in terms of cooling under nominal operating conditions, but in the case of high external heat fluxes, the risk factor for triggering thermal runaway increases. In addition, cylindrical and prismatic cells are provided with a safety valve that opens when the pressure inside the battery reaches a threshold due to gas production, to prevent it from exploding; pouch cells are not provided with this valve and therefore tend to swell during gas production inside the cell. This phenomenon also occurs during normal battery use, due to the decomposition of the electrolyte over time. In the experimental setup, a resistance heater was used to generate the heat flow. The thermal runaway phenomena obtained during the tests for the two cells show different characteristics:

- the 38 Ah cell presents a deflagration with the release of thermojets without the presence of flame in the initial phase. It then starts the combustion process once the cell components are exposed to air. The 78 Ah cell, on the other hand, begins the thermal runaway process directly with the combustion phase, without the presence of explosions or thermojets.
- The prismatic cell performs a gas release due to the opening of the safety valve, while for the pouch cell this phase does not occur
- For both the 38 Ah cell and the 78 Ah cell, a higher heat flux corresponds to a lower characteristic time; the characteristic time starts when the cell is exposed to the heat flux and includes all phases until the fire is extinguished.
- For the 38 Ah cell, the characteristic time varies from about 2500 s to 500 s depending on the intensity of the heat flux.
- The characteristic time of the pouch cell varies between 350 s and 100 s, significantly less than the prismatic cell.
- The heat released by the 78 Ah cell is higher than that of the 38 Ah cell, and the internal surface temperature is also higher for the 78 Ah cell.

The results obtained from the study [59], show how the incident heat flux can change the behaviour of the cells to which they are exposed. Moreover, it can be seen that two cells of different conformation react quite differently to the same thermal loads; the prismatic cell examined showed a time required to initiate thermal runaway approximately 7 times longer than the pouch cell with the same thermal flux (10 kW/m^2). Under the most intense heat flux conditions, the prismatic cell resisted almost twice the time with respect to the pouch; this behaviour must

be taken into account especially in the event of an accident scenario, where a few seconds can make the difference for the occupants of the vehicle to escape the danger. However, the difference in capacity between the two cells must also be taken into account: a battery with a larger capacity also implies a larger amount of material available for combustion and also larger batteries have a bigger exposed surface, which allows a greater heat exchange with the heat source [59]. Among the data obtained, a very important one is the Heat Release Rate (HRR), which translates into the thermal power developed by the cells during all phases of the thermal runaway: for the 38 Ah cell, the HRR varies between 10 and 75 kW depending on the heat fluxes, while for the 78 Ah pouch cell, HRR stabilises steadily at around 150 kW [59]. These thermal power values were triggered by a heat flux coming from an external source in the experimental setup (external heater), but often batteries of this type are placed close to each other to optimise space and maximise storage capacity for the same volume: this characteristic creates dangerous scenarios that can trigger chain reactions capable of self-feeding and expanding very quickly, as shown in the 3D model obtained in another study [15] in figure 21.

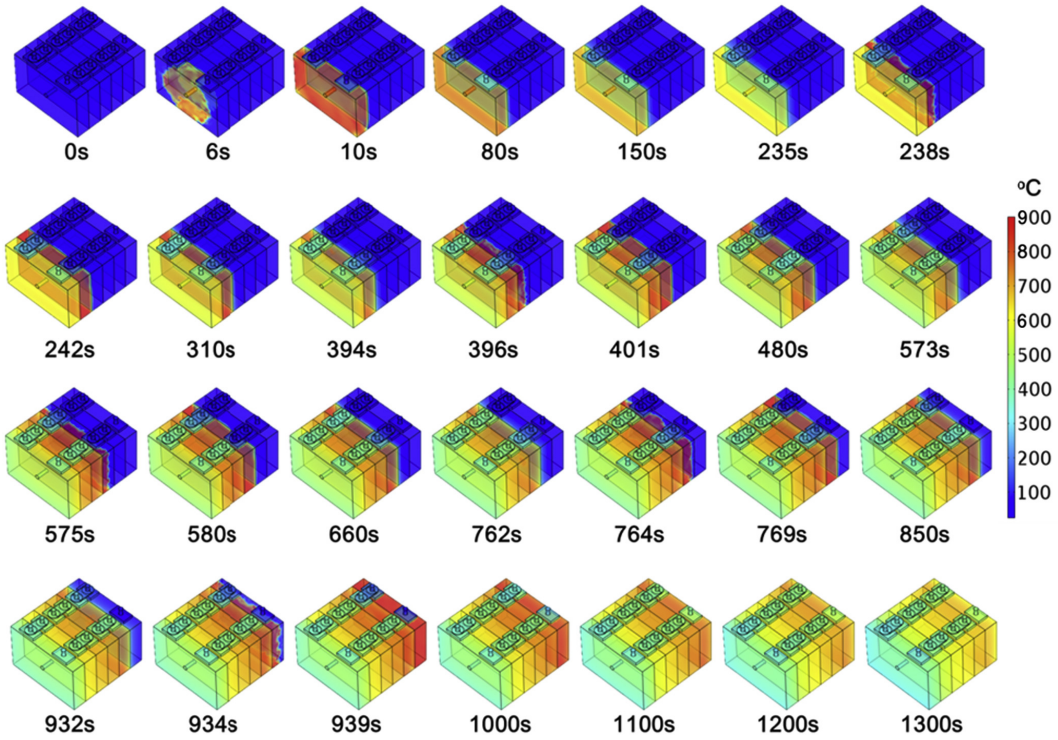

Figure 21: Temperature distribution on thermal runaway model [15]

Another study [7], analysed the thermal runaway propagation phenomenon for

cylindrical 18650 cells, a type of battery often used as a storage system for electric cars. The batteries were left inside the packaging used for transport, positioned with positive pole upward in a 10x10 and 6x6 configuration; in both configurations, one battery in the central position was removed to be replaced by a 500 W cylindrical resistance heater. Approximately 500 seconds after the heater is switched on, a phase of smoke release from inside the pack begins due to the opening of the safety valve of the cells positioned close to the heater; the cylindrical cells are equipped with a safety valve unlike the pouch cells analysed in the previous study. After about 800 s, the batteries closest to the heater begin to ignite and the flames then spread to the nearby cells; the fire that has spread provides heat to the entire battery pack and as the safety valves open, jet fires are produced due to the ignition of the gases leaking from the batteries. After a period of stationary combustion, jet fires appear again and propagate very rapidly; after these phases, the cells and the cardboard box burn until extinction, which occurred at around 1700 seconds [7]. It can be noticed that the ignition phase takes several time; this is due to the heat exchange mechanisms that the heater employ to transfer heat to adjacent cells. Due to their shape, the contact surface between one cell and another is small compared to prismatic or pouch cells, which instead have a large contact surface area, this allows a faster heat propagation. Tests were carried out in the 2 configurations 6x6 and 10x10, and the Heat Release Rate (HRR) was measured, like in the previous study: in the first 6x6 configuration, a peak value of approximately 80 kW was measured, while in the test in the 10x10 configuration, the peak value recorded reached a value of 450 kW. In terms of thermal energy released, in the first case a Total Heat Release (THR) of 4364 kJ was obtained while in the second configuration the energy released was 16490 kJ [7]. These numbers further confirm the correlation between the amount of mass of material available for ignition and the amount of energy released during the fire phase: the greater the number of accumulated batteries, the greater the amount of energy released. Furthermore, it can be seen how the method of heat propagation influences the time necessary for the thermal runaway: the fire that then fuels the thermal runaway starts from a single cell that overheats until itself ignites; once flames take possession of an area, propagation becomes inevitable and accelerates faster as more material ends up being used as fuel. The heat exchange process is governed, in the first phase, by convection and conduction (the latter being disadvantaged due to the poor contact surface between the cells); irradiation contributes particularly when temperatures begin to rise, as it is correlated by the difference of two temperature raised to the forth power. Once the combus-

tion phase begins, the heat transferred by irradiation becomes preponderant and the chain reaction becomes unstoppable: the fire causes a sudden rise in temperature and the thermal gradient allows propagation even to more distant cells, which ignite more easily. For this reason, preventing the ignition of overheated cells can prevent the propagation of thermal runaway to adjacent cells, especially in the case of cylindrical ones, which have an advantage due to their difficulty in transmitting heat one to another (due to the gaps between individual cells) and because their configuration allows for easier cooling and insulation.
The last form of abuse is the mechanical one: this is probably the one that most concerns the automotive sector; while driving on the road, the components of a car are mechanically stressed by the roughness of the road causing vibrations that act repeatedly for thousands of kilometres. In addition to these, there are also environmental conditions that can further aggravate the situation, such as extreme heat or cold. In addition to the ordinary phenomena that damage the car's components, there are also the extraordinary events that, unfortunately, occur: accidents. During impacts with objects or other vehicles, the components inevitably undergo deformations; these deformations may affect the organs for the transfer of motion or the structural part of the vehicle: this implies a risk for the occupants in a direct way because they may be injured during the impact, but if this does not occur, it does not represent a form of danger. In the case of the battery pack, on the other hand, this is a risk that is not directly related to the impact, but rather to what could happen in the minutes following it: the deformation or perforation of the cells can trigger a thermal runaway, as in the case of thermal and electrical abuse. The problem with this form of abuse is that unfortunately it cannot be detected by the BMS in the same way as in the case of an overtheating or short circuit; in these two scenarios, the battery management system's measurements can detect abnormal temperature or current values and alert the driver, so that the he can intervene to ensure the safety of the vehicle's occupants and those in its proximity. Mechanical abuse is an extreme stress to which batteries are subjected and requires strategies to prevent the consequences as quickly as possible. Specifically, a mechanical deformation triggers a chain of electrical and thermal phenomena that are then the actual drivers of thermal runaway: the simple deformation does not represent a risk, but is more the triggering phenomenon. For example, the piercing of a cell by an object made of conductive material causes its internal short circuit, as already discussed in the section on electrical abuse. Another problem is posed by vibrations and sudden shocks: these phenomena can cause the contacts to become partially detached from the battery poles, leading to

an increase in resistance to the passage of electrons, which results in an increase in temperature during the passage of current due to the Joule effect. Finally, an impact during an accident can cause the battery to deform or fracture, and with it the damaging of the separator, triggering an internal short-circuit; this is why cells are designed to resist, at least up to a certain threshold, the stresses without deforming excessively.
In order to reproduce the mechanical abuse, tests are carried out in the laboratory to understand the dynamics by which the thermal runaway develops; one of the most important is the nail penetration test, which consists of piercing the cell with a nail of a fixed diameter and material to trigger the internal short circuit and thus the thermal runaway. The procedures for the test follow the Society Automotive Engineers' standard J2464 and require the nail material to be mild steel with a diameter of 3 mm; the penetration speed must be greater than or equal to 8 cm/s and the nail must be oriented perpendicular to the cell's electrodes [45]. This is a destructive test after which the cell can no longer be reused. The material with which the penetration is carried out is also responsible for the resulting internal short circuit: the nail made of a metallic material creates a direct contact point between the anode and cathode, and since it is a conductive material, it allows current to flow between the two electrodes. A study [1] shows how the material of the nail with which the penetration test is carried out affects the result: the perforation was carried out with copper, steel and plastic nails. The cell voltage measurements carried out during the test show that the copper nail caused the cell to short-circuit to 0 V in almost all cases; the steel nail, on the other hand, short-circuited 4 out of 10 cells, while the remaining 6 cells maintained a constant voltage of around 3.5 V. In the case of the plastic nail, no drop in voltage was observed: for all 6 cells tested, the measured voltage remained constant at around 4.2 V even hours after penetration. These results show that the nail works exactly as a medium for the current to flow through and is therefore responsible for the internal short circuit; in the case where the puncture medium is an electrical insulator (such as plastic), the cell is damaged but the current cannot find a way to flow through the cell and therefore cannot trigger the thermal runaway. In another study [36], LiNiCoMn 18650 batteries were subjected to the nail penetration test; the cells were punctured by a 3 mm in diameter nail at different charge levels (0%, 50%, 75% and 100%). The cell surface temperature trends during the tests at different SOCs show that for fully charged and 50% charged batteries, no thermal runaway occurred. For batteries charged to 75%, thermal runaway occurred in 3 out of 4 cases and finally, for fully charged batteries, thermal runaway occurred

in all cases. In the cases where the thermal runaway did not occur, the temperatures measured on the cell surface always remained below 100 °C, while in the worst case with a fully charged cell, the maximum temperature found was 465 °C. While the maximum temperature increases as the state of charge increases, the time required to reach it decreases as the state of charge increases: the higher the state of charge, the shorter the time to maximum temperature. The state of charge therefore influences both the gravity of the phenomena obtained by the cell penetration and the speed with which these events happen [36]. About the effect of the penetration zone, this apparently causes the triggering of the thermal runaway in all cases; in addition, the zone of the cell where the maximum temperature is reached does not change, it almost always occurs around the central area of the cell. The depth of penetration of the nail, on the other hand, affects the number of layers affected by the short circuit, since the electrodes are rolled on top of each other: the greater the depth of penetration, the greater the number of layers in which the electrodes are short-circuited, causing a greater current flow and consequently more heat. Finally, the study shows that penetration speed does not seem to influence the thermal runaway triggering: all cells perforated at different nail speeds experienced thermal runaway [36].
Cells subjected to mechanical abuse may not immediately show the symptoms of an imminent thermal runaway: during an impact, the battery pack may be subjected to insufficient deformation to break the separator and bring the two electrodes into direct contact. In these situations, deformations could happen inside some cells, changing their geometry and creating internal defects that, over time, could propagate to the point of triggering thermal runaway. If the thermal runaway is triggered some time after the accident, it constitutes a greater risk than if it occurs immediately after the accident: in the latter case, measures to contain the risk and protect people are taken immediately; in the case of damage that develops over a long period of time and acts silently, on the other hand, there are no signs to warn people of the imminent danger, but it can occur at any time. In the event of an accident, the cells must be to integrity control in order to avoid this risk. The effects of deformation caused by mechanical stress without irreversible damage were analysed in a study [17]: 3 Ah $LiCoO_2$ pouch cells were subjected to deformation up to the maximum limit before rupture; cells subjected to different degrees of deformation were then tested in different charge/discharge cycles under different temperature conditions and then compared with those not subjected to deformation. The cells were deformed in a vertical direction relative to the cross-section in the middle area without triggering thermal runaway, but with

consequences for the internal structure of the battery. The electrodes suffered major damage, especially at higher strain values, while at lower stresses, only deformations without any particular breakage within the cell were evident. A total of 48 cells were subjected to charge/discharge cycles following the deformations; 4 batteries showed a gradual loss of voltage and swelling, due to the breakage of the separator, which caused an internal short circuit. The damaged cells, however, did not trigger the thermal runaway because the heat generated during the short-circuit was not high enough. The short-circuit phenomenon, however, did not occur immediately after the mechanical tests, but after a few work cycles. The cells analyzed in this study were subjected to lower levels of mechanical stresses with respect to those required to trigger the thermal runaway: the deformation was therefore not sufficient to fully break the separator and bring the two electrodes into direct contact, but this did not prevent the phenomenon from occurring in the following time; moreover, the behaviour of the "stressed" cells did not deviate much from that of the undamaged ones, making the damage phenomenon difficult to identify and therefore more dangerous. Especially in mobility applications, thousands of cells of this type are stored in confined spaces and, as mentioned above, the triggering of a chain reaction can start from a single faulty cell and then very quickly spread to the entire storage system; for this reason, it is very important to know the weak points of this technology, so as to anticipate possible safety risks and minimise the chance of these happening..

The forms of abuse that batteries can suffer are many, and unfortunately the situations in which these can occur are not so far from ordinary use to be ignored; moreover, the causes of thermal runaway are often multi-factorial and sometimes interconnected, such as mechanical and electrical stress. The consequences of poor management of this storage system can be very serious and must be avoided by all means. Unfortunately, it is not possible to eliminate the risk of such phenomena to occur: for this purpose, strategies to contain them are required to prevent the propagation of thermal runaway, which will be analysed in the next section.

2.3 Management of incidental events

The stresses to which batteries are subjected during their use in stationary conditions, and even more in mobility applications, can cause them to become irreversibly damaged, resulting in dangerous and sometimes fatal reactions for those in their proximity. The phenomena that can trigger thermal runaway have previously been analysed, and by understanding these events, it is possible to adopt solutions that can prevent their development and contain them if the means of prevention are not sufficient. The stresses are therefore mainly thermal, mechanical and electrical. Thermal stress is caused by incorrect management of the cell temperature control system: this management is performed by means of sensors in the BMS, which has the task of monitoring the cell temperature in every moment. From the previous paragraphs, it has been possible to understand that the dynamics of the cell's internal reactions for the production of electric current are strongly influenced by temperature, in fact it modifies the ion exchange characteristics and the internal resistivity of the cell. Optimum operating conditions require a cell temperature between 20 °C and 40 °C [18]: under these conditions, battery life is maximised and the risk of thermal problems is reduced. Temperatures slightly above or below this range do not pose a direct problem, but, especially for values below 0 °C, they can irreparably damage the battery. During use in low temperature conditions, the slowdown of ion exchange reactions can cause lithium to accumulate on the anode, especially when the electrical current demand is high; these deposits can accumulate to the point that they perforate the separator and bring the anode and cathode into direct contact, causing an internal short circuit. On the other hand, high temperatures cause both a loss of efficiency and thus shorten the life of the battery, and decomposition of the electrolyte; in addition, they can trigger the cell fire. To prevent the triggering of these phenomena, the BMS constantly monitors the internal temperature of the battery pack, and adopts cooling and heating procedures to keep the cells inside safe temperature ranges. During heavy duty use, the high current demand causes the cell temperature to rise, requiring an appropriate cooling system. The most common cooling systems use air (forced or natural convection), water and phase change materials (PCM). PCMs are materials that release or absorb heat at a constant temperature during phase change: the energy exchanged comes from the latent heat, of fusion or solidification, and allows a better heat exchange than a traditional material precisely because during the phase change process, the temperature of the medium remains constant, until the complete change of phase. In a study [41], was analyzed the heat exchange behaviour of 18650 batteries wrapped

in a volume of PCM subjected to forced air. The material surrounding the cells was disposed in 3 different configurations: in an ellipse positioned parallel and perpendicular to the air flow and in a circular geometry, but always maintaining a constant amount of material. The simulations show that with the same PCM material used, the highest battery temperature is found in the vertical ellipse configuration: due to the reduced space between cells, the air in the direction of the batteries cannot diffuse towards the inner cells, which therefore start to heat up more. On the other hand, the best one is the horizontal ellipse configuration, with the absolute lowest maximum temperature, even compared to the configuration with circular distribution: this is due to the greater surface area exposed in the direction parallel to the air flow; this allows easier heat removal by convection and a reduced pressure drop due to the greater cross-section for the passage of air. Another method of cooling batteries involves the use of forced air, which removes heat as it passes between the individual cells. The distance between cells is a key parameter for thermal management, as a larger gap allows easier passage of air with less pressure drop, but the greater the space, the smaller the quantity of cells that can be contained for the same volume. Increasing the cell spacing therefore promotes heat exchange but at the same time reduces the amount of energy that can be stored. Air cooling has the advantage of being easier to implement and manage, but has a low convective heat exchange coefficient as a limiting factor. The thermal power exchanged by convection is expressed by the formula:

$$Q = h_{air} * A_{cell} * (T_{cell} - T_{air}) \tag{14}$$

where:
h_{air}: convective heat transfer coefficient of air
A_{cell}: external surface of the cell
T_{cell}: temperature of the external surface of the cell
T_{air}: temperature of air in contact with the external surface of the cell
The amount of heat removed per unit of time therefore depends on the surface area of the cell exposed to the air, the temperature difference between the cell and the air, and finally the heat exchange coefficient: the coefficient does not have a fixed value but depends on many factors such as air speed, density and viscosity of the fluid. There are therefore several ways to increase the power exchanged and thus the cooling capacity; it is possible to intervene by increasing the contact surface of the cells by means of finned banks, but this further contributes to increasing the effective size of the cell. The most convenient choice for increasing heat exchange

without modifying the cell configuration is to improve the convective heat exchange coefficient; this parameter depends on the type of fluid being considered (which possesses specific thermo-fluid-dynamic characteristics) but also on the dynamics of the fluid: to characterise convection heat exchange, some detailed information is required. The flow of a fluid with an undisturbed initial velocity in one direction is modified by the presence of obstacles along the direction of propagation. The flow may be in a laminar or turbulent way: in the first case, the fluid particles move in an organised manner and it is possible to identify the flow lines along which these particles move; in the second case, the flow is irregular and difficult to predict, and presents variations in velocity and pressure along the direction of propagation. The transition from laminar to turbulent flow is due to the interactions the fluid has along the way and the disturbances it encounters, especially when it comes into contact with objects that obstruct the flow. A dimensionless parameter to distinguish the laminar and turbulent flow is the Reynolds number, defined as[39]:

$$Re = \frac{\rho V l}{\mu} \tag{15}$$

where:
ρ: density of fluid
V: velocity of fluid
l: characteristic length of the body in contact with the fluid
μ: viscosity of fluid
It can be seen that the dimensionless number is influenced both by the physical characteristics of the fluid, such as its density and viscosity, and by the dynamics of the flow, such as the initial velocity: the Reynolds number increases as the fluid's velocity and its density increases. Thanks to this number, and others, it is possible to determine the convective heat transfer coefficient a fluid has when removing or supplying heat. An increase in the heat transfer coefficient corresponds to a greater ability of the fluid to remove the heat produced by the batteries during work cycles, limiting the risk of overheating. Thanks to the Reynolds number, it is possible to understand how a liquid, theoretically, has advantages in terms of heat removal over an aeriform like air. In a study [33], was analyzed the effectiveness of a liquid cooling system based on five different types of fluorocarbons. In addition to the cooling capacity, the environmental impact resulting from the disposal of these liquids was analysed: in all cases, due to their organic-based structure, the cooling liquids degrade very easily without damaging the atmosphere. The types of coolants analysed are: High boiling point coolant and Low boiling point

coolant. The first have boiling temperatures between 49 °C and 82 °C, while the seconds have boiling temperatures around 34 °C. Tests showed that the 3500 mAh 18650 cells cooled with ambient air during charge-discharge cycles (9900 mA during discharge and 5000 mA during charging) reached a maximum temperature of 80 °C and maintained an average temperature of around 65 °C. With respect to coolants, low boiling point coolants recorded the lowest maximum temperature, at around 35 °C (equal to the boiling temperature of the coolant), while high boiling point coolants showed a lower cooling capacity, however, better than that of air, reaching maximum temperatures ranging between 50 °C and 60 °C. The study in question also analysed the SOH (State of Health) of the cells subjected to the different cooling fluids after 100 charge/discharge cycles, the results of which are shown in figure 22

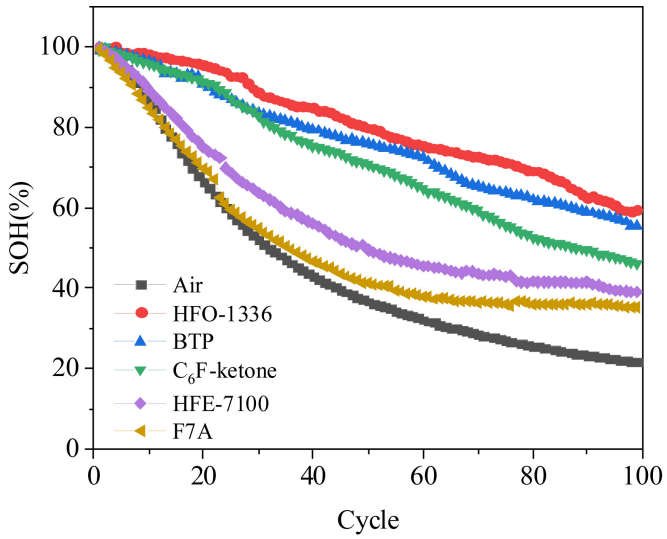

Figure 22: SOH of cell with different cooling technology [33]

It can be seen that the most significant degradation is for cells cooled with ambient air, while the best results are obtained for low boiling temperature coolants (red, blue and green curves); in between the two are cells cooled with high boiling temperature liquids (purple and gold curves). These results show that the temperature at which the cells are maintained has a significant influence on their service life, especially when subjected to high operating currents (in this case, 9000 mA for both charging and discharging). After 100 cycles, the air-cooled cell posses a much lower state of health than liquid-cooled cells, making the liquid-cooled one the best solution [33]. This type of coolant also plays a key role in the prevention of thermal runaway in the event of a malfunction: as analysed above, the triggering

of thermal runaway is a multifactorial event, but one that always results from a rapid temperature rise in a cell. The heat flux generated by a single battery can subsequently trigger the thermal runaway of cells in the proximity, promoting a chain reaction. Liquid cooling compared to air cooling therefore implies a higher cooling efficiency of the cells both in terms of maximum temperature and average temperature during duty cycles; but it has been shown to prevent the triggering of thermal runaway caused by the overheating of a cell [33]. In the previously reported study on thermal runaway propagation between 18650 cells placed in transport packages [7], was demonstrated the risk of an overheated cell triggering a chain thermal runaway reaction to adjacent cells: this phenomenon is difficult if not impossible to contain once the reaction is triggered, due to the high temperatures reached during the combustion phase. One of the advantages of the liquid cooling system is its ability to prevent the phenomenon of cell overheating, with the consequent risk of thermal runaway chain reaction [33]. In the case of air cooling, the heat removed from the overheated cell (simulated by a 300 W electric heater) was not sufficient to prevent the cells in the vicinity from heating up; for the cells immersed in the organic coolant (both high and low boiling point), the temperature increased, but not enough to trigger thermal runaway, reaching a stationary temperature between 100 °C and 120 °C depending on the type of coolant. Finally, it was possible to demonstrate a high degree of compatibility between the liquid refrigerants and the cells: in fact, after 3 months of immersion, only one type of organic liquid showed a corrosive reaction on the cell casing, while for the other liquids, no substantial differences were noticed [33]. Organic liquid cooling therefore proves to be an excellent candidate as a medium for cooling battery packs, thanks to its high heat removal capacity and at the same time allows the introduction of new strategies for thermal management: the containment effect of thermal runaway by the organic liquid gives the control system more time to predict a possible anomaly, and thus guarantees, at least outside of accident scenarios, greater safety for the vehicle occupants.
In this section, were reported the types of abuse that the cells can suffer during their use: the consequences of such forms of abuse can be very serious and for this reason the correct management of such a storage system is very important. In the next section, the experimental data obtained on 18650 cells subjected to mechanical abuse will be reported: the data obtained is used to characterise the consequences of perforation of these cells with consequent triggering of thermal runaway; the characterisation of this phenomenon is carried out by means of sensors capable of monitoring the behaviour of the cell during perforation.

3 Experimental section

3.1 Methodology and experimental setup

In this section, the results obtained from perforation tests performed on 18650 lithium-ions cells are collected. The aim of this type of test is to measure, through the use of probes, the phenomenon of thermal runaway induced by perforation of the cell: this is a situation that does not occur during ordinary use, but rather in the event of an accident.
Experimental tests were carried out at the Energy Center Lab in Turin, on LG INR 18650 M29 batteries with a capacity of 2850 mAh; additional technical specifications are shown in the following table.

Technology	Li-NiMnCoO2
Nominal Capacity	2850 mAh
Nominal Energy	10.5 Wh @ 0.2C
Nominal Voltage	3.67 V
Charging Voltage	4.2 V
Charging Current	0.5C (1375 mA)
Max Charge Current	1C (2750 mA)
Max Discharge Current	10 A
Operating Temperature range	-30 - 60 °C
Weight	45 g

Table 3: LG cell data sheet

The tested cells were subjected to a cycling process in order to verify the actual capacity and to reproduce the behaviour in ordinary use. Every tested cell is charged up to a voltage of 4.2 V at the manufacturer's declared nominal charging current of 1375 mA. The recharge process was performed by Arbin Instruments BT-2000 Battery Tester, as shown in figure 23. The charging process followed the standard Constant Current - Constant Voltage method (CC-CV) showed in picture 24 and the ambient temperature of the room in which the charge-discharge process is performed is maintained at 20 °C.

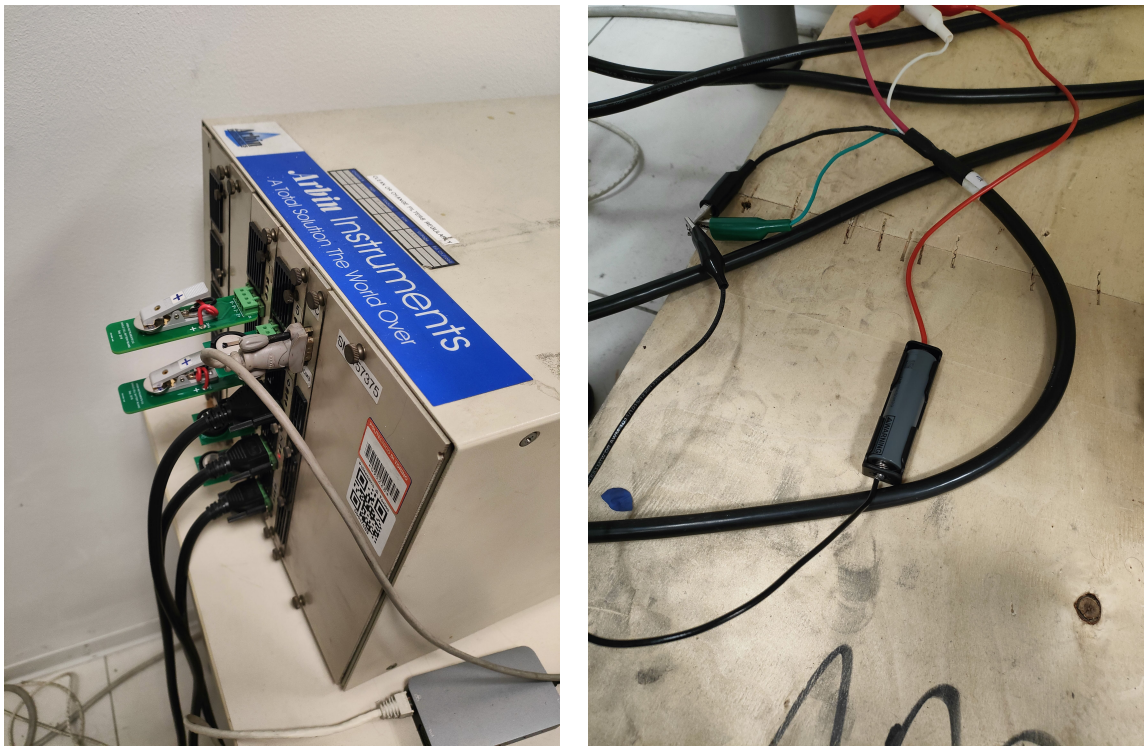

Figure 23: Battery Tester (left) LG cell during charging phase (right)

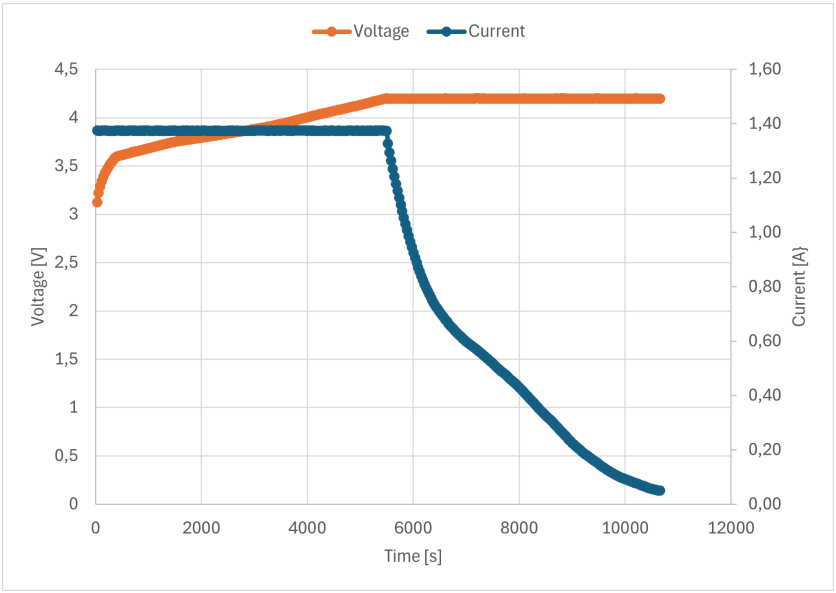

Figure 24: Recharge process of LG 18650 for experimental test

Nail Testing procedure was performed inside the Thermal Hazard Technology EV+ Accelerating Rate Calorimeter (ARC): this device is able to perform battery

testing on different sizes of batteries according to the following specifications:

- Battery test capacity from 18650 up to small modules (1-130 Ah)
- Heated walls to simulate adiabatic conditions and thermal imaging camera
- NPCO-CS option: Pneumatic nail penetration and crush with controlled speed
- Chamber dimensions: 40 cm diameter x 44 cm depth
- Temperature range inside the heated chamber: ambient to 300 °C
- Thermocouple specifications: resolution 0.001°C, precision <0.2% and accuracy 0.7%
- Pressure range: 0-200 bar

The device is composed by 2 sections, one inside the other: where the nail test takes place is the calorimeter assembly and this section is enclosed by the blast box; the external part has the function of extracting exhaust gases which can exit from the test box and also has the purpose to protect the user. The top part of the calorimeter is closed by a heavy lid to contain the explosion and also the gases that are produced after the penetration phase. A scheme of the assembly is shown in picture 25.

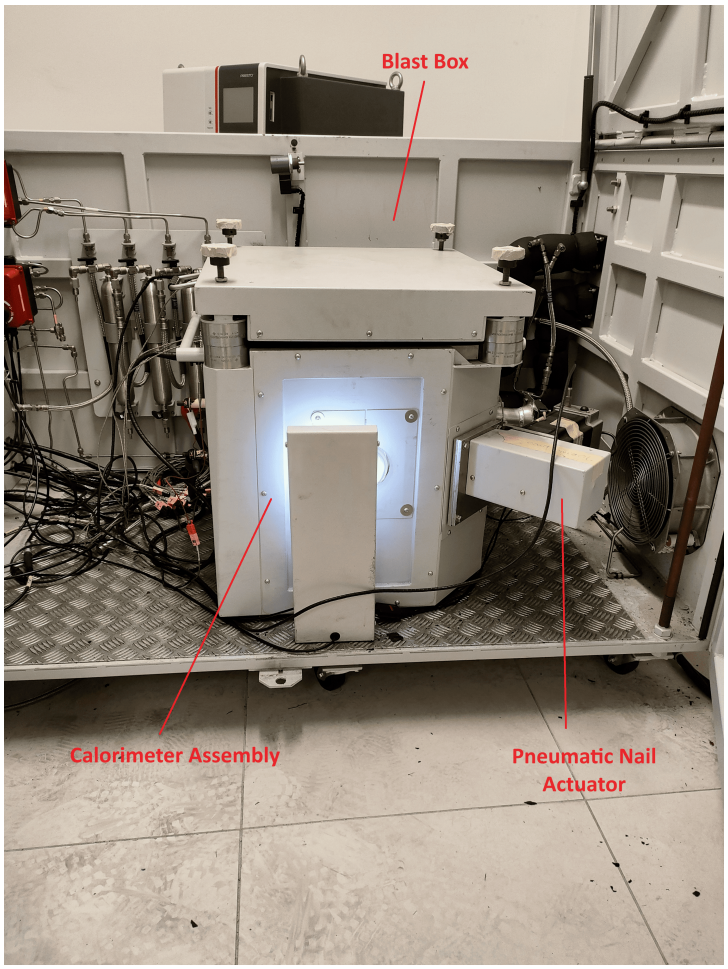

Figure 25: THT EV+ ARC assembly

After the charging process, the 18650 LG cells are extracted from the battery tester and the voltage is measured to verify the state of charge. After this step starts the calibration procedure of the nail, which consists in a manual control of the pneumatic actuator to push forward the tip of the nail until reaching the necessary depth to pierce the battery (this procedure is carried out before the positioning of the cell). Once the zero position is set manually, the command "initialize" allows the retraction of the nail in backward direction; now the battery can be positioned: the cell is placed with the positive pole oriented upwards, then the thermocouple is kept in direct contact with the cell thanks to high temperature scotch tape (the fixing point of the thermocuple is roughly in the middle of the cell). In the end, the battery is kept adherent to the wall of the calorimeter with layers of the same high temperature tape to avoid the its rotation or the displacement during the perforation. The configuration of the cell is shown in figure 26

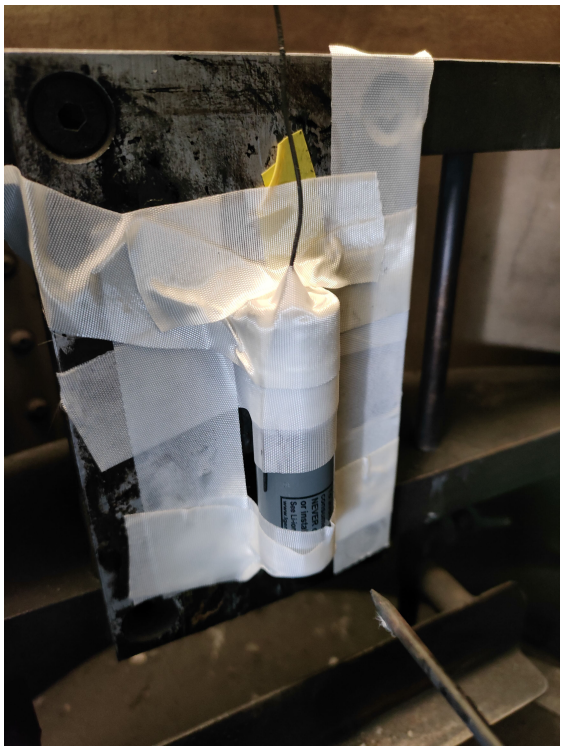

Figure 26: 18650 cell configuration before nail penetration procedure

On the left side of the calorimeter, a hole allows the insertion of an external probe to monitor the gas production during the thermal runaway; the exhaust gas probe Testo 330 was used, and its specifications are reported in the table below

Parameter	**Precision**
O_2	±0.2 Vol.%
CO	±20 ppm (0...400 ppm) ±5 % d. v.m. (401...2000 ppm) ±10 % d. v.m. (2001...4000 ppm)
NO	±2 ppm (0...39,9 ppm) ±5 % d. v.m. (40. . . .2000 ppm) ±10 % d. v.m. (2001...3000 ppm)
CO_2	±75 ppm + 3 % d. v.m. (0...5000 ppm) ±150 ppm + 5 % d. v.m. (5001...10000 ppm)

Table 4: Testo 330 gas probe precision range

The gas probe was added to the experimental configuration to evaluate the composition of gases produced after the thermal runaway triggering, in particular,

it was possible to measure the production of carbon monoxide (CO) and nitrogen monoxide (NO). CO is a toxic gas and it is produced during incomplete combustion of organic material with low concentration of oxygen: it is considered dangerous for human health since it bonds with hemoglobin and reduces the capability of blood to transport oxygen and high concentrations can lead to death [38]. NO is also a product of combustion and its formation is linked to the oxidation process of Nitrogen present in the ambient air thanks to high temperature generated during the combustion. It is dangerous for human health and high concentrations can reduce breathing capacity [38].
In addition to the LG 18650 cells, are subjected to nail testing Samsung batteries INR18650-15L, whose specifications are reported in the following table.

Technology	Li-NiMnCoO2
Nominal Capacity	1500 mAh
Nominal Voltage	3.6 V
Charging Voltage	4.2 V
Charging Current	0.5C (750 mA)
Max Charge Current	4000 mA
Max Discharge Current	18 A
Operating Temperature range	-20 - 60 °C
Weight	43 g

Table 5: Samsung cell data sheet

These cells are recovered from a battery pack and the number of charge-discharge cycles to which they were subjected is unknown, but surely higher than a thousand. The chemistry of the cathode is the same as the LG cells, the only difference is the capacity, which, in case of Samsung cells, is lower. After the extraction of the cells from the battery pack, the positive and negative poles were cleaned from welding points, to ensure a safe contact point for the charger. Then, each battery is tested to discover the residual capacity (the testing was performed with a total discharge up to 2.8 V and then a full recharge up to 4.2 V with nominal declared currents). The retained capacity found is:

Cell 1	1058 mAh
Cell 2	1011 mAh
Cell 3	1071 mAh
Cell 4	1089 mAh
Cell 5	1053 mAh

Table 6: Samsung cells retained capacity

Each cell has lost around 30 % of its nominal capacity but there is not a large difference in terms of capacity between one and another, probably thanks to the BMS they were connected to inside the battery pack. Before the start of the testing procedure, some parameters need to be defined: the nail diameter is 3 mm and the speed has been set to 8 cm/s, as stated by the Society Automotive Engineers' standard J2464. The set point temperature was also selected and once reached, a 5 minutes timer starts before the nail moves forward. The heating process is fairly slow, around 0.2-0.3 °C/min and once the nail is pushed forward, the instrument starts the "seek" phase, in which it is expected a rapid increment in temperature and the sampling time increases. Once the perforation has occurred, the nail goes backward to detach from the cell. All batteries are left at least one day inside the calorimeter box to allow the gases to be extracted and expelled from the chamber for safety reasons.

3.2 Results and comparison

In this section the data obtained from the nail testing is collected and is composed by samples obtained from the software of the THT ARC EV+ by means of the thermocouple and the thermal camera positioned inside the blast box and also data obtained from the gas probe positioned inside the calorimeter box; after the extraction from the chamber, pictures of the cells are taken as further evidence. To better understand the results it is necessary to point out some issues that appeared during the experimental phase: due to violence of the thermal runaway, some temperature samples obtained are not to be considered, at least in some parts, correct due to the detachment of the thermocouple from the battery.

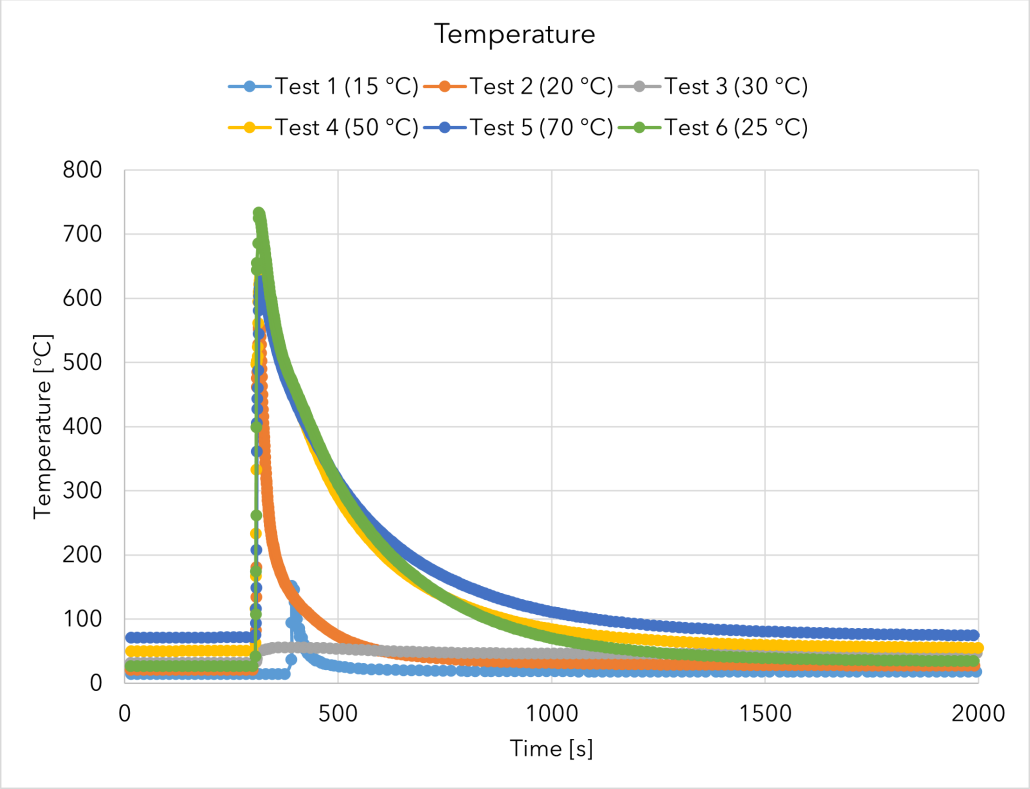

Figure 27: LG cells temperature profiles

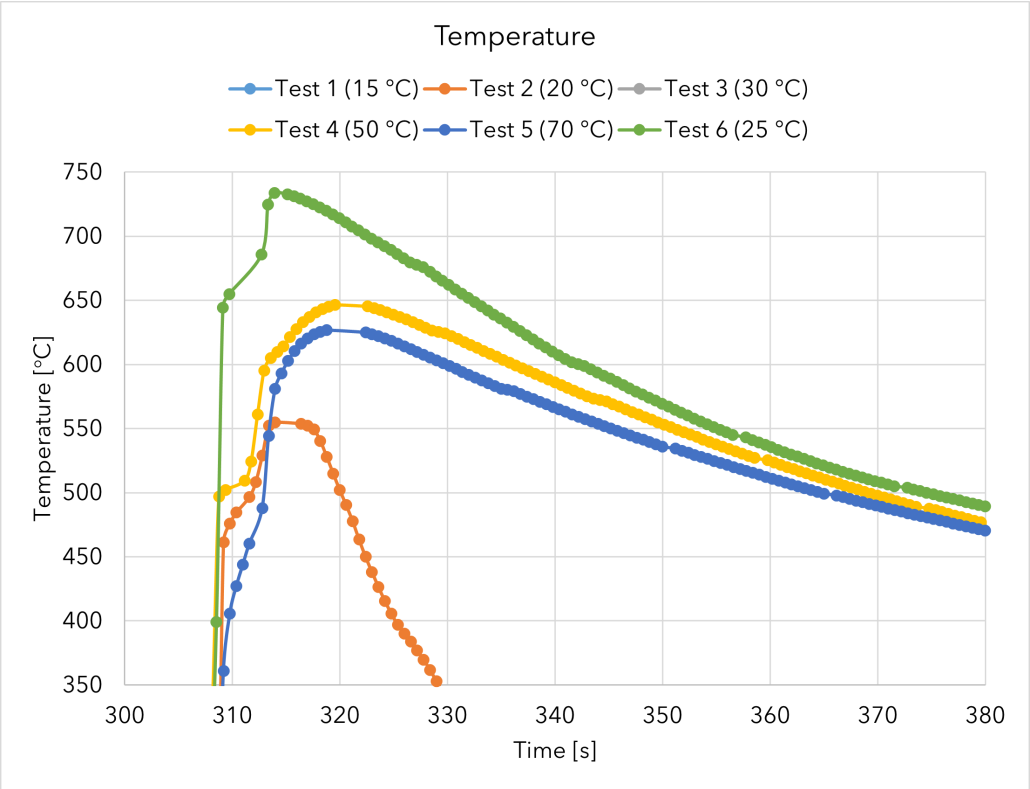

Figure 28: LG cells temperature profiles (zoom)

In figure 27 is reported the global temperature profile of each cell in different ambient conditions, from a minimum temperature around 15 °C and a maximum of 70 °C: as can be noticed, temperature profiles of Test 3 (30 °C) and Test 1 (15 °C) are the result of the thermocouple detachment; while for Test 2, the temperature sensor remained in contact with the cell during the nailing phase and detached later probably during the retraction of the nail. The increment in temperature is very fast after the perforation and it is possible to appreciate some analogies between the cells at different temperatures: the yellow and blue curves, respectively at 50 °C and 70 °C can almost overlap and both reached a maximum temperature around 650 °C. For the orange curve and the green curve obtained at 20 °C and 25 °C the behaviour is also similar but there is no certainty about the maximum temperature reached during the test at 20 °C because of the detachment of the temperature sensor when the nail is retracted; this theory is confirmed by the strong difference in the cooling curve: for test 4, 5 and 6 the cooling behaviour is the same and also slower if compared with the test 2. The only difference is the final temperature after the cooling process, which is of course lower as the ambient temperature of the test is lower and this allows a faster cooling process

of the cell once the internal heat generation stops. Another common behaviour can be noticed in the change of slope of the curves: for a period of time around 5 seconds, the slope of all 4 curves decreases slightly and then increases again right before the maximum temperature. This change is related to the evaporation of the electrolyte due to the high temperature developed inside the cell: the amount of heat generated by the current flowing inside the cell causes the evaporation of the electrolyte; it is an endothermic reaction, which absorbs heat produced inside the cell, modifying the gradient of temperature. To better understand this behaviour, temperature rates, expressed as °C/min, are obtained by data collected from the thermocouple, and once put in comparison, an interesting behaviour appeared.

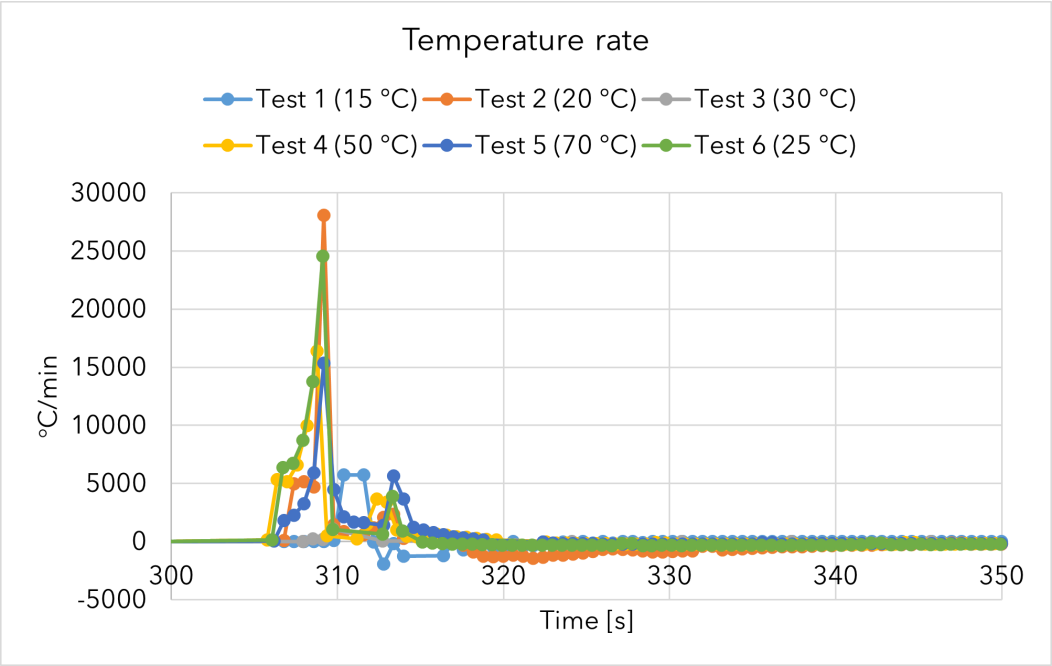

Figure 29: LG cells temperature rate profiles

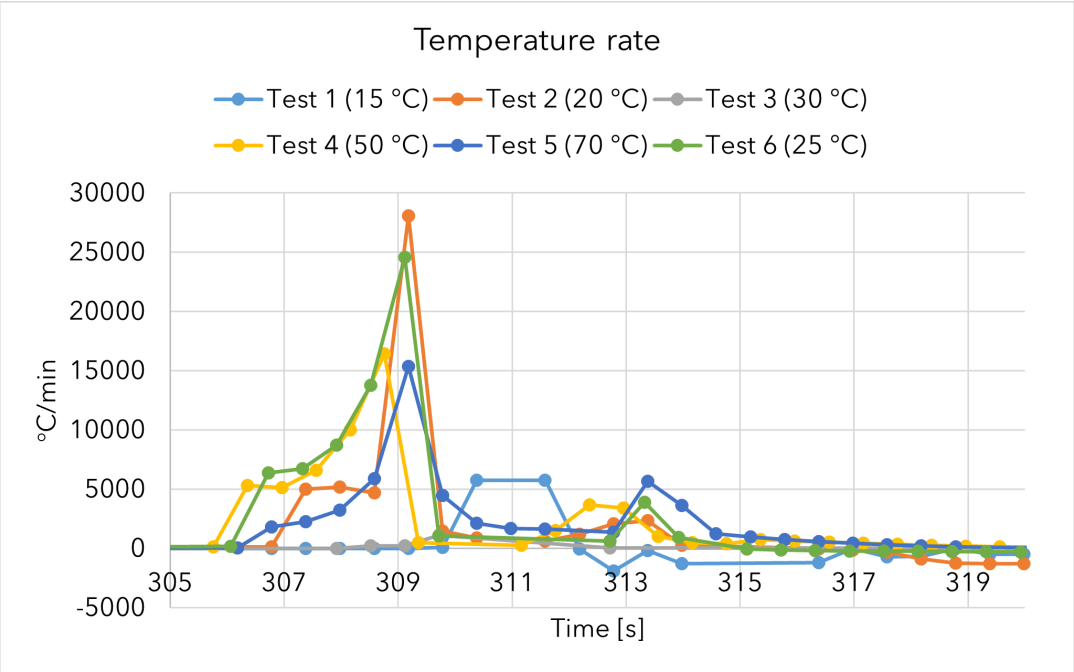

Figure 30: LG cells temperature rate profiles (zoom)

In terms of maximum reached temperature it is not possible to classify all the batteries since in some cases the thermocouple has detached from the cell, but focusing on the gradient of temperature with respect to time (°C/min), two distinguished behaviours appear, as shown in figure 29 and zoomed in figure 30. The temperature rate curves appear to be coupled: the behaviour of Test 2 is similar to that of Test 6 (respectively at 20 and 25 °C) since the green curve reaches a first maximum point at 25000 °C/min while the orange curve maximum point is at around 28000 °C/min. Another similar behaviour with lower increase rate is found for Test 4 which is similar to Test 5 (respectively 50 °C and 70 °C): the yellow curve reaches a maximum point at around 17000 °C/min while the blue curve finds its maximum point a little bit lower at 16000 °C/min. All curves present the first maximum point between 15000 °C/min and 28000 °C/min, followed by a second maximum point between 3000 °C/min and 5500 °C/min obtained after the evaporation of the electrolyte, which caused a partial decrement of the temperature rate. With this data it is noticeable that increasing the temperature of the environment, the violence of the reaction reduces. Also the duration of the thermal runaway is comparable, they all started at around 305 s and ended at around 315 s, while the time needed for the battery to reach the ambient temperature (which varies between a minimum of 20 °C and a maximum of 70 °C) in all cases

is higher than 2000 s. Thanks to the temperature rate is possible to understand the dynamic of the thermal runaway right after the puncturing of the nail, and from this data appears that increasing the initial temperature of the cell (between 20 °C and 70 °C), the temperature increment rate decreases. Another parameter obtained from the ARC is the pressure inside the chamber, which helps to understand what happened after the penetration and with respect to the temperature is proven to be a less difficult parameter to record.

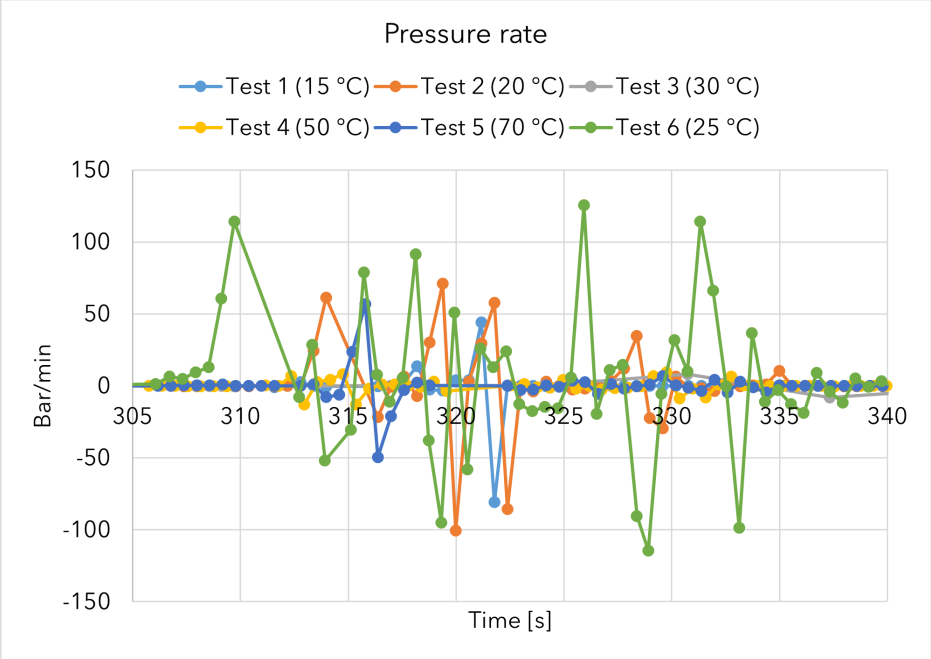

Figure 31: LG cells pressure rate profiles (zoom)

The pressure increase rate is expressed as the pressure variation with respect to time (Bar/min), which is shown in figure 31. Also in this case the highest values are recorded for the test performed at lower temperature (20 °C and 25 °C), while lower values are recorded for the high temperature tests (50 °C and 70 °C). The higher values are obtained for the Test 6 at 25 °C, followed by lower peak values for Test 2 at 20 °C. This information helps to confirm that, at least as first hypotheses, the lower the temperature, the higher the violence of the thermal runaway. The day after the nail test, batteries are removed and placed one close to another in order to take pictures; photos of the LG 18650 are reported in the following pages.

Figure 32: Test 1 15 °C (left) Test 2 20 °C (right)

Figure 33: Test 3 30 °C (left) Test 4 50 °C (right)

Figure 34: Test 5 70 °C (left) Test 6 25 °C (right)

In first place it is possible to notice that the upper part of the cell, where the pressure valve is positioned, is the one with most deposits of carbon particles since on the top is where gases are able to exit after the penetration. Batteries of test 2, 3 and 6, respectively 20 °C, 30 °C and 25 °C in addition to the deposits of carbon on the top part, present other breaking points on the case different from the penetration point of the nail. Additional fracturing points can be symptoms of a higher internal pressure inside the battery: the sudden gas production induced by the heat generated inside the cell can cause the rupture of other parts of the cell in addition to the safety valve, especially if the zone of breakage is already subjected to intense heat. In all cases, the additional breaking points are positioned in the medium-top section of the cell (Test 2) or near the puncturing point of the nail (Test 3 and Test 6). The most stressed points in fact are reported to be, from the thermal point of view, the middle section where the nail puts in short circuit the cell because of the concentration of electric current; the other stressed point is the top part where hot gases tend to accumulate and then release after the safety valve opening [36]. Pictures of the cells can further help to characterize the behaviour during the abuse; the presence of a higher number of cracks on the external surface for batteries tested between 20 °C and 30 °C can confirm the previous hypothesis: the lower the initial temperature of the cell, the higher the violence of the thermal runaway.
Another useful instrument to characterize the nail test is the infra-red camera:

in the following pages are reported screenshots of the videos recorded inside the chamber; the pictures captured from the video are sampled every 5 s. With the help of the videos it is possible to understand what happened inside the chamber also when the thermocouple detached from the battery, at least from a qualitative point of view. Thanks to the recorded videos it is possible to see also the escape of the gases from the top part of the cell. Around 1 minute after the puncturing, the cell temperature becomes uniform with the metal plate to which it is fixed. As the temperature inside the chamber increases, the time required to the cell to merge with the plate decrease and also it is more difficult to distinguish the image since the temperatures of the cell and the surroundings become closer. In all the performed tests, after the nail hits the battery, the heat propagates almost instantaneously from the center of the cell towards the poles; after the complete discharge of the cell (due to the internal damage), it starts to cool down faster with respect to the middle section both because of the larger surface exposed to the air and also because the middle section is where electric current is concentrated and for this reason is the hottest part.

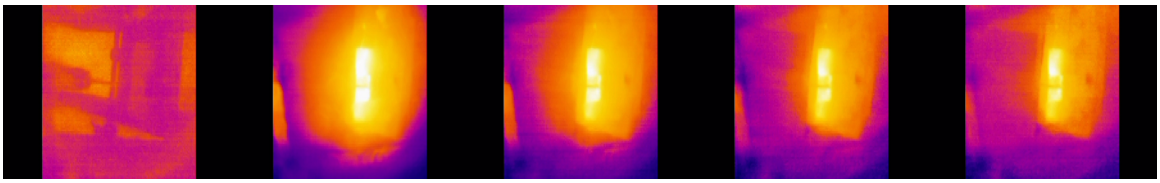

Figure 35: Test 2 20 °C

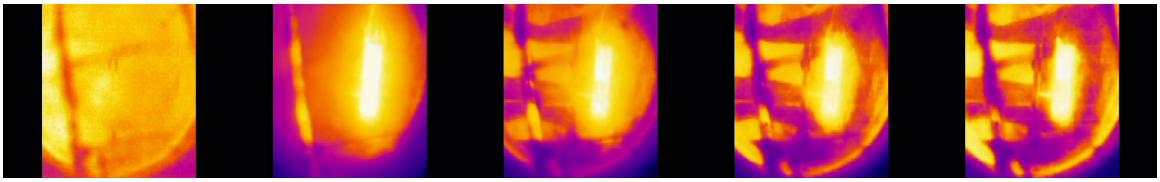

Figure 36: Test 3 30 °C

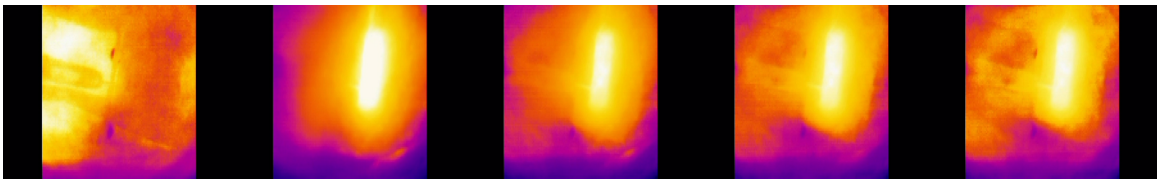

Figure 37: Test 4 50 °C

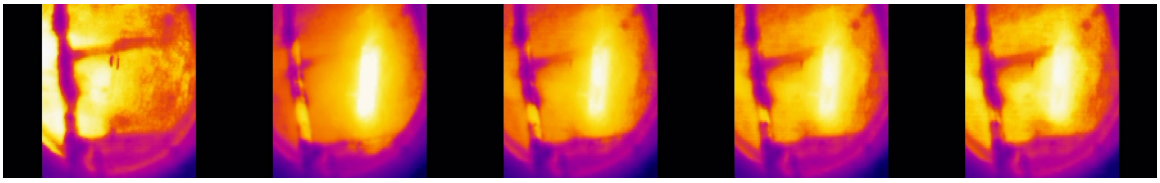

Figure 38: Test 5 70 °C

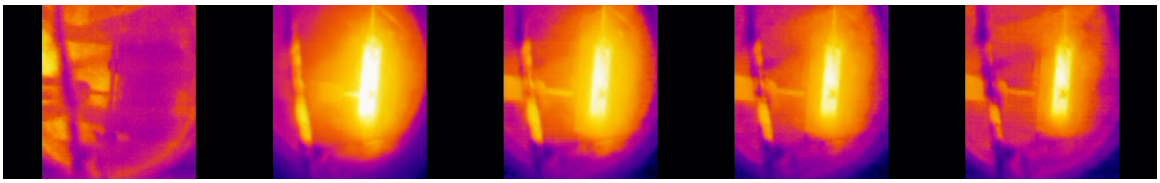

Figure 39: Test 6 25 °C

For what concerns the gas production, the main parameters recorded from the gas probe are: CO, NO, $\%O_2$, $\%CO_2$.

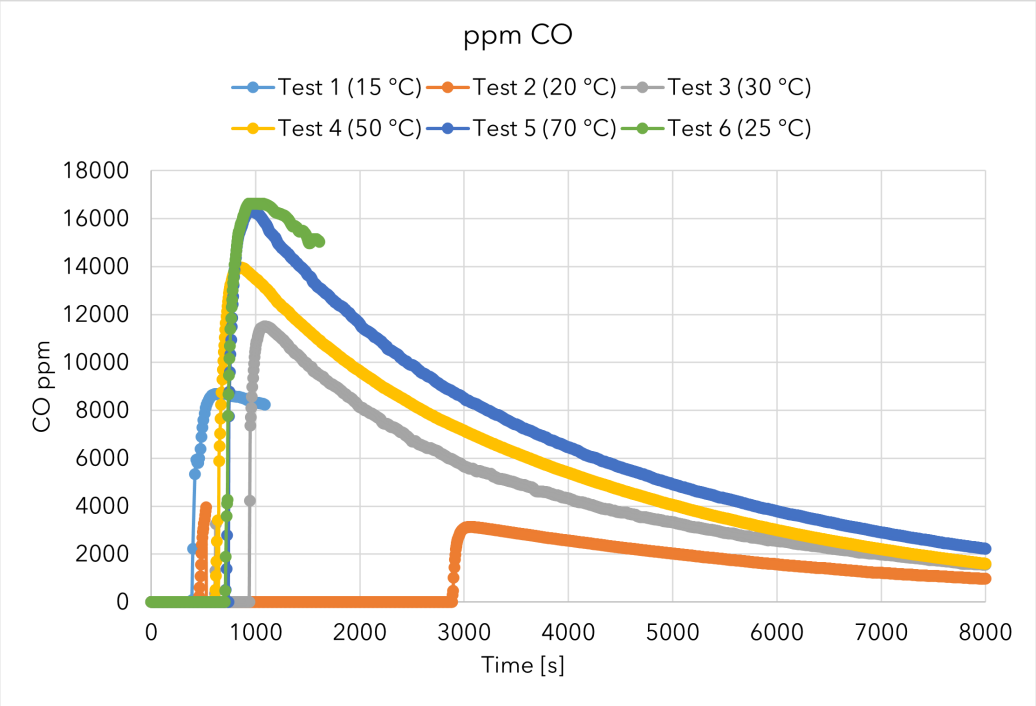

Figure 40: LG cells CO concentrations

Graphs of CO and NO concentrations expressed in ppm are reported in figure 40 and in figure 41. Unfortunately, due to connection problems with the probe, some information was lost during the acquisition. The results, at least for the first 5 tests, showed that increasing the ambient temperature increase both the production of carbon monoxide and nitrogen monoxide. The highest CO value recorded is around 16000 ppm for test 6 (25 °C), very close to the maximum for the high temperature test at 70 °C (Test 5); for the NO is noticeable also an increasing production with the increasing temperature inside the chamber, again with the exception of test performed at 25 °C. Unfortunately, for Test 2, due to connection problem, the maximum values for NO and CO are unknown.

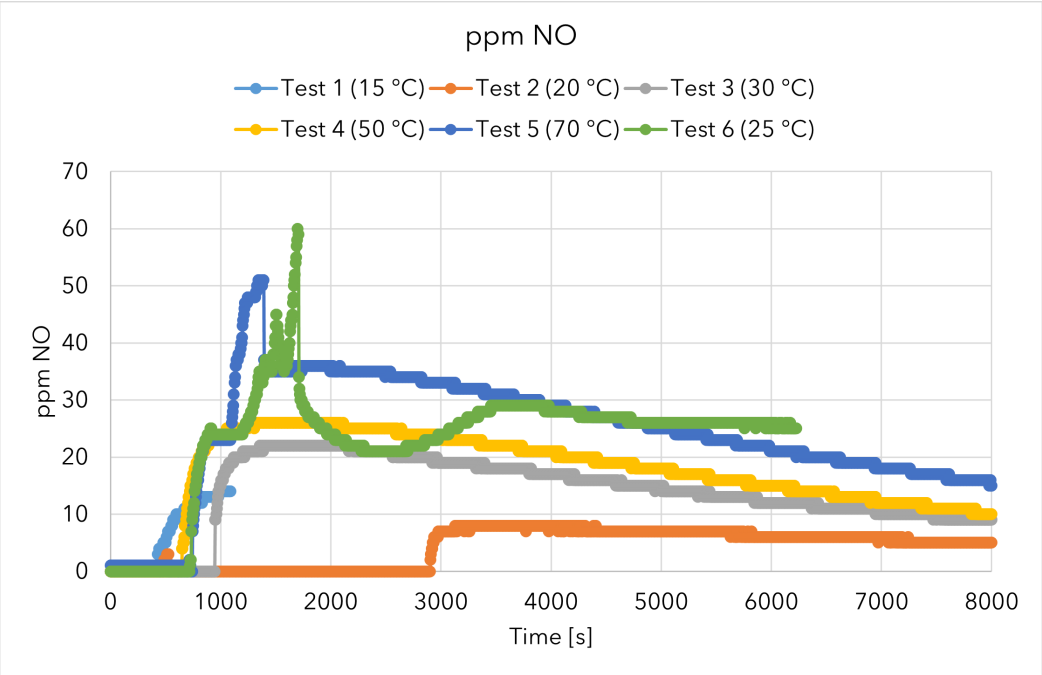

Figure 41: LG cells NO concentrations

Values of $\%O_2$ and $\%CO_2$ are reported in figure 42 and figure 43; it is possible to notice that the lowest concentration of oxygen after the combustion and the highest concentration of carbon dioxide are obtained for test 2 and test 6. Tests performed at higher temperature, test 4 and test 5, on the other hand, consumed a lower amount of oxygen and produced also a lower quantity of CO_2. From the data obtained by the gas probe, the amount of oxygen available for combustion in percentage terms is lower, as the volume of air increases with temperature; the lower temperature allows an higher amount of oxygen in the same volume and the higher the amount of oxygen, the easier is the oxidation process during the combustion phase. From the consumption of oxygen and production of CO_2, it is evident that thermal runaway occurred at lower temperature (20 and 25 °C) are favoured with respect to the ones at higher temperature (50 and 70 °C).

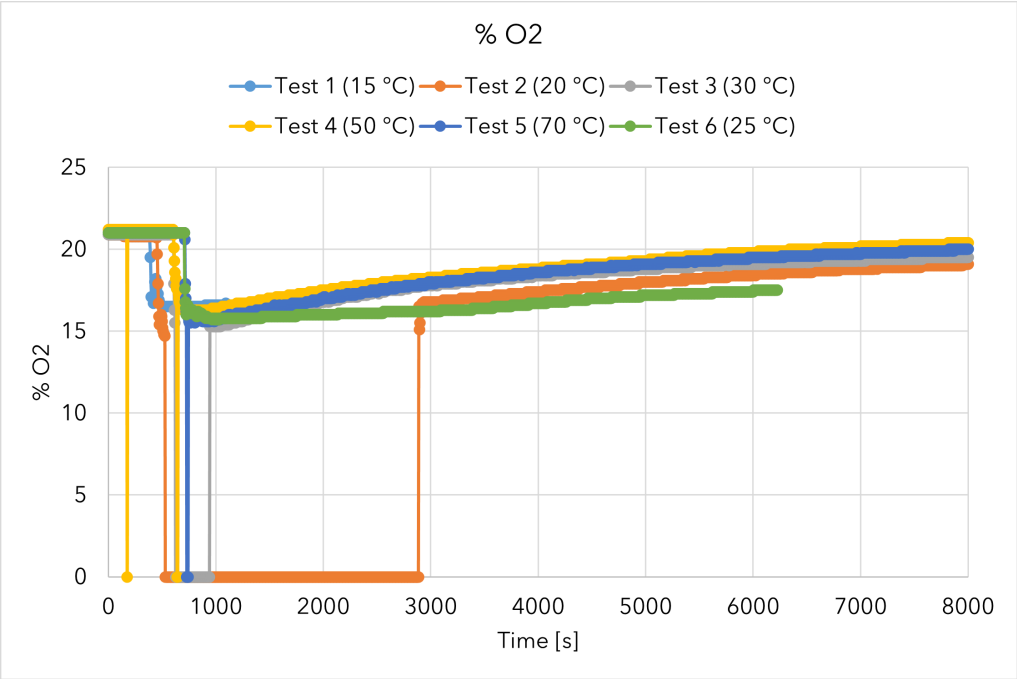

Figure 42: LG cells $\%O_2$

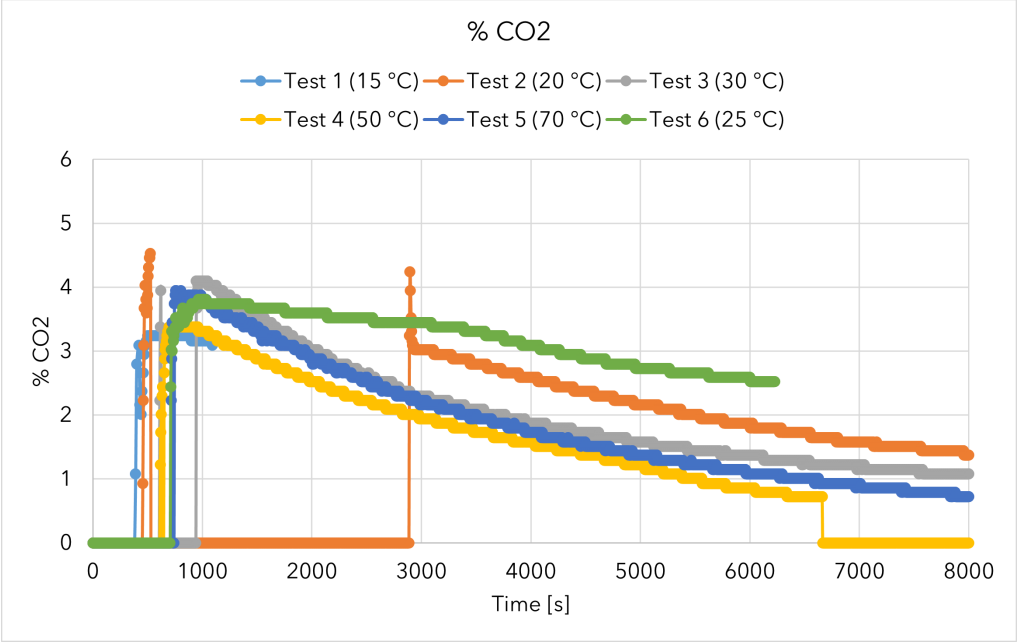

Figure 43: LG cells $\%CO_2$

After the analysis on LG INR18650 M29 (new cells), nail test are performed on Samsung INR18650-15L, which are batteries removed from a battery pack and

which were subjected to a number of cycles higher than a thousand. All batteries have lost around 30 % of their nominal capacity (1500 mAh), but are proven as still working. As before, batteries are placed inside the chamber to perform the nail test. Results of temperature profiles are reported in figure 44

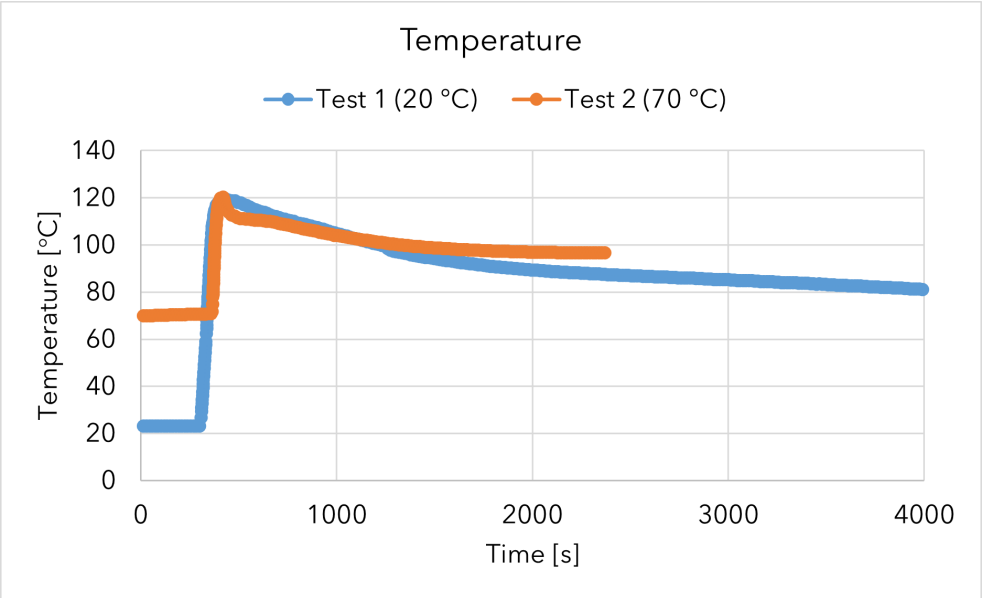

Figure 44: Samsung cells (cycled) temperature profiles

Due to problem during the tests, temperature measurements were stopped before the full cooling process, but the maximum temperature was recorded. It is clear that the maximum temperature is much lower with respect to new cells. In both cases, the maximum recorded temperature is 120 °C (a third penetration test, reported as Test 0, was performed at 20 °C but the data was not saved, also in that case the maximum temperature was 116 °C). In comparison with new cells, at same environment temperature, the maximum surface temperature was 550 °C for test at 20 °C and 730 °C for test at 25 °C, while for 70 °C the maximum was reached at 630 °C; with this data is clear how the ageing process influences the thermal runaway. Another difference is the duration of the discharge process: for new batteries, after the triggering of the thermal runaway, the internal heat generation destroys the cell and after 2000 s the temperature of the cell reaches an equilibrium condition with the environment. For cycled cells, the heat generation is not sufficient to trigger the thermal runaway and destroy the cell, so the heat generation lasts longer (cell's temperature of Test 1 was higher than 40 °C after 20000 s). These results are even more surprising if the difference in the maximum discharge current is considered: from data sheets, reported in table 3 and

table 5, the maximum discharge currents are respectively 10 A for the LG and 18 A for the Samsung cell. Despite the higher maximum discharge current declared, the ageing process has reduced the ability of the electrolyte and the electrodes to exchange ions, so that when high current is demanded, in this case due to internal short circuit, the voltage of the battery drops very quickly and so does the current. The ageing process is related to many factors so that is impossible to say certainly, in this case, which one is the main cause. A study, [35], reports that the main reasons for battery ageing are the loss of active material and Lithium plating. These phenomena reduce the amount of available Lithium ions during the charge/discharge; the reduction of ions is, for example, connected to the increment of the thickness of the SEI (Solid Electrolyte Interphase): this thin layer separates the anode and the cathode from the electrolyte stabilizing the cell. The Lithium ions consumed during this process are no longer able for the charge/discharge phases, reducing the actual capacity of the cell (as found in table 6). Ageing of the cell is an inevitable phenomenon that can be promoted by charge current, high and low temperature and cut-off voltage to make some examples [35]. Samsung cells employed in this nail test were subjected to a normal use cycling and for this reason the cause of their damaging is mainly related to the time and cycling. A zoomed portion of the maximum temperature is reported in figure 45.

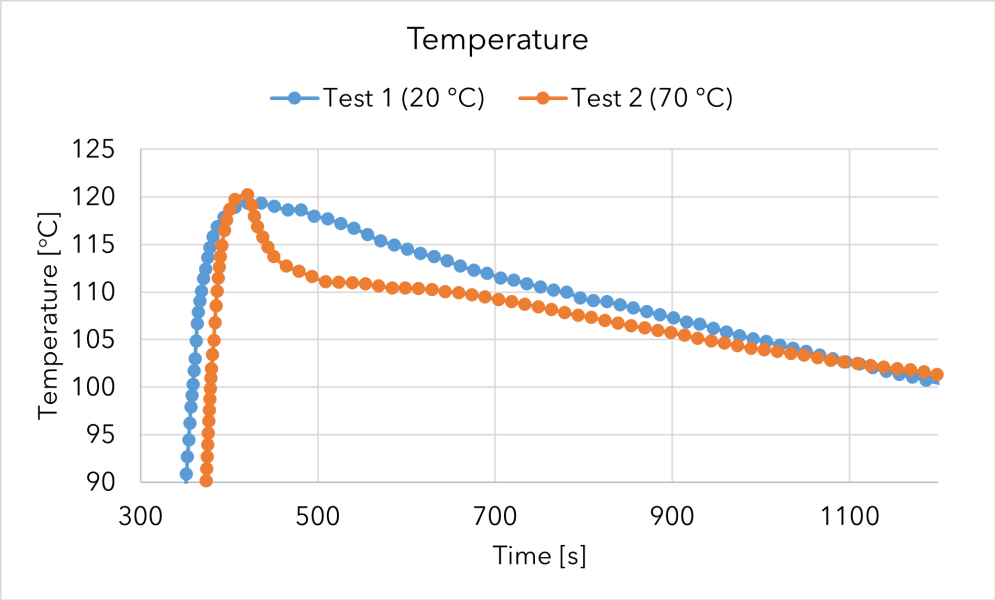

Figure 45: Samsung cells (cycled) temperature profiles (zoom)

Also the temperature increase rate is much lower with respect to the new cells, due to the lower maximum temperature and also due to the higher amount of time

requested to reach it; the reaction after the puncturing appears to be slower and less violent, but more persistent and lasting. Figure 46 shows the temperature rate of the cells: the maximum value of increase in temperature recorded for cycled cells is 320 °C/min for Test 2 at 70 °C, while for new cells the maximum is around 28000 °C/min for Test 2 at 20 °C. Also the duration of the heat generation is different: for cycled cells, the heat generation that caused an increase in temperature lasted for 60 seconds at 20 °C and, around 30 seconds for test at 70 °C; for new cells, the increase in temperature lasted for a maximum of 10 seconds due to the damage of the cell. For Test 1, the first maximum at around 280 °C/min is followed by a constant value around 80 °C/min (evaporation of the electrolyte) and then another relative maximum value around 240 °C/min. While, for the second test at 70 °C, the maximum value recorded is slightly higher (320 °C/min) followed by a lower value at 120 °C/min due to again the evaporation of the electrolyte.

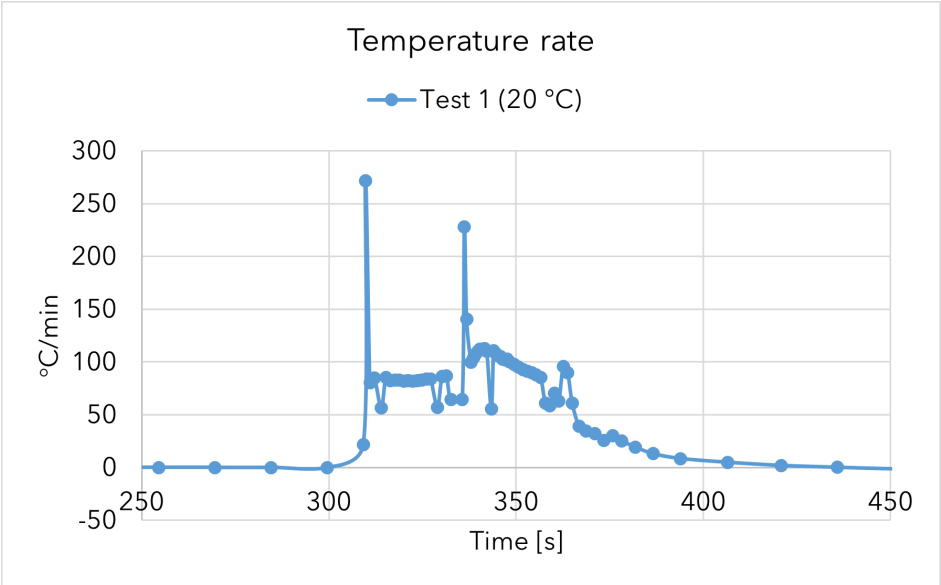

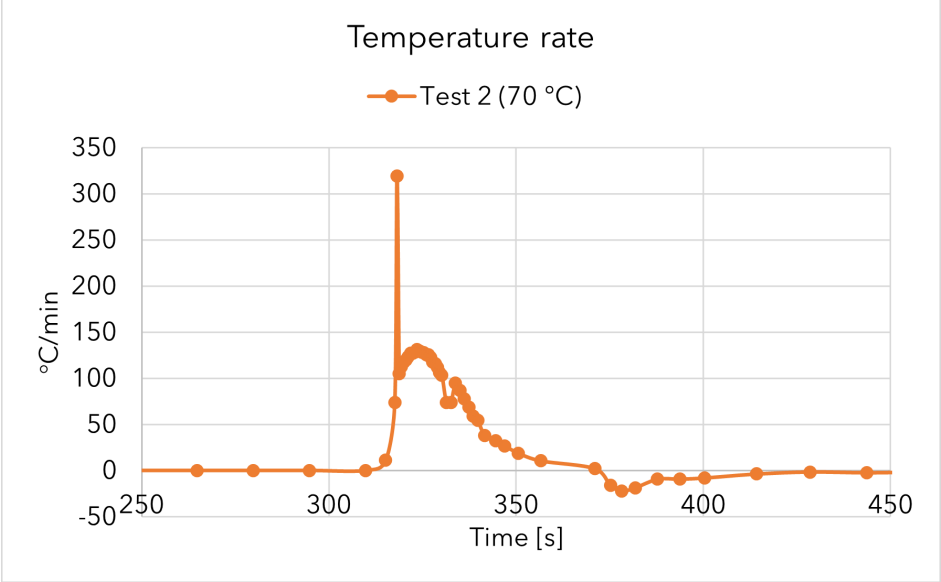

Figure 46: Samsung Temperature rate zoom Test 1 (up) Test 2 (down)

The effect of the lower surface temperature recorded after the nail penetration is also confirmed by the pictures taken after the extraction from the chamber, reported below.

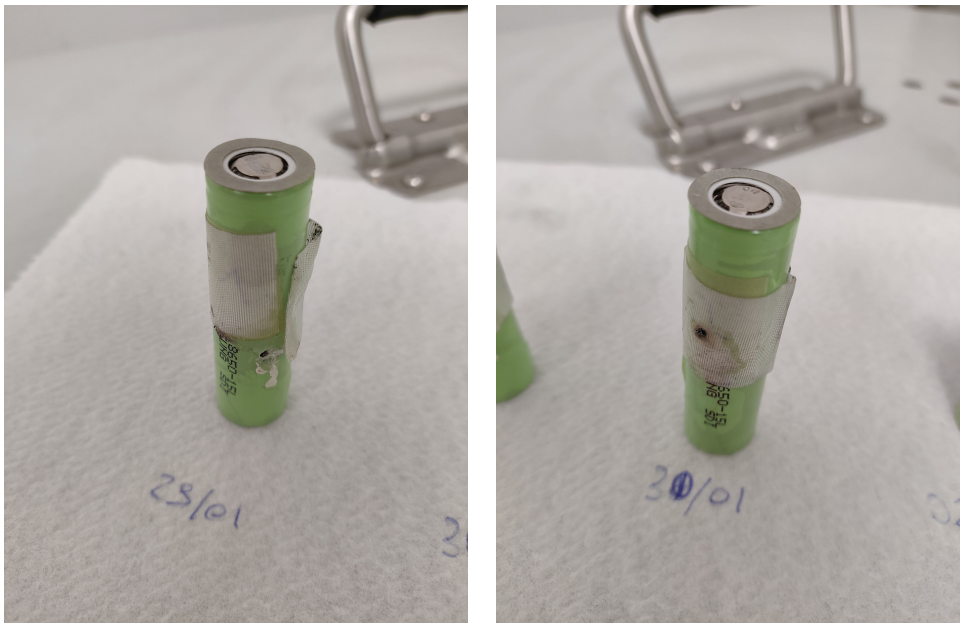

Figure 47: Samsung cells (cycled) Test 0 20 °C (left) Test 1 20 °C (right)

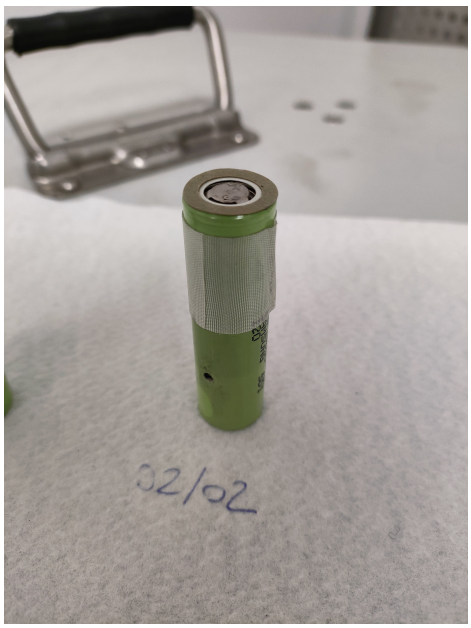

Figure 48: Samsung cell (cycled) Test 2 (70 °C)

Pictures of the cells after nail tests reported in figure 47 and figure 48 confirm what has been obtained from the thermocouple: all cells are not externally damaged, differently from new cells, the plastic wrap around the case has not shrank and has not burned; there is not carbon deposit on top size and no evi-

dent damages on the external surface are noticeable. From the videos obtained by the infra-red camera it is possible to appreciate the difference during the spread of the heat after the nail penetration: for new cells, right after the nail hit the cell, the heat generation is almost instantaneous and the image of the cell becomes bright with respect to the surrounding environment; the heating process of the Samsung battery is much slower and starts from the center of the cell and then spreads to the top and bottom part. The temperature difference is noticeable especially for tests performed at 70 °C: during the test for the new cells, shown in figure 38, the background, after the penetration, becomes dark because the temperature is much lower in comparison with the one of cell (around 600 °C); for the cycled battery at 70 °C, shown in figure 50, the background remains almost of the same color of the picture before the nail test, representing the fact that the temperature difference between the walls of the chamber and the battery is not so high since the cell's temperature is around 120 °C.

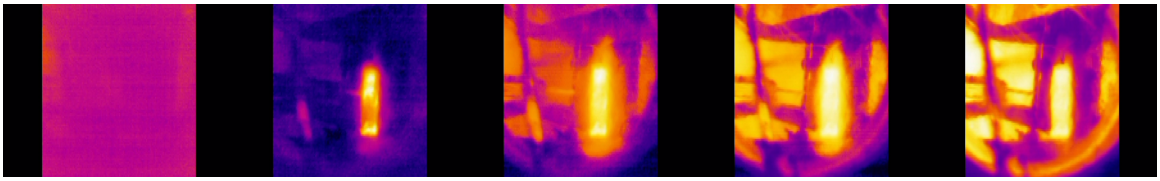

Figure 49: Samsung Test 1 20 °C

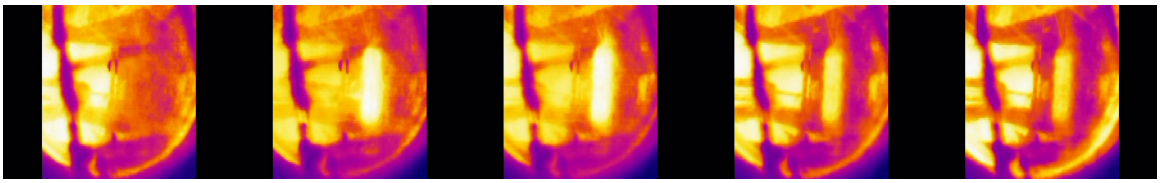

Figure 50: Samsung Test 2 70 °C

The data obtained from the gas probe is also collected and, despite some connection problems, many differences in comparison with new cells can be noticed.

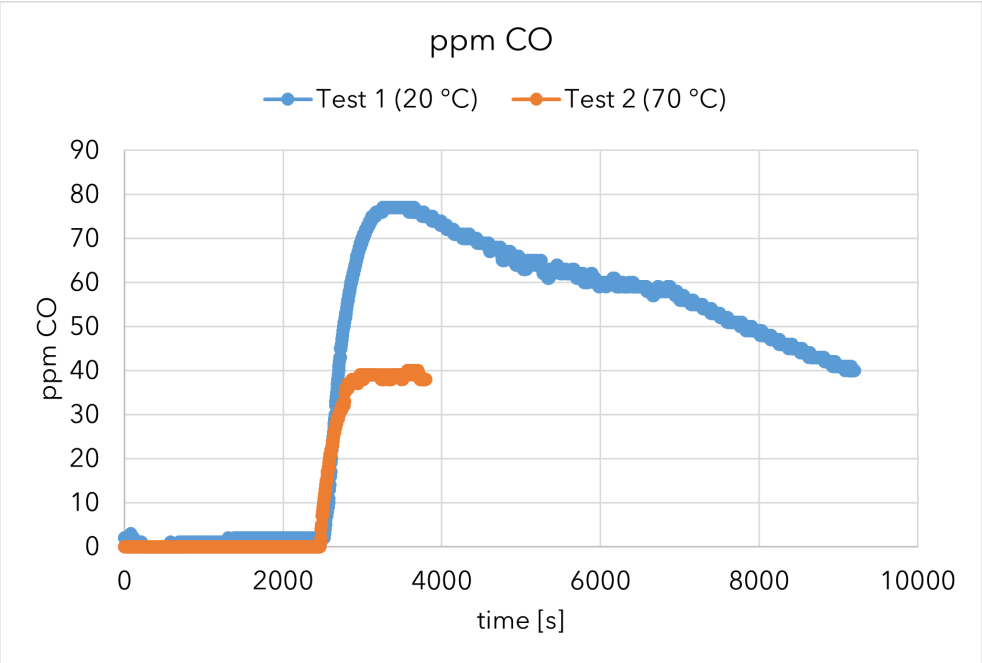

Figure 51: Samsung cells (cycled) CO concentrations

Because of much lower temperature, the gas production is considerably lower in comparison with new cells, for the CO, maximum value recorded is around 80 ppm for the test at 20 °C and, in contradiction with what obtained previously, a lower amount of carbon dioxide is produced increasing the temperature, even if the numbers can be considered close one to the other if compared to 16000 ppm recorded during tests for new cells. About the Nitrogen monoxide, NO, which in the previous test varied between a minimum of 15 ppm for Test 1 at 15 °C and a maximum of 60 ppm for Test 6 at 25 °C, in this case the values varied between 1 and 2 ppm; these values confirm that the production of NO is related to the high temperature reached inside (and outside) the cell: the oxidation process of Nitrogen requires high temperature, which, in case of aged cells, is not reached. Lastly, these results are confirmed by the percentage of oxygen: it is evident a small reduction in the concentration of O_2 that is mostly related to the production of other gaseous species since no combustion is evident. The $\%CO_2$ graph is not reported since in both cases, no production of this gas was evident. Graphs of the produced gases are reported in figure 51, 52 and 53.

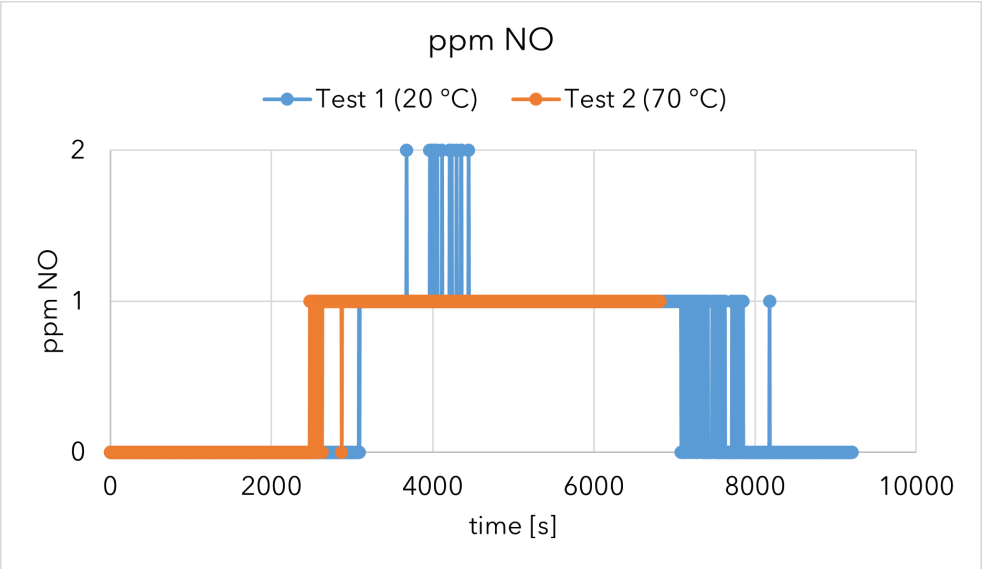

Figure 52: Samsung cells (cycled) NO concentrations

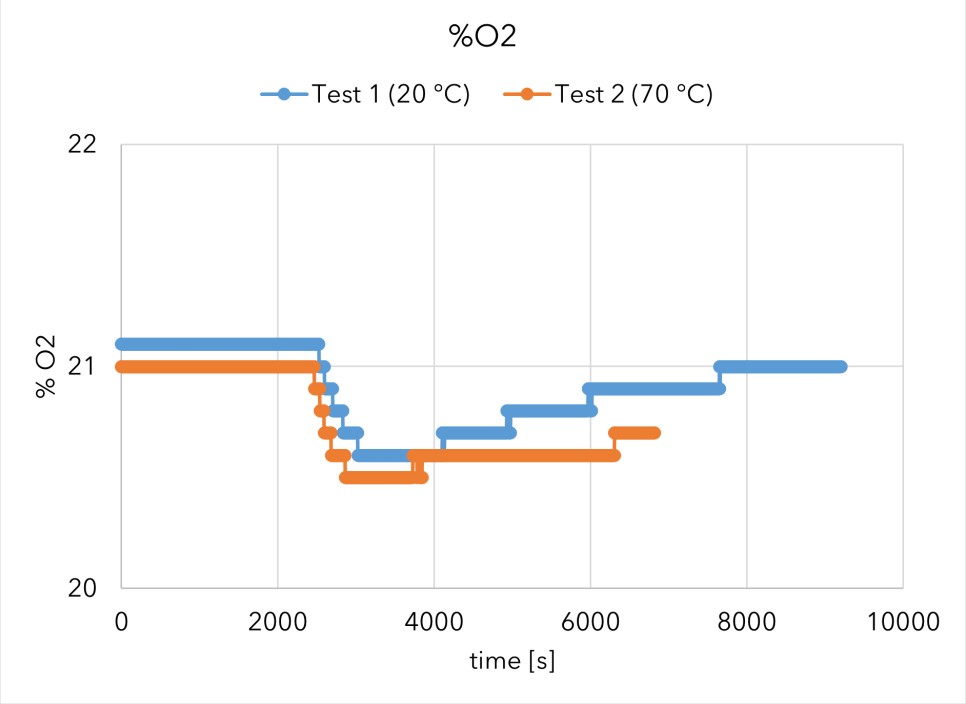

Figure 53: Samsung cells (cycled) $\%O_2$

In addition to nail testing, 2 cells were subjected to overheating inside the chamber to understand the effect of high temperature on the thermal runaway triggering. To perform this test, some parameters of the ARC need to be adjusted but

in comparison with nail testing, the temperature rate increment is faster and this allows a lower time to reach high temperatures. As before, the cell is positioned inside the chamber and blocked with high temperature tape in contact with the thermocouple. During the Test 1 a new LG cell at 100% SOC is used while during the Test 2 a cycled Samsung cell is used also charged at 100%. The setpoint temperature of the calorimeter is set to 150 °C, and can be increased during the test. In figure 54, it is shown the temperature profile of both the new and the cycled cell; the new cell started the self-heating process at around 140 °C, followed by the thermal runaway. The cycled cell, Test 2, has been heated up to 165 °C and no evident self-heating process was detected, and also no thermal runaway occurred, even increasing the temperature 25 °C more with respect to the new cell. The maximum temperature recorded during thermal runaway is 1300 °C, but after consulting videos recorded by the infra-red camera, it can be noticed that due to pressure release on top of the cell during thermal runaway, the battery slipped downward and probably the tip of the thermocouple was invested by the hot gases generated inside the cell. Even if the temperature profile is not a perfect representation of the surface temperature, is still a qualitative parameter to understand the temperature at which the self-heating has started.

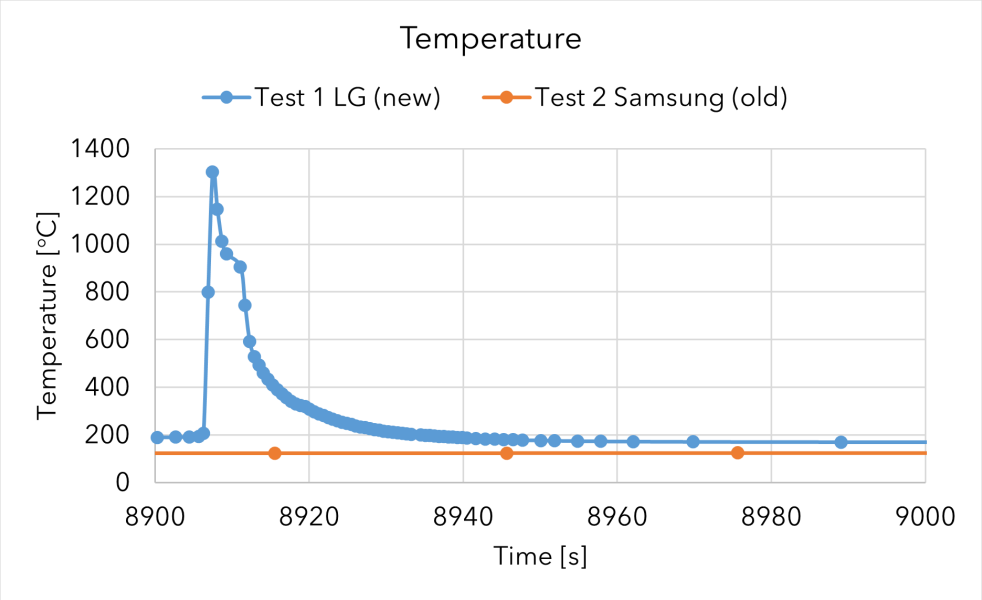

Figure 54: Overheating Temperature profiles

During the heating process of the batteries, both of them presented a decrease in surface temperature, as shown in figure 55. This behaviour is related to the

evaporation of the electrolyte after the safety valve opening: gases generated inside the cell increase the internal pressure until the safety valve opens and with the reduction of pressure starts the endothermic process of evaporation, which subtract heat from the cell and thus reduces its surface temperature [31]. The valve opening happened at different temperatures: the LG valve opened at 133 °C while the Samsung opened at 121 °C; if the threshold pressure is assumed to be the same, as hypothesis, this result proves that the gas production due to decomposition of the electrolyte starts earlier for aged cells.

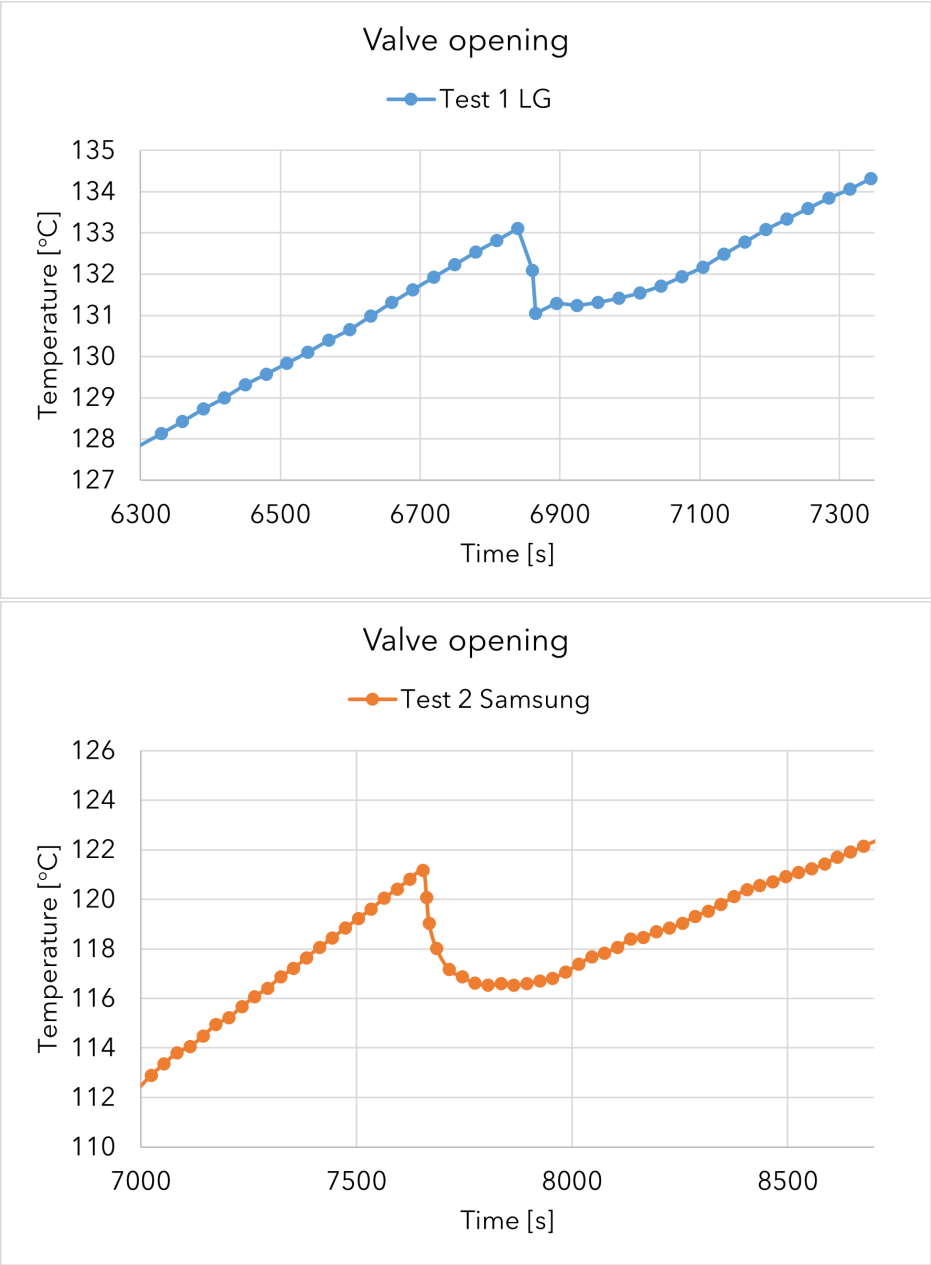

Figure 55: Valve Opening Test 1 LG (up) Test 2 Samsung (down)

Finally in figure 57, it is shown a comparison in temperature profiles for both cells: it is clear how in Test 1 the increment starts slowly at around 140 °C (temperature rate is around 1-2 °C/min) and becomes faster when the cell's temperature reaches 160 °C; after that point the thermal runaway starts. For Test 2, on the other hand, it is noticeable a slight change in the temperature gradient at around 135 °C, but not sufficient to trigger thermal runaway; the heating process of the

chamber is carried out until 165 °C and then stopped since nothing relevant happened. In both tests, the gas probe was inserted but due to problems during the saving process, in both cases results were lost. For Test 2 last recorded value was at 164 °C and results are: 346 ppm for the CO, 20,1 %O_2 and NO 2 ppm; values for the first test are assumed to be much higher since combustion occurred. In figure 58, is reported the sequence of screenshots obtained from the video of the infra-red camera: the time between each picture is also in this case around 5 seconds. It is evident that the cells starts to heat-up quickly and in the last picture a change in the shot framing is noticeable: this difference is related to the impact of the cell with the bottom of the chamber which caused the displacement of the camera. From the video is clear that after the self-heating process started at 140 °C, the gas production inside the cell increases until a violent expulsion of hot gases from the top happens; this phenomenon generates a downward push that detached the battery from the plate. To further confirm what occurred inside the chamber, in figure 56 are reported pictures of the cells after the extraction.

Figure 56: LG cell overheating (left) Samsung cell overheating (right)

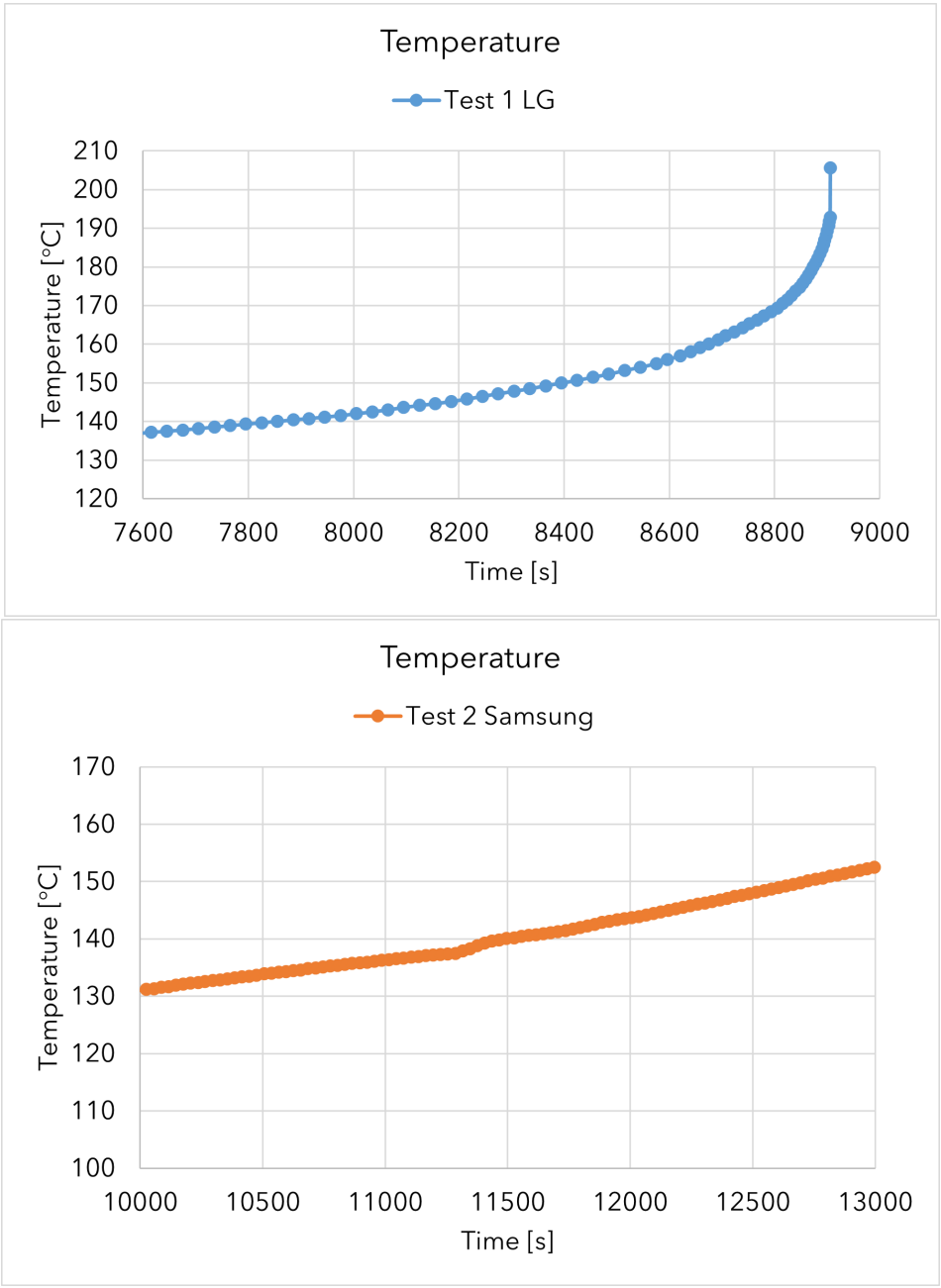

Figure 57: Temperature gradient zoom Test 1 LG (up) Test 2 Samsung (down)

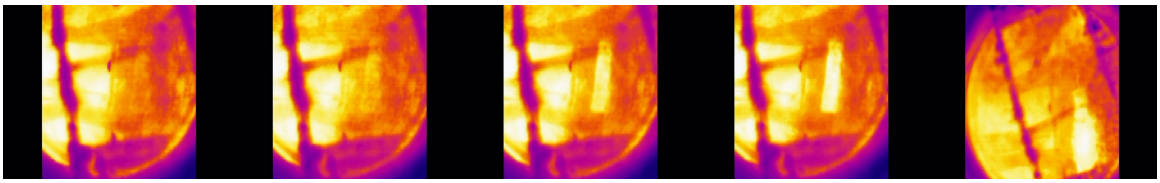

Figure 58: Samsung Test 1 150 °C

After all tests (nail and overheating) the cells are weighed to evaluate the mass consumption. The initial weight of the LG cell is 45 g and the initial weight of the Samsung cell is 43 g.

Cell	Weight [g]	Weight loss [%]
LG Cell 1 nail test 15 °C	25,6	43,1
LG Cell 2 nail test 20 °C	28,3	37,1
LG Cell 3 nail test 30 °C	24,5	45,6
LG Cell 4 nail test 50 °C	23	48,9
LG Cell 5 nail test 70 °C	25	44,4
LG Cell 6 nail test 25 °C	24,9	44,7
Samsung Cell 0 nail test 20 °C	42	2,3
Samsung Cell 1 nail test 20 °C	42	2,3
Samsung Cell 2 nail test 70 °C	40,8	5,1
LG Cell 1 overheating test 150 °C	17,8	60,4
Samsung Cell 1 overheating test 150 °C	40,6	5,6

Table 7: Cell's weight comparison after each test

All LG cells have lost around 40 % of their initial weight due to combustion, while cycled Samsung cells retained the majority of their initial mass since no combustion occurred. The lowest weight was recorded for the overheated LG cell (17.8 g). This value proves that the worst combustion process is obtained in overheating conditions rather than under mechanical abuse. The video of the IR-camera confirms this hypothesis since the explosion during overheating was so violent to detach the cell from the wall; this event has never occurred in all previous test conditions. The higher weight loss is obtained for the overheating test performed on the new cell, around 60% of mass is lost during the combustion phase. A study confirms this data [54]: the amount of mass lost during the thermal runaway is linked to the amount of heat provided to the cell; during nail testing the reaction is very violent but also really fast, on the other hand the slow heating phase which happens during overheating test, allows more uniform conduction of thermal en-

ergy. The heat generation inside the cell is after the nail penetration lasts around 10 s, after the cell is irreversibly damaged and the reaction is not anymore able to sustain itself, stopping or at least, slowing down the mass consumption. While for self heating, the process is more gradual allowing a uniform propagation of heat and for a longer amount of time, in figure 57 it is shown the heat generation phase, which starts at 7600 s (at 136 °C) and finishes with the thermal runaway triggering 1300 s after. This heat generation allows a higher consumption of material and thus a higher consumption of mass inside the cell. The same phenomenon is not found for older cells, since the internal heat generation is never triggered.

3.3 Conclusions

The abuses to which Lithium-ions batteries can be subjected to are multiple and differentiated. In this work, literature review allowed a general overview about the 3 main types of abuse: thermal, electrical and mechanical. The experimental section prove to be a difficult part to implement because of the high temperature and the high amount of heat generated during the tests; nevertheless, the obtained results can be useful to better understand the effect of ageing on LIBs during abuse conditions. For new cells, in this case LG 18650, the violence of the reaction and also the temperature increment appear to be higher if the cell is kept in optimal temperature range conditions (20-25 °C); even if in 1 case is not possible to be certain about the maximum reached temperature due to detachment of the thermocouple, the previous consideration is partially confirmed by data recorded from the calorimeter in terms of pressure gradient and gas concentration. For new cells, optimal temperature conditions are more dangerous in case of penetration of the case, since a faster reaction is produced with respect to higher temperature conditions. After the penetration phase, a high amount of toxic gases like CO and NO are produced due to combustion phase inside the cell. In all temperature conditions, for new cells, the thermal runaway is really violent but positive temperature increments lasts around 10 s in each test: after this period of time, the cell is completely broken and no longer able to produce current an thus sustain the reaction. The same tests performed on aged cells obtained completely different results. The first difference is the maximum reached temperature, which for new cells is around 730 °C while for cycled cells is 120 °C; the second difference is that cycled cells take more time to reach the maximum temperature and also the cooling process is much longer: while new cells after 2000 s from penetration already have reached the ambient temperature, cycled cells are still between 90 and 100 °C, proving that the discharge process is still happening but in a less violent manner. After visual inspection is clear that cycled cells do not burn since no carbon deposits are present on the surface and the plastic wrap is still intact; new cells, on the other hand, because of high temperature, are able to produce a higher amount of gases, like NO, CO and CO_2 while the production of this gases is very limited for cycled cells. Lastly, even with thermal abuse the cycled cells prove to be much safer if compared to new ones: for new cell the self-heating process followed by thermal runaway started at around 130 °C while even after reaching 160 °C no self-heating and no thermal runaway are detected for cycled cells. After different experimental tests on mechanical and thermal abuses in different temperature conditions, it is evident that a cycled battery loses with time its reactivity

together with its retained capacity, if compared to a new one; this is a phenomenon which presents disadvantages in terms of usage of the storage mean, but, on the other hand, guarantees a higher level of safety in case of accident.

References

[1] Ahmed Abaza et al. “Experimental study of internal and external short circuits of commercial automotive pouch lithium-ion cells”. In: *Journal of Energy Storage* 16 (2018), pp. 211–217. ISSN: 2352-152X.

[2] Sayem M. Abu et al. “State of the art of lithium-ion battery material potentials: An analytical evaluations, issues and future research directions”. In: *Journal of Cleaner Production* 394 (2023), p. 136246. ISSN: 0959-6526.

[3] Muhammad Umair Ali et al. “Towards a Smarter Battery Management System for Electric Vehicle Applications: A Critical Review of Lithium-Ion Battery State of Charge Estimation”. In: *Energies* 12.3 (2019). ISSN: 1996-1073. URL: https://www.mdpi.com/1996-1073/12/3/446.

[4] *AutoinsuranceEZ https://www.autoinsuranceez.com/*.

[5] Elaheh Bazdar et al. “Compressed air energy storage in integrated energy systems: A review”. In: *Renewable and Sustainable Energy Reviews* 167 (2022), p. 112701. ISSN: 1364-0321.

[6] “bp Statistical Review of World Energy”. In: (2022). URL: https://www.bp.com/en/global/corporate/energy-economics/statistical-review-of-world-energy.html.

[7] Mingyi Chen et al. “Investigation on thermal and fire propagation behaviors of multiple lithium-ion batteries within the package”. In: *Applied Thermal Engineering* 157 (2019), p. 113750. ISSN: 1359-4311.

[8] Gianfranco Chicco. *Smart Electricity Systems*. A.Y. 2022-2023.

[9] The International Council on Clean Transportation. “European vehicle market statistics: Pocketbook 2022/2023”. In: (2023).

[10] Minh Phuong Do et al. “Fruit waste-derived lixiviant: A viable green chemical for lithium-ion battery recycling”. In: *Journal of Cleaner Production* 420 (2023), p. 138303. ISSN: 0959-6526.

[11] *Dominion Energy https://www.dominionenergy.com/*.

[12] Jiaqiang E et al. “Effects of heating film and phase change material on preheating performance of the lithium-ion battery pack with large capacity under low temperature environment”. In: *Energy* 284 (2023), p. 129280. ISSN: 0360-5442.

[13] *Eco Lihtium Battery https://www.ecolithiumbattery.com/*.

[14] Hauke Engel, Patrick Hertzke, and Giulia Siccardo. “Second-life EV batteries: The newest value pool in energy storage”. In: *McKinsey & Company* (2019).

[15] Xuning Feng et al. “A 3D thermal runaway propagation model for a large format lithium ion battery module”. In: *Energy* 115 (2016), pp. 194–208. ISSN: 0360-5442.

[16] Meike Fleischhammer et al. “Interaction of cyclic ageing at high-rate and low temperatures and safety in lithium-ion batteries”. In: *Journal of Power Sources* 274 (2015), pp. 432–439. ISSN: 0378-7753.

[17] Johanna K. Stark Goodman et al. “Lithium-ion cell response to mechanical abuse: Three-point bend”. In: *Journal of Energy Storage* 28 (2020), p. 101244. ISSN: 2352-152X.

[18] Husam Abdulrasool Hasan et al. “Thermal performance assessment for an array of cylindrical Lithium-Ion battery cells using an Air-Cooling system”. In: *Applied Energy* 346 (2023), p. 121354. ISSN: 0306-2619.

[19] *https://www.batteryuniversity.com/*.

[20] *https://www.europarl.europa.eu/portal/en*.

[21] *https://www.iea.org/reports/key-world-energy-statistics-2021/*.

[22] *https://www.irena.org/*.

[23] Abhishek Jaiswal. “Lithium-ion battery based renewable energy solution for off-grid electricity: A techno-economic analysis”. In: *Renewable and Sustainable Energy Reviews* 72 (2017), pp. 922–934. ISSN: 1364-0321.

[24] Taskin Jamal et al. “Fuelling the future: An in-depth review of recent trends, challenges and opportunities of hydrogen fuel cell for a sustainable hydrogen economy”. In: *Energy Reports* 10 (2023), pp. 2103–2127. ISSN: 2352-4847.

[25] Manish Kumar Kar, Mehmet Ali Recai nal, and Chenna Rao Borra. “Alumina recovery from bauxite residue: A concise review”. In: *Resources, Conservation and Recycling* 198 (2023), p. 107158. ISSN: 0921-3449.

[26] F M Nizam Uddin Khan et al. “Design and optimization of lithium-ion battery as an efficient energy storage device for electric vehicles: A comprehensive review”. In: *Journal of Energy Storage* 71 (2023), p. 108033. ISSN: 2352-152X.

[27] F.M. Nizam Uddin Khan et al. “Maximizing energy density of lithium-ion batteries for electric vehicles: A critical review”. In: *Energy Reports* 9 (2023). Proceedings of 2022 7th International Conference on Renewable Energy and Conservation, pp. 11–21. ISSN: 2352-4847.

[28] Felix Leach et al. “The scope for improving the efficiency and environmental impact of internal combustion engines”. In: *Transportation Engineering* 1 (2020), p. 100005. ISSN: 2666-691X.

[29] Pierluigi Leone. *Thermal Design and optimization*. A.Y. 2021-2022.

[30] Pengwei Li et al. “Progress, challenges, and prospects of spent lithium-ion batteries recycling: A review”. In: *Journal of Energy Chemistry* (2023). ISSN: 2095-4956.

[31] Shuo Li et al. “Constant-rate heating-induced thermal runaway in 18650-type Li-ion cells charged/discharged at 1 °C: Effect of undischargeable Li at anode”. In: *Journal of Power Sources* 505 (2021), p. 230082. ISSN: 0378-7753.

[32] Xiaojun Li and Alan Palazzolo. “A review of flywheel energy storage systems: state of the art and opportunities”. In: *Journal of Energy Storage* 46 (2022), p. 103576. ISSN: 2352-152X.

[33] Xiutao Li et al. “A liquid cooling technology based on fluorocarbons for lithium-ion battery thermal safety”. In: *Journal of Loss Prevention in the Process Industries* 78 (2022), p. 104818. ISSN: 0950-4230.

[34] Niranjanmurthi Lingappan et al. “A comprehensive review of separator membranes in lithium-ion batteries”. In: *Renewable and Sustainable Energy Reviews* 187 (2023), p. 113726. ISSN: 1364-0321.

[35] Jialong Liu et al. “Aging behavior and mechanisms of lithium-ion battery under multi-aging path”. In: *Journal of Cleaner Production* 423 (2023), p. 138678. ISSN: 0959-6526.

[36] Binbin Mao et al. “Failure mechanism of the lithium ion battery during nail penetration”. In: *International Journal of Heat and Mass Transfer* 122 (2018), pp. 1103–1115. ISSN: 0017-9310.

[37] Ning Mao et al. “An investigation on thermal runaway behaviours of lithium-ion battery with Li(Ni0.6Co0.2Mn0.2)O2 cathode induced by overcharge under different heat dissipation conditions”. In: *International Journal of Heat and Mass Transfer* 217 (2023), p. 124677. ISSN: 0017-9310.

[38] *Ministero della Salute https://www.salute.gov.it/*.

[39] Bruce R. Munson et al. *Meccanica dei Fluidi*. 2016.

[40] A.G. Olabi et al. "Critical review of energy storage systems". In: *Energy* 214 (2021), p. 118987. ISSN: 0360-5442.

[41] Xinrui Qi et al. "Study of circular, horizontal and vertical elliptical enclosures filled with phase change material in thermal management of lithium-ion batteries in an air-cooled system". In: *Journal of Energy Storage* 53 (2022), p. 105041. ISSN: 2352-152X.

[42] Andrea Carpignano Raffaella Gerboni. *Valutazione di impatto ambientale e LCA*. A.Y. 2022-2023.

[43] Massimo Santarelli. *Polygeneration and Advanced Energy Systems*. A.Y. 2022-2023.

[44] Michael H. Severson et al. "An integrated supply chain analysis for cobalt and rare earth elements under global electrification and constrained resources". In: *Resources, Conservation and Recycling* 189 (2023), p. 106761. ISSN: 0921-3449.

[45] *Society of Automotive Engineers' https://www.sae.org/*.

[46] Ziyou Song et al. "Benefit assessment of second-life electric vehicle lithium-ion batteries in distributed power grid applications". In: *Journal of Energy Storage* 56 (2022), p. 105939. ISSN: 2352-152X.

[47] *Swedish Civil Contingencies Agency https://www.msb.se/en/*.

[48] Alberto Tenconi. *Sistemi di propulsione elettrica per i trasporti*. A.Y. 2019-2020.

[49] Wenxuan Tong et al. "Solid gravity energy storage: A review". In: *Journal of Energy Storage* 53 (2022), p. 105226. ISSN: 2352-152X.

[50] *U.S. energy information administration https://www.eia.gov/*.

[51] *Vistra Corp. https://vistracorp.com/*.

[52] Hao Wang et al. "Battery and energy management system for vanadium redox flow battery: A critical review and recommendations". In: *Journal of Energy Storage* 58 (2023), p. 106384. ISSN: 2352-152X. DOI: https://doi.org/10.1016/j.est.2022.106384.

[53] Mohammad Waseem et al. "Battery technologies and functionality of battery management system for EVs: Current status, key challenges, and future prospectives". In: *Journal of Power Sources* 580 (2023), p. 233349. ISSN: 0378-7753.

[54] Ola Willstrand et al. “Impact of different Li-ion cell test conditions on thermal runaway characteristics and gas release measurements”. In: *Journal of Energy Storage* 68 (2023), p. 107785. ISSN: 2352-152X.

[55] Yu Yang et al. “Towards a safer lithium-ion batteries: A critical review on cause, characteristics, warning and disposal strategy for thermal runaway”. In: *Advances in Applied Energy* 11 (2023), p. 100146. ISSN: 2666-7924.

[56] Ryutaka Yudhistira, Dilip Khatiwada, and Fernando Sanchez. “A comparative life cycle assessment of lithium-ion and lead-acid batteries for grid energy storage”. In: *Journal of Cleaner Production* 358 (2022), p. 131999. ISSN: 0959-6526.

[57] Antong Zhang et al. *2060: Civilization, Energy, and Progression of Mankind on the Kardashev Scale*. 2022. arXiv: 2208.12617 [cs.CY].

[58] Jiangong Zhu et al. “A method to prolong lithium-ion battery life during the full life cycle”. In: *Cell Reports Physical Science* 4.7 (2023), p. 101464. ISSN: 2666-3864.

[59] Kaiyu Zou and Shouxiang Lu. “Comparative study on the influence of incident heat flux on thermal runaway fire development of large-format lithium-ion batteries”. In: *Process Safety and Environmental Protection* 176 (2023), pp. 831–840. ISSN: 0957-5820.

[60] Ghassan Zubi et al. “Lithium-ion battery-packs for solar home systems: Layout, cost and implementation perspectives”. In: *Journal of Energy Storage* 32 (2020), p. 101985. ISSN: 2352-152X.

[61] Ghassan Zubi et al. “The lithium-ion battery: State of the art and future perspectives”. In: *Renewable and Sustainable Energy Reviews* 89 (2018), pp. 292–308. ISSN: 1364-0321.